HIGH TEMPERATURE TRANSPORT MEASUREMENTS

ON n-TYPE GaSb AND GaAs

by

Joseph Basinski

Ph.D. Thesis 1972

LIST OF CONTENTS

ABSTRACT

The considerable variation reported in the literature for the Γ_1 - L_1 minima separation and its temperature dependence in GaSb, suggested the need for further critical study to resolve these apparent discrepancies.

In this work measurements of magnetoresistance and Hall coefficient as a function of magnetic field and temperature were made on samples of Tellurium doped GaSb in the temperature range 25° to 200°C. Also the Hall coefficient at constant magnetic field and the zero field conductivity were measured up to a temperature of 360° on these n-type samples and up to 550°C on an undoped p-type sample. The results were analysed on the basis of a model including three conduction bands with minima at Γ_1, L_1 and X_1, and two valence bands. The non-parabolicity of the Γ_1 conduction band was taken into account. A zero temperature Γ_1 - L_1 band separation of 0.099 eV and a temperature dependence of -3.4×10^{-5} eV/°K was obtained. Also, the temperature variation of electron mobilities in the Γ_1 and L_1 minima was obtained from the results. This temperature variation of electron mobility $\mu_1(T)$ in the Γ_1 band was explained using a model involving four scattering mechanisms; viz. polar optical, screened Coulomb, interband and spacecharge. It is shown that the anomalously low electron mobility in the Γ_1 band of GaSb reported in the literature, can be understood when proper account is taken of the screened Coulomb scattering by both ionized impurities and the heavy electrons in the L_1 minima. These calculations also give an estimate of the value of the interband coupling constant, D_{12}, of 4.1×10^8 eV/cm for scattering between Γ_1 and L_1 bands.

It is well established that the lowest conduction band in GaAs has a minimum at the centre of the Brillouin zone. However, the positions in k-space of the next lowest set of minima have been in doubt. Experimental results strongly

favour these subsidiary minima to be in the <100> directions. On the other hand calculations based on various theoretical models predict the sets of minima to lie in either or both <100> and <111> directions.

An attempt is made here to resolve this problem by making Hall coefficient and conductivity measurements on a number of heavily Tellurium doped n-type GaAs samples in the temperature range 20^{o} to 600^{o}C. The results were analysed using three possible conduction band models. From these analyses it was concluded that the most probable model involves the Γ_1, Δ_1 and L_1 minima with absolute zero temperature band separations of 0.381 eV and 0.488 eV for the $\Gamma_1 - \Delta_1$ and $\Gamma_1 - L_1$ respectively.

ACKNOWLEDGEMENTS

First of all I wish to express my sincere thanks to my supervisor, Professor J. C. Woolley for his support, guidance and encouragement during the course of this work.

The help of all the professors in this department is deeply appreciated, in particular that of Professor Y. P. Varshni and Dr. K. S. Song for many discussions on scattering and band structure. I have benefited also from many stimulating and helpful discussions with my colleagues, especially Dr. C. C. Y. Kwan, Mr. R. Glinski, Mr. S. Rosenbaum and Mr. D. Demars.

I also wish to thank Miss L. Sawyer and Mrs. D. Perron for typing this manuscript.

The capable and prompt attention of all the workshop staff is gratefully acknowledged, as well as the able assistance of R. Hart.

I would also like to express my thanks to my wife Joan, daugters Teresa and Jane for their patience during the course of this work.

Finally, I acknowledge the financial assistance of the National Research Council of Canada through the P.I.E.R. Fellowship.

LIST OF TABLES

LIST OF FIGURES

CHAPTER I INTRODUCTION

This thesis is mainly concerned with the conduction band structure of GaSb and GaAs, and electron mobility in their conduction bands. The introductory discussion given below is divided into two separate parts dealing with the problems of GaSb and GaAs respectively.

GaSb

The compound semiconductor GaSb has been investigated experimentally and theoretically since about 1955 and its band structure is now quite well understood. However, uncertainties still exist in the values of several band parameters.

It was established by Zwerdling et al. (59Z1) that the lowest conduction band minimum in GaSb is at the centre of the Brillouin zone $(\Gamma_1)^*$ 0.813 eV above the valence band at absolute zero. This value, the principal energy gap in GaSb, was later confirmed by Adachi (69A2) who reanalysed Zwerdling et al.'s results including the non-parabolic effects.

Sagar (60S1) showed, from transport measurements under pressure, that a set of four equivalent minima are at the zone boundaries in the <111> directions $(L_1)^*$, at approximately 0.08 eV above the Γ_1 minimum. Ehrenreich (61E1) estimated that the next lowest set of minima are at the <100> zone boundaries $(X_1)^*$ and lie about 0.3 - 0.4 eV above the principal Γ_1 conduction minimum. Later, Kosicki and Jayaraman (68K1) obtained a value of 0.315 ± .015 eV for the $\Gamma_1 - X_1$ separation from the pressure dependence of the resistivity at room temperature.

* The notation for symmetry of the band extrema used here is a standard group theoretical notation first used by Bauckaert, Smoluchowski and Wigner (36B1). When the symmetry of a band extremum is in doubt, then standard crystallographic notation is used describing the directions in k-space.

Although theories of two band behaviour have been developed, in practice the application of these is difficult; either because the bands are of complex form (e.g. heavy hole valence band) or because experimental conditions which are required to ensure that both bands are populated (e.g. application of high pressures or temperatures, or heavy doping of samples) do not comply with assumptions on which the theories are based. However, the small energy separation of the Γ_1 and L_1 minima in GaSb ensures that samples can be chosen so that carriers are present in both bands at normal pressure and in a temperature range in which the theories are applicable. Consequently band parameters for the Γ_1 and L_1 bands can be determined from transport measurements on GaSb.

Table I-1 shows some reported values for the Γ_1 and L_1 minima separation, E_2, and its temperature dependence, α_2. It can be seen from this Table that considerable disagreement exists between these values. This wide variation can be traced, in most cases, to assumptions made in the analyses of experimental results, in particular the values chosen for the electron effective mass in the two bands and, in the case of theoretical calculations, to the model chosen.

Part of the work described here is concerned with obtaining reliable values of E_2 and α_2, as well as explaining the observed low mobility in the Γ_1 band. This was achieved by making accurate experimental measurements of the Hall coefficient and conductivity as a function of both magnetic field and temperature on appropriate samples of GaSb at temperatures where, (a) the experimental data are sensitive to E_2 and α_2 and (b) analysis can be carried out with a minimum number of assumptions. To this end, experiments were carried out at and above room temperature, in contrast to previously reported measurements which were invariably made at lower temperatures. The reason for this is that above about $20^{o}C$ n-type

samples can be chosen in which the total number of electrons, distributed over conduction bands, will remain constant with temperature. Under these conditions the analysis of experimental data is simplified and results are more reliable.

In the following sections we shall review the pertinent literature on GaSb and critically discuss the band parameters given.

The reported values of effective mass of electrons in the Γ_1 band vary between 0.040m, determined by Yep and Becker (66Y1) from de Haas-Shubnikov measurements at liquid helium temperature, and 0.049m obtained by Piller (63P1) from Faraday rotation measurements at liquid nitrogen temperature. Since Kane (56K1) has shown that the Γ_1 band in III-V compounds cannot be considered parabolic, it is insufficient to quote effective mass values other than the bottom of the band effective mass at absolute zero, m^*_{oo}, without quoting the Fermi energy and temperature. Only the mass given by Yep and Becker has been corrected for non-parabolicity of the band, but Piller (63P1) obtained a value of 0.053m at absolute zero using an approximate Kane band in his analysis of Faraday rotation data. This latter value can not be regarded as reliable because of the assumptions involved in its derivation. The optical results of Aubin et al. (69A3) on the alloy system (GaIn)Sb when extrapolated to the GaSb end of the ternary section, give the bottom of the band effective mass as between 0.042 and 0.043m at room temperature.

Several values of the effective mass in the L_1 minima can be found in the literature. Becker et al. (61B1) report a value of 0.027m for the density of states effective mass, m^*_{2d}, which they derived from measurements of Hall effect, conductivity and magnetoresistance at low temperatures. Piller (63P1) on the other hand derived a value of .228m from his Faraday rotation data in agreement with 0.226 by Van Tongerloo and Woolley (69T1) based on similar measurements. Theoretical

calculations of Cohen and Bergstresser (66C1), using pseudo-potential method lead to a value of 0.276m, but the band separations they calculate do not agree with experimentally obtained values. More recently Zhang and Callaway (68Z1, 69Z1) also using pseudo-potential method, but including non local terms, arrived at a value of 0.238m for this effective mass, but in contrast to Cohen and Bergstresser's calculation, they force the band separations to agree with experimentally determined values by adjusting their pseudo-potentials. The ellipticity parameter K_2, (the ratio of longitudinal to transverse effective mass, $K_2 = m^*_{2\ell}/m^*_{2t}$), was obtained experimentally by Piller (64P1), who reports a value of 8.4, from analysis of Faraday rotation measurements which he interprets using a two band model. A value of $K_2 = 10$ was also reported by Averous et al. (70A1) which was deduced from transport measurements on GaSb, analysis of which was also based on a two band model. The two theoretical calculations mentioned above give values of K_2 of 9.54 (66C1) and 13.5 (68Z1).

The effective mass of electrons in the X_1 band has not been obtained experimentally. In their analysis of resistivity as a function of pressure, Kosicki et al. (68K1) use 1.2m, established for the total density of states mass, M^*_{3d}, in the Δ_1 minima from Si, which they assume to be the appropriate value for the same band in GaSb.

Pitt (69P2), in analysing his experimental data of Hall coefficient and resistivity at high pressures, on the other hand used a value of 0.9m, which he obtained from similar measurements on GaAs for the minima in <100> direction. The pseudo-potential calculations, mentioned above, of Cohen and Bergstresser (66C1) and of Zhang and Callaway (68Z1) give values for the longitudinal, m^*_ℓ, and the transverse, m^*_t, effective masses. If a multiplicity of three is assumed, i.e.

minima at the zone boundary with symmetry, X_1, this leads to total density of state effective mass values of 1.0m and 0.87m respectively. Also, these values of m_ℓ^* and m_t^* give ellipticity parameters, K_3, of 5.6 and 6.9.

The low electron mobility in the Γ_1 conduction band, the value of which has usually been obtained as $\sim 0.4 m^2/V.sec.$ at room temperature (e.g. Sagar 60S1; Ehrenreich 61E1; Harland and Woolley 66H1) has long been thought to be anomalously low. Baxter et al. (67B1) suggested that this low mobility can be explained if the scattering is predominantly ionized impurity and if the high degree of compensation in n-type samples is taken into account and the heavy electrons populating the L_1 minima are considered to add to this scattering. That is, in addition to ionized impurities, the heavy electrons which have a mobility of $\sim 1/6$ of those in the Γ_1 band, will act as Coulomb scattering centres. Baxter et al. took as an example Sagar's (60S1) sample 1B and calculated the ionized impurity mobility based on this model to be $0.65 m^2/V.sec.$ They combined this with the total lattice mobility of $1.4 m^2/V.sec.$ estimated by Ehrenreich (61E1) to obtain a combined value of $0.44 m^2/V.sec.$ at room temperature, in good agreement with experiment.

Electron mobilities in the L_1 band also have been obtained from pressure experiments at room temperature by Pitt (69P2) and by Rosenbaum (72R1), values of between 0.04 and $0.05 m^2/V.sec.$ being derived. These agree well with values of .04 to $.065 m^2/V.sec.$ deduced by Sagar (60S1) from the analysis of the two band Hall effect.

Pitt (69P1) has also obtained a value of $\sim .004 m^2/V.sec.$ for the electron mobility in the X_1 band at room temperature. This seems somewhat low in comparison with the mobility observed in Si for the Δ_1 minima, but compares well with the mobility measured in the GaP principal conduction band which has the same symmetry

(68M1), and with the mobility of electrons in the Δ_1 band of GaAs when doping is taken into account.

From the foregoing brief review of the conduction band parameters in GaSb, it seems clear that the largest disagreements exist in the value of the $\Gamma_1 - L_1$ separation and its temperature dependence. Also the model which was used by Baxter et al. (67B1) seems to oversimplify the problem of scattering in the Γ_1 band. We shall attempt to clarify these problems in Chapter IV of this thesis.

It was suggested by Bate (62B1) that group VI impurity levels in III-V compounds are associated with the minima of subsidiary conduction bands. Harland and Woolley (66H1) found that the total electron concentration in their Te-doped GaSb increased with increasing temperature. To account for this they postulated an impurity level situated between the Γ_1 and L_1 minima. Recently Pitt (69P2) obtained an ionization energy $\sim$0.02 eV for Te donors in GaSb below the L_1 minima. For this reason the experimental measurements on n-type GaSb which are analysed in Chapter IV were performed at and above room temperature to ensure that all the available donors are ionized and hence the total electron concentration remains constant.

GaAs

Gallium Arsenide is probably one of the most studied III-V compounds because of its potential for device applications as well as purely academic interest. However, a serious gap exists in the understanding of the conduction band structure of this material. It is well established that, as in GaSb, the lowest conduction band in GaAs has its minimum at the centre of the Brillouin zone with Γ_1 symmetry. The problem arises as to the position in k-space of the next lowest set of minima.

Essentially, the experimental results suggest that the first subsidiary minima are ∿.4 eV above the Γ_1 minimum in the <100> direction and have Δ_1 or X_1 symmetry, but these results are not conclusive. Theoretical calculations using different methods of analysis, on the other hand, do not agree on whether the first subsidiary minima are in the <100> or <111> direction, nor do they agree on the relative energy separations of these sets of minima.

Since the first subsidiary minima in GaAs lie at about 0.4 eV above the Γ_1 minimum, in order to study these subsidiary minima by transport measurements, it is necessary to use heavily doped samples and elevated temperatures. Therefore measurements of Hall coefficient, at a constant magnetic field, and of conductivity were made from 20 to 600°C on samples with room temperature electron concentrations of from 5×10^{23} to $5 \times 10^{24} m^{-3}$. Measurements of magnetoresistance as a function of magnetic field were also made at 450°C, but these could not be analysed on the same model as those as GaSb. The results of Hall coefficient and conductivity were analysed on three models involving possible arrangements of subsidiary conduction bands. It was possible to choose the most probable model from these analyses on the basis of overall consistency in explaining experimental data.

Data concerning the subsidiary valleys in the conduction band structure of GaAs are reviewed in the following paragraphs. A more extensive review of the conduction band structure of GaAs can be found in the article by Gray (70G1). Photoemission studies of James et al. (68J1, 68J2) and Spicer and Eden (68S1) show transitions to subsidiary minima at about 0.35, 0.45 and 0.95 eV above the Γ_1 minimum and were interpreted as being transitions to the minima at the X_1, L_1 and X_3 points in the Brillouin zone. The identification of the lowest of these minima is consistent with the results of an analysis based on a two band model by Ehrenreich (60E1) and

using data on the high temperature Hall coefficient. This analysis shows that there are six equivalent minima at 0.36 eV above the Γ_1 minimum with a combined density of states mass of 1.2m. By analysing data on the resistivity as a function of pressure, Ehrenreich (60E1) was able to deduce a variation with pressure of the position of these minima relative to the valence band. Since this pressure coefficient and the above effective mass were reasonably close to the corresponding values observed for the Δ_1 minima in silicon, Ehrenreich concluded that the subsidiary minima in GaAs were probably also in the <100> direction . Experiments on Ga(AsP) alloys are in agreement with Ehrenreich's conclusion. These show that the positions of the <100> minima in the phosphide rich alloys, when extrapolated back to zero phosphorous content lead to a Γ_1 - Δ_1 separation of about 0.4 eV (60E1). The conclusion is also consistent with work of Harris et al. (70H1) on the variation of the threshold field for Gunn oscillations with uniaxial compression along various directions. Measurements by Balslev (68B1) of the indirect absorption from the Γ_1 minimum to a subsidiary band, as a function of uniaxial compression along various directions, also reveal minima in the <100> directions at a somewhat higher energy of 0.43 eV at liquid nitrogen temperature.

Although the above evidence strongly suggests that the lowest subsidiary minima are in the <100> directions, it is worth noting that it cannot at this stage be regarded as conclusive. The first reason for this is that Ehrenreich's analysis (60E1) does not lead directly to the density of states in the subsidiary minima, but to the product of the density of states and the factor $e^{-\alpha/k}$, where α is the linear temperature coefficient of the Γ_1 - Δ_1 band separation and k is Boltzmann's constant. With α assumed to be zero, Ehrenreich (60E1) could determine only that the density of states mass lies between 0.9 and 1.7m. More recent experiments on GaAs under pressure have given the value of 0.38 eV at room temperature for the energy separation of

the minima (67H1) and 0.85m for the density of states mass (70P1, 70P2), but it was necessary in both these cases to assume either the density of states (67H1) or energy separation (70P1, 70P2) to deduce these values. Also, even if the <100> minima are the lowest at high pressure in GaAs, as seems almost certain, it does not necessarily follow that the <100> minima are the lowest at zero pressure. The <100> and <111> minima could cross before the <100> minima could start to influence the transport properties. This arrangement of the minima would not necessarily conflict with the data on the band gap of Ga(AsP) alloys, particularly since any non-linear variation of the band gap with composition was not taken into account in the extrapolation of the data (68L2).

As was already pointed out, band structure calculations (66C1, 69J1, 66P1, 70C1, 68H1) do not consistently predict the relative position of the <100> and <111> minima, the latter being calculated to be from as much as 0.5 eV below to 0.4 eV above the <100> minima. Pseudo-potential calculations of Cohen and Bergstresser (66C1) predict the <111> minima to be 0.1 eV below the <100> minima, whereas Jones and Lettington (69J1), using the same method but a different form of pseudo-potential, have recently calculated the <111> minima to be 0.4 eV above the <100> minima. The k.p calculations of Pollak et al. (66P1) place the <111> and <100> minima at about the same energy. The <111> minima are found to be below the <100> minima in the OPW calculations of Collins et al. (70C1), the separation being 0.44 eV, although the <100> minima occur in this case 0.8 of the way to the X point, i.e. have Δ_1 symmetry. On the other hand, Herman (68H1) has shown that it is possible to adjust the Fourier coefficients of the potential used in the OPW calculation to obtain close agreement with the observed transition energies between the various minima throughout the band structure. He found that if X_1 and L_1 minima were taken to lie 0.35 and 0.43 eV respectively above the Γ_1 minimum then a good overall fit to the experimental data

was obtained.

The bottom of the band effective mass in the Γ_1 band of GaAs has been measured by various methods (65M1; 68S2; 69C1; 68V1), the values obtained vary between 0.064m and 0.067m, i.e. close agreement exists for this parameter. On the other hand, no experimentally determined values have been reported for the effective mass in the <111> minima for GaAs. However, the k.p perturbation calculations of Pollak et al. (66P1) predict values of 0.97m and 0.116m for the longitudinal and transverse mass respectively, from which a density of states mass of 0.235m and an ellipticity parameter of 8.4 are calculated.

Electron mobility in the Γ_1 band has been investigated by Ehrenreich (60E1), Fortini et al, (70F1), Moore and Ehrenreich (66M1), Moore (67M1) and Ikoma (70I1). Ehrenreich has shown that in pure samples, the electron mobility is limited by polar optical scattering with a resulting room temperature value of 0.93m/V sec. Polar optical mobility was also calculated for GaAs by Fortini et al.(70F1) and compared to Hall mobility measurements on a pure sample ($n \sim 10^{20} m^{-3}$ at $350^{o}C$) over a wide temperature range. They found good agreement up to room temperature, but at higher temperatures, calculations lead to a higher mobility than those experimentally observed. Fortini et al. suggest that the disagreement may be accounted for by omitting in their calculations the effects of multiphonon scattering and neglecting the temperature dependence of the dielectric constant. Ehrenreich (60E1) has also made calculations of combined polar optical and ionized impurity scattering using variational techniques, he showed that at room temperature the calculated mobility was in good agreement with the measured mobility as a function of doping, except in the high doping range. Later Moore and Ehrenreich (66M1) showed that in order to have better agreement at high doping concentrations, i.e. $N_I > 7.5 \times 10^{23} m^{-3}$, quantum mechanical corrections had to be made to the Brooks-Herring ionized impurity mobility relation.

Making these corrections, they found excellent agreement with experimental results at liquid nitrogen temperature, and slightly less acceptable agreement at 300°K. Ikoma (70I1), on the other hand, made measurements of Hall mobility up to 600°C on samples doped with less than $1 \times 10^{23} m^{-3}$ tellurium donors, and obtained reasonably satisfactory agreement above 200°C between his experimental results and calculated values. The calculations included two phonon resonance, polar optical and interband scattering between Γ_1 and Δ_1 minima. However, some heavier doped samples had a measured mobility of roughly half the calculated value, indicating that scattering at elevated temperatures was underestimated by Ikoma's model.

The mobility at room temperature in the Δ_1(or X_1) minima of GaAs has been deduced from the Hall coefficient and resistivity measurements under pressure . Hutson et al. (67H1) deduced $0.011 m^2$/V.sec. whereas Pitt and Lees (70P2) derived $0.035 m^2$/V.sec. for the electron mobility in the <100> minima. This discrepancy may be explained by the use of different effective mass values for these minima. Thus, Hutson et al. used the density of states mass of 1.2m obtained by Ehrenreich (60E1), i.e. six equivalent minima; whereas Pitt and Lees derived a value of 0.85m, which was based on a 3 equivalent minima model. Conwell and Vassel (68C1) calculated the mobility to be $0.0145 m^2$/V.sec. by taking into account acoustic, polar optical and equivalent intervalley scattering by optical phonons. This value agrees well with the value of $0.015 m^2$/V.sec. obtained earlier by Lees et al. (67L1) from hydrostatic pressure measurements assuming 6 equivalent valleys. Calculations of James et al. (69J2) which include equivalent intervalley and deformation potential scattering, give a mobility in this band of $0.012 m^2$/V.sec.

TABLE I-1

E_2 eV	α_2 eV/°k x 10^4	Ref.
0.074	-3.	(60S1)
	~1.	(61C1)
	1.1	(63P1)
0.084 *	0.8	(66H1)
0.084	0.59	(68L1)
0.083	0.55	(69B1)
0.08	2.1	(70A1)
0.077	-2.	(70R1)
0.04	-1.8	(70S1)
0.058	1.4	(71S1)

* Liang (68L1) uses the value of E_2 obtained by Harland and Woolley (66H1)

Table I-1: The values of E_2 and α_2 reported in the literature.

CHAPTER II

THEORY

CHAPTER II THEORY

Theory necessary to the understanding of the work presented in this thesis will be reviewed here. When proofs of certain expressions may be found in the literature these will not be repeated but references will be given; any underlying assumptions used will be critically discussed. The author's own contribution when applicable will be pointed out.

II-1 The Effective Mass

The concept of effective mass has been discussed in various standard texts (e.g. Kittel, 53K1). However, since there are different definitions of effective mass depending on the nature of the external force being applied, a summary of those which will be used in later chapters in dealing with the analysis of experimental results is presented in Table II-1.

II-2 Form of the Energy Bands, the Kane Model

Theoretical calculations of band structure are generally a formidable problem. The necessity of determining band structure in solids has led to a number of different approximations which make the problem more tractable. By using the "one electron" approximation, various theories can be developed to give the energy band scheme of solids. One of these is the semi-empirical $k.p$ perturbation theory developed by Kane (56K1) which describes the band shapes at and in the vicinity of critical points. The present work is in part concerned with the band parameters of the Γ_1 conduction band of GaSb and GaAs. In both these compounds the Γ_1 conduction band is limited to a small range in k space, so that of the available methods of calculations, the $k.p$ representation is most suitable. The results of the $k.p$ perturbation theory developed by Kane will thus be used.

We shall start with the E vs k relation obtained from the Kane model and use this relation to derive expressions which will later be used in the analysis of experimental data.

First order perturbation theory led Kane to an 8 x 8 secular determinant, the solution of which is

$$E'[E'(E' - E_o)(E' + \Delta) - k^2P^2(E' + 2/3\Delta)] = 0 \qquad \text{II-1}$$

where $E' = E - \hbar^2k^2/2m$, energy being measured from the top of the valence band.

E_o is the principal gap

Δ is the spin orbit splitting of the valence band

P is a matrix element

m is the electron rest mass

It should be pointed out at this point that solution II-1 is obtained when only three valence bands and one conduction band are taken into account, neglecting the interaction of higher conduction bands. This model has been used extensively and has proved to be satisfactory for the III-V compounds (e.g. InSb, 71Z1) so that the approximation seems to be justified in this case.

It has been shown by Aubin (69A1) that a general solution to equation II-1 for the conduction band is of the form

$$E' = \frac{E_o}{2}\left[-1 + \left(1 + \frac{\beta k^2P^2}{E_o^2}\right)^{1/2}\right] \qquad \text{II-2}$$

where

$$\beta = \frac{4 + 8\eta/3}{1 + \eta}$$

and

$$\eta = \Delta/E_o$$

Hence, replacing E' in II-2 gives

$$E = \frac{\hbar^2 k^2}{2m} + \frac{E_o}{2}\left[\left(1 + \frac{\beta k^2 P^2}{E_o^2}\right)^{1/2} - 1\right] \qquad \text{II-3}$$

Using the definition of cyclotron and band curvature effective mass given in Table II-1, we can now derive the variation of the effective mass with k i.e.

$$\frac{1}{m_c^*} = \frac{1}{m} + (E_o^2 + \beta k^2 P^2)^{-1/2} \beta P^2 / 2\hbar^2 \qquad \text{II-4}$$

$$\frac{1}{m_e^*} = \frac{1}{m_c^*} - \frac{\beta^2 P^4 k^2}{2\hbar^2 E_o^3}\left(1 + \frac{\beta P^2 k^2}{E_o^2}\right)^{-3/2} \qquad \text{II-5}$$

Thus the bottom of the band effective mass m_o^* is obtained when $k = o$, i.e.

$$\frac{1}{m_o^*} = \frac{1}{m} + \frac{\beta P^2}{2\hbar^2 E_o} \qquad \text{II-6}$$

which now gives the well known relation for the square of the matrix element P^2,

$$P^2 = \frac{3\hbar^2/2m \;\; E_o(E_o + \Delta)\;(m/m_o^* - 1)}{(3E_o + 2\Delta)} \qquad \text{II-7}$$

Eliminating P^2 and β from II-3 we obtain the $E(k)$ relation in terms of the basic measurable band parameters

$$E = \frac{\hbar^2 k^2}{2m} + \frac{E_o}{2}\left[\left\{1 + \frac{4\hbar^2 k^2}{2mE_o}\;(m/m_o^* - 1)\right\}^{1/2} - 1\right] \qquad \text{II-8}$$

The same relation was obtained by Cardona (61C1) who assumed that $E' << E_o + 2/3\Delta$. It should be noted that for large energy gap E_o and small effective mass the above relation reduces to the standard parabolic band, in which case the effective mass

is independent of energy

$$E = \frac{\hbar^2 k^2}{2m^*} \qquad \text{II-9}$$

We can invert relation II-8 to obtain $k(E)$ i.e.

$$k^2 = \left(\frac{m^2 E_o}{\hbar^2 m_o^*}\right) \left[1 + \frac{2Em_o^*}{E_o m} - \left(1 + \frac{4Em_o^*}{E_o m}\left(1 - \frac{m_o^*}{m}\right)\right)^{1/2}\right] \qquad \text{II-10}$$

Another form of the $k(E)$ relation can be derived starting with equation II-1 and assuming that $E >> h^2k^2/2m$ which simplifies the relation to

$$E(E + E_o)(E + E_o + \Delta) - k^2P^2(E + E_o + 2/3\Delta) = 0 \qquad \text{II-11}$$

from which one obtains

$$k^2 = \frac{E(E + E_o)(E + E_o + \Delta)}{(E + E_o + 2/3\Delta)P^2} \qquad \text{II-12}$$

It was shown by Aubin (69A1) that for InSb both relations II-10 and II-12 are good approximations to the Kane model and agreed very well with the $k(E)$ expression derived by Kolodziejczak (66K2) who included the effect of higher and lower bands by second order perturbation theory. We expect therefore that in the case of GaSb and GaAs where the interaction of valence and conduction bands is weaker, the above expressions would be a still better approximation to the Kane model than for InSb.

Indeed, it can be seen from Kolodziejczak's calculations (66K2) that for both GaAs and GaSb the inclusion of the upper and lower bands does not significantly affect the Kane model, at least in the Fermi energy range of about +0.1eV to -0.1eV. encountered in the experiments described here. Seiler et al. (69S1) have considered the effect of the L_1 minima on the isotropy of the Γ_1 minimum in GaSb and found that the distortion is very small, hence to a good approximation we can consider

that the Γ_1 band in GaSb is isotropic.

Ehrenreich (57E1) has pointed out that the Kane model is strictly valid only at absolute zero. Hence E_o appearing in the Kane expression is the band gap at absolute zero. Further, at finite temperatures the value of E_o is affected both by lattice distortion and interaction with the phonon field. However, Ehrenreich (57E1) suggests that the band curvature, which determines the effective mass, depends only on the lattice dilation, and therefore that E_o in the Kane model should be replaced by E_o^*, the "effective mass band gap" where E_o^* is the value the band gap would have if only lattice dilation effects were considered. The above effect was considered also by Ravich (66R1) who derived the changes with temperature in the effective mass, due to electron phonon interaction, as a function of the temperature variation of the band gap for InSb and InAs.

The effective mass band gap E_o^* may be expressed in the form (68T1)

$$E_o^* = E_{oo} - \left(\frac{E_{oo} - E_o}{a}\right) \qquad \text{II-13}$$

where E_{oo} is the intrinsic band gap at absolute zero and "a" is a parameter which determines the relative effect of lattice dilation and interaction of phonon field on the band gap.

II-3 Electron Scattering in III-V Compounds

It can be shown that under steady state conditions Boltzmann's transport equation can be written in the form

$$\hbar^{-1} \frac{df}{dE} (F \cdot \text{grad}_k E) = \left.\frac{df}{dE}\right|_{\text{coll}} \qquad \text{II-14}$$

where F is the applied field, f is the distribution function under the applied field.

The collision term on the right of the equation is responsible for restoring f to its equilibrium value. If the deviation from equilibrium is small it is possible to write the collision term in the form,

$$\left.\frac{df}{dt}\right|_{coll} = - \frac{f - f_o}{\tau} \qquad \text{II-15}$$

where f_o is the equilibrium distribution function and τ is a relaxation time, then II-14 becomes

$$\hbar^{-1} \frac{df}{dE} (F. \text{ grad}_k E) = - \frac{f - f_o}{\tau} \qquad \text{II-16}$$

The validity of the relaxation time approximation is discussed in many standard texts (e.g. Blatt, 68B2) and will be assumed here.

The magnitude, energy and temperature dependence of τ will depend on the scattering mechanism, which will now be discussed. It should be pointed out that the following discussion does not attempt to exhaust all the possible scattering processes, nor does it treat them very rigorously since full derivations can be found in the references quoted.

II-31 Lattice Phonon Scattering

II-311 Acoustic Phonon, "deformation potential" scattering

For acoustic mode vibrations, the wavelength is large compared with the interatomic distance and the vibrational energy is relatively small. It was pointed out by Bardeen and Shockley (50B1) that the long wavelength acoustic vibrations which produce a small perturbation on the periodic potential of a crystal, can be

used to calculate the motion of an electron neglecting the periodic potential. They introduced the name "deformation potential" for this type of effective potential which can be produced by long wavelength acoustical waves. The relaxation time, due to this scattering is given by

$$\tau_{a\ell} = \frac{\rho U_\ell^2 \quad \hbar^4}{8\pi^3 (2m^*)^{3/2} \; kT \; E_1^2 \quad E^{1/2}} \qquad \text{II-17}$$

where ρ is the density, U_ℓ is the velocity of the longitudinal waves in the crystal and E_1 is the deformation potential energy defined by

$$\Delta E_c = E_1 \quad \Delta V/V_o \qquad \text{II-18}$$

Here ΔE_c is the change in energy of the bottom of the conduction band due to a small change ΔV in the original volume V_o.

For ellipsoidal constant energy surfaces it was shown by Herring and Vogt (56H1) that E_1 is related to Ξ_d and Ξ_u deformation potential constants which depend on the symmetry of the minima considered.

II-312 Optical Phonon Scattering

(a) It has been shown by Ehrenreich (60E1) that polar optical scattering is dominant in conduction bands with Γ_1 symmetry in III-V compounds. Ehrenreich (60E1) derived, (using variational techniques) an expression for the mobility due to combined polar optical and ionized impurity scattering. The present measurements were taken at $T > 300^oK$, hence other scattering mechanisms such as interband scattering have to be included so that Ehrenreich's expression becomes inapplicable. Therefore we shall make use of the expression for the relaxation time due to polar scattering derived by Conwell and Vassell (68C1). In the case of a parabolic band

the relaxation time τ_{po} is given by:

$$\frac{1}{\tau_{po}} = \frac{eE_o\ (2N_{q\ell} + 1)}{[2m^* E]^{1/2}} \qquad \text{II-19}$$

and for a non-parabolic band with spherical symmetry this becomes

$$\frac{1}{\tau_{po}} = eE_o\ (2N_{q\ell} + 1)\ (2m_o^*\ \gamma)^{-1/2}\ \frac{d\gamma}{dE} \qquad \text{II-20}$$

where

$$eE_o = \frac{e^2 m_o^*\ (\hbar\omega_\ell)}{4\pi\hbar^2}\ \left(\frac{1}{\kappa_\infty} - \frac{1}{\kappa_o}\right) \qquad \text{II-21}$$

$$N_{q\ell} = \left[\exp\left(\frac{\hbar\omega_\ell}{kT}\right) - 1\right]^{-1} \qquad \text{II-22}$$

and

$$\gamma = \frac{\hbar^2 k^2}{2m_o^*} \qquad \text{II-23}$$

where ω_ℓ is the optical phonon frequency, κ_∞ and κ_o are the high frequency and static dielectric constants respectively.

It was pointed out by Conwell and Vassell (68C1) that the expression for τ_{po} was derived assuming only wave functions with S symmetry. For higher energies the admixture of p functions causes the expression to be less accurate. However, at these higher energies other scattering mechanisms, such as interband, become more important in both GaAs and GaSb and hence this error may be neglected.

(b) In semiconductors with band structure such that two bands have minima close in energy, the scattering of carriers between the two bands may be important in determining the mobility of carriers in either one or both bands. This scattering is usually termed "interband" scattering.

In polar semiconductors such as III-V compounds and their alloys, this scattering mechanism is possible with an absorption or emission of an optical phonon, since a large change in wave vector k is necessarily required when the two minima are at different symmetry points in the Brillouin zone. An expression for τ_{ib} was also derived by Conwell and Vassell (68C1) and is

$$\frac{1}{\tau_{ib}} = \frac{D_{12}^2 (M_d^*)^{3/2}}{\sqrt{2\pi}\ \hbar^3\ \rho\omega_{12}} \times \frac{1}{e^{x_{12}} - 1}$$

$$\times \left[(E + \hbar\omega_{12} - E_{12})^{1/2} + e^{x_{12}}(E - \hbar\omega_{12} - E_{12})^{1/2}\right] \qquad \text{II-24}$$

where D_{12} is the coupling constant, ω_{12} the angular frequency for transition between the two bands, $x_{12} = \hbar\omega_{12}/kT$ (k = Boltzmann constant). E_{12} is the energy separation of the two minima and $M_d^* = \nu^{2/3} m_d^*$. The integer ν represents the number of equivalent minima.

II-32 Scattering by Lattice Defects

II-321 Scattering by ionized impurities

The problem of scattering by ionized impurities was originally treated by Conwell and Weisskopf (50C1) who considered Rutherford scattering by each ion independently. The divergence arising from the increasing contribution of small angle scattering was removed by arbitrarily cutting off the scattering cross sections at a distance $r^{-1} = N_I^{1/3}/2$, where N_I is the impurity density. In later work Brooks and Herring (51B1) and Dingle (55D1), used a screened Coulomb potential, which takes care of the divergence difficulty, this arises from the fact that charge carriers distribute themselves around the impurity and cancel its field at large

distances. This leads to a relaxation time τ_I given by an expression of the following type (59S1);

$$\tau_I = \frac{16\pi\,(2m^*)^{1/2}\,\kappa_o^2\,E^{3/2}}{e^4\,N_I\,f(z)} \qquad \text{II-25}$$

where f(z) is a slowly varying function of E and is given by $f(z) = \ell n(1+z) - z/(1+z)$, here $z \equiv 2(k\,a)^2$ and "a" is the screening distance which is a function of the carrier density, temperature and energy of the carrier.

The above screening relation was derived by quantum-mechanical treatment and is based on the Born approximation, which implies that the range of validity of the treatment is given by $z >> 1$. When this is violated as in the case of high impurity concentration or at very low temperatures the accuracy of the calculation of mobility may be suspect.

Using the results obtained by Dingle (55D1), Beer (63B1) has given a relation for z of the form:

$$z = \frac{8\,\kappa_o m^* kTE}{e^2\hbar^2 n}\,\frac{F_{1/2}(\eta)}{F_{-1/2}(\eta)} \qquad \text{II-26}$$

where n is the carrier concentration in the conduction band and F's are Fermi integrals defined by:

$$F_r(\eta) = \int_o^\infty \frac{x^r\,dx}{1 + e^{x-\eta}} \qquad \text{II-27}$$

where η is the reduced Fermi energy E_F/kT.

More recently Moore and Ehrenreich (66M1) and later Moore (67M1) have extended the above theory by including quantum mechanical corrections to the semi-classical Brooks-Herring treatment. They derive the following expression for the mobility:

$$\mu_I = \mu_I^* / \{1 + \sigma_B + \sigma_M + \sigma_D\} \qquad \text{II-28}$$

where μ_I^* is the Brooks-Herring mobility and the correction terms σ_B, σ_M and σ_D are defined by Ehrenreich and Moore (66E1) and contain some formidable integrals which Moore (67M1) solved numerically for GaAs.

The above relations are valid only for parabolic bands. Taking the non-parabolicity into account, it was shown by Kolodziejczak (66K1) that the relaxation time for ionized impurity scattering may be written in the form

$$\tau_I = \frac{8\pi \kappa_o^2 (2\gamma)^{3/2} m_o^{*\,1/2} dE/d\gamma}{e^4 N_I f(z)} \qquad \text{II-29}$$

where z is now given by

$$z = \frac{16\pi^2 \kappa_o \hbar \gamma}{e^2 (2m_o^*)^{1/2} (kT)^{1/2} L_1^{1/2}(\beta,\eta)} \qquad \text{II-30}$$

$L_1^{1/2}(\beta, \eta)$ is an integral defined as

$$L_k(\beta, \eta) = \int_o^\infty \left(-\frac{df_o}{dx}\right) (x + \beta x^2)^n (1 + 2\beta x)^k \, dx \qquad \text{II-31}$$

and

$$\beta = \frac{kT}{E_o} \quad , \quad \eta = \frac{E_F}{kT}$$

However, if we have multiple charged scattering centres and carriers present in more than one band, Kolodziejczak relations II-30 and II-31 have to be modified to take this into account. Baxter et al. (67B1) have shown that this can be done by replacing N_I in equation II-29 by $\sum_i Q_i N_i$, where Q_i and N_i are the charge and density of the i'th scattering centre respectively. They have also shown that in order to take into account the difference of screening by the carriers in the different bands z must be replaced by

$$z = \frac{8m_o^* Ea^2 \, d\gamma/dE}{\hbar^2} \qquad \text{II-32}$$

where a is the screening distance given by Dingle (55D1)

$$\frac{1}{a^2} = \frac{e^2}{\kappa_o kT} \frac{\partial n_i}{\partial \eta} \qquad \text{II-33}$$

and n_i is the density of carriers in band i.

II-322 Spacecharge Scattering

It was suggested by Weisberg (62W1) that the anomalously low mobility of electrons observed in some III-V compounds is due to scattering by spacecharge regions in the material. These spacecharge regions are formed by randomly distributed acceptor impurities compensating the donors, which would tend to produce intrinsic or even p-type regions. To provide the appropriate potential difference with respect to the uncompensated material, a region of spacecharge will be formed. By assuming that these regions are impenetrable spheres to the quasi free electrons, Conwell and Vassell (68C1) obtain an expression for the relaxation time due to spacecharge scattering for parabolic bands,

$$\tau_{sc} = (N_s Q_s)^{-1} [m^*/2E]^{1/2} \qquad \text{II-34}$$

where N_s is the density of the impenetrable spheres and Q_s their scattering cross section.

For non-parabolic bands this relaxation time is

$$\tau_{sc} = (N_s Q_s)^{-1} (m_o^*/2\gamma)^{1/2} \, d\gamma/dE \qquad \text{II-35}$$

It is of interest to note that unlike impurity scattering this process becomes more important as the energy of electrons increases.

II-33 Other Scattering Mechanisms

There are various other scattering mechanisms which play a role in carrier scattering in semiconductors, among these are piezo-electric and neutral impurity. Both of these can be shown to be unimportant in GaAs and GaSb at the temperatures at which experimental data for this thesis were obtained. However, electron-electron and electron-hole interactions can become important at elevated temperatures and in the intrinsic region. These interactions will be discussed further in a later chapter dealing with the experimental results on GaSb.

II-4 Carrier Mobility

When an electric field E_x is applied to a semiconductor in direction x, the average drift velocity of a carrier will be given by

$$v_x = \mu E_x \qquad \text{II-36}$$

where the proportionality constant μ is called the carrier mobility; it is positive for holes and negative for electrons. This mobility is given by

$$\mu = \frac{e \langle \tau \rangle}{m_e^*} \qquad \text{II-37}$$

for parabolic bands, where $\langle \tau \rangle$ is an average over all energies of the electron distribution.

If the band is non-parabolic (e.g. Kane Band), the effective mass is a function of energy and therefore must be included in the averaging process, and the mobility may be written as

$$\mu = e \left\langle \frac{\tau}{m_e^*} \right\rangle \qquad \text{II-38}$$

However, it has been pointed out by Sosnowski (64S1) that the second term in equation II-5 cancels out in the Boltzmann equation. Consequently, it is the cyclotron mass that enters into the solution and all expressions entering the transport. Therefore m_e^* appearing in II-38 should be replaced by m_c^*. Zawadzki (62Z1) has shown that for spherical constant energy surfaces the average $\langle \tau/m_c^* \rangle$ is given by

$$\left\langle \frac{\tau}{m_c^*} \right\rangle = \frac{\int_0^\infty \left(-\frac{\partial f}{\partial E}\right) \frac{\tau}{m_c^*} k^3 dE}{\int_0^\infty \left(-\frac{\partial f}{\partial E}\right) k^3 dE} \qquad \text{II-39}$$

where $f = f_o$ the equilibrium Fermi-Dirac distribution factor for small E_x.

For parabolic bands this becomes

$$\langle \tau \rangle = \frac{\int_0^\infty \left(-\frac{\partial f_o}{\partial E}\right) \tau E^{3/2} dE}{\int_0^\infty \left(-\frac{\partial f_o}{\partial E}\right) E^{3/2} dE} \qquad \text{II-40}$$

and under the condition of non-degenerate statistics $-\frac{\partial f_o}{\partial E}$ may be replaced by f_o, and in this limit f_o (= exp[-E/kT]) is the Boltzmann distribution function.

In cases when more than one scattering mechanism affects the carriers, the resultant relaxation time may be written in the form

$$\tau^{-1} = \sum_i \tau_i^{-1} \qquad \text{II-41}$$

where "i" runs over all the scattering modes. This relation assumes that the scattering mechanisms are independent of one another, which in effect is an approximation, since in the case of lattice and ionized impurity scattering, for example, an electron may be scattered by a lattice phonon while in the field of an

impurity. However, this approximation is usually made in semiconductor work and will be adopted here.

II-5 The Hall Effect

II-51 "Two band" Hall coefficient

In most III-V compounds the conduction band structure is such that when two non equivalent minima are partially occupied by carriers one of these is the Γ minimum, which is isotropic but non-parabolic, and the others are the minima in the <111> or <100> directions. These latter minima have ellipsoidal energy surfaces and can be taken as parabolic. In addition, the electron effective mass of the ellipsoidal minima are much greater than that in the minimum at Γ (e.g. Madelung 64M1, p. 352).

The theory developed below is therefore applicable to the band structures of III-V compounds and, although it may be suitable for other materials it is important to ensure that the assumptions made in deriving these expressions are still valid.

For the case of two non-interacting bands it was shown by Chambers (52C1) that the Hall coefficient is given by

$$R = \frac{R_1\sigma_1^2\,(1 + \sigma_2^2 R_2^2 B^2) + R_2\sigma_2^2\,(1 + \sigma_1^2 R_1^2 B^2)}{(\sigma_1 + \sigma_2)^2 + \sigma_1^2\sigma_2^2\,B^2(R_1 + R_2)^2} \qquad \text{II-42}$$

This expression as it stands can not be used directly with experimental results to give useful information about the parameters of the two bands. However, with some manipulation a more convenient form is developed here, from which the band

parameters σ_1, σ_2, R_1 and R_2 can be calculated from experimental results. This development is shown below. At B = 0 the expression II-42 reduces to:

$$R_o = \frac{R_1\sigma_1^2 + R_2\sigma_2^2}{\sigma_o^2} \qquad \text{II-43}$$

where $\sigma_o = \sigma_1 + \sigma_2$, the zero field conductivity. Let the change in Hall coefficient $R - R_o = \Delta R$, then:

$$\frac{\Delta R}{R_o} = \frac{\sigma_1^2\sigma_2^2(R_1 + R_2)[(\sigma_1 + \sigma_2)^2 R_1R_2 - (R_1 + R_2)(R_1\sigma_1^2 + R_2\sigma_2^2)]\, B^2}{(R_1\sigma_1^2 + R_2\sigma_2^2)[(\sigma_1 + \sigma_2)^2 + \sigma_1^2\sigma_2^2 (R_1 + R_2)^2 B^2]} \qquad \text{II-44}$$

with further manipulation we obtain:

$$-\frac{R_o}{\Delta R} = \frac{(R_1\sigma_1^2 + R_2\sigma_2^2)(\sigma_1 + \sigma_2)^2}{\sigma_1^2\sigma_2^2 (R_1 + R_2)(R_1\sigma_1 + R_2\sigma_2)^2} B^{-2}$$

$$+ \frac{(R_1\sigma_1^2 + R_2\sigma_2^2)(R_1 + R_2)}{(R_1\sigma_1 - R_2\sigma_2)^2} \qquad \text{II-45}$$

$$= sB^{-2} + a \qquad \text{II-46}$$

where

$$s = \frac{(R_1\sigma_1^2 + R_2\sigma_2^2)(\sigma_1 + \sigma_2)^2}{\sigma_1^2\sigma_2^2(R_1 + R_2)(R_1\sigma_1 - R_2\sigma_2)^2} \qquad \text{II-47}$$

$$a = \frac{(R_1\sigma_1^2 + R_2\sigma_2^2)(R_1 + R_2)}{(R_1\sigma_1 - R_2\sigma_2)^2} \qquad \text{II-47}$$

Hence a plot of $-\frac{R_o}{\Delta R}$ vs. B^{-2} will give a straight line, with the slope s and intercept "a" each depending on the four band parameters R_1, σ_1, R_2 and σ_2. To solve for these factors two more relations between these and experimentally measurable quantities, are needed; these are given by the equations for R_o and σ_o. The solution of the four equations then gives:

$$\sigma_1 = \frac{\sigma_o}{2} \left[1 + \sqrt{\frac{c}{c+4}}\right] \qquad \text{II-49}$$

$$\sigma_2 = \frac{\sigma_o}{2} \left[1 - \sqrt{\frac{c}{c+4}}\right] \qquad \text{II-50}$$

where

$$c = -\frac{\sqrt{sa}}{R_o\sigma_o} \left[R_o\sigma_o + \sqrt{\frac{a}{s}}\right]^2 \qquad \text{II-51}$$

and

$$R_1 = \frac{1}{2\sigma_1 - \sigma_o} \left[R_o\sigma_o + \frac{\sigma_2}{\sigma_1}\sqrt{\frac{a}{s}}\right] \qquad \text{II-52}$$

R_2 can then be obtained from the equation II-43 for R_o.

The choice of sign in the above expressions containing square roots depends on the relative magnitude of σ_1 and σ_2. The signs given correspond to $\sigma_1 > \sigma_2$.

The above treatment shows that as long as the expression for two band Hall coefficient holds; i.e. B is small enough so that no quantum effects are present (Blatt 68B2, p. 216), measurement of R as a function of magnetic field B in principle can give information on the carrier concentration and mobility of carriers in the two bands. The main difficulty in obtaining this information, provided accurate experimental results of R and B can be obtained, is in the calculation of the carrier density n_i (i = 1, 2) from the respective Hall coefficients. This difficulty is inherent in the expression due to the usual lack of understanding of scattering

mechanisms in a band, and hence in the knowledge of the scattering factor $r = \left(\frac{\langle\tau_i^2\rangle}{\langle\tau_i\rangle^2}\right)$. Further discussion of this point is postponed till later chapters dealing with analysis of experimental results.

II-52 Multiband Hall coefficient

It is an easy step to extend the two band expression for R to any number of bands, say q, i.e.:

$$R = \frac{\sum_i D_i/B}{(\sum_i A_i)^2 + (\sum_i D_i)^2} \quad , \quad i = 1, \text{-----} q \qquad \text{II-53}$$

where

$$A_i = \sigma_i/(1 + \sigma_i^2 R_i^2 B^2) \qquad \text{II-54}$$

and

$$D_i = R_i \sigma_i^2 B/(1 + \sigma_i^2 R_i^2 B^2) \qquad \text{II-55}$$

We can write this expression in terms of carrier concentrations n_i and mobilities, μ_i, i.e.:

$$R = \frac{\sum_{i=1}^{q} (r_i F_i e\, n_i \mu_i^2)/(1 + \zeta_i^2)}{\left[\sum_{i=1}^{q} (e\, n_i \mu_i)/(1 + \zeta_i^2)\right]^2 + \left[\sum_{i=1}^{q} (e\, n_i \mu_i \zeta_i)/(1 + \zeta_i^2)\right]^2} \qquad \text{II-56}$$

where $\zeta_i = r_i F_i \mu_i B = \mu_{H_i} B$, and μ_H is the Hall mobility defined by $\mu_H = R\sigma$.

The conductivity σ is then given by

$$\sigma = e \sum_{i=1}^{q} n_i \mu_i \qquad \text{II-57}$$

When the density of holes becomes appreciable so that they contribute to the transport, their effect is easily taken into account by additional terms in equations II-56 and II-57.

II-6 Magnetoresistance

When a magnetic field is applied to a conductor, as in the case of Hall effect, the resistance of the conductor will invariably increase. When the field is applied, the trajectories of electrons between collisions will acquire a curvature. This means that the component of motion in the direction of applied electric field will be reduced by the presence of the magnetic field, effectively increasing the resistance. This phenomenon will be briefly discussed for the case of two models.

II-61 One band magnetoresistance

It can easily be shown that for a simple band with isotropic constant energy surfaces and constant relaxation time, the magnetoresistance will be zero. There are two cases when the magnetoresistance for carriers in one band is non zero; a) when the constant energy surfaces are non spherical and b) when the relaxation time is a function of energy.

For a) in the case of low magnetic fields and ellipsoids with major axes along <100> and <111> directions the appropriate expressions can be found in Smith (59S1, p.124). Smith also gives a definition of the "magnetoresistance coefficient" (ξ) as

$$\xi + 1 = \frac{\langle \tau^3 \rangle \quad \langle \tau \rangle}{\langle \tau^2 \rangle^2} \qquad \text{II-58}$$

Thus in case b) when the relaxation time is a function of energy and the band is not parabolic, the above expression becomes

$$\xi + 1 = \frac{\left\langle \frac{\tau^3}{m_c^3} \right\rangle \quad \left\langle \frac{\tau}{m_c} \right\rangle}{\left\langle \frac{\tau^2}{m_c^2} \right\rangle^2} \qquad \text{II-59}$$

II-62 Two band magnetoresistance

It is well known that for K = 1 and τ= constant, magnetoresistance vanishes (e.g. Smith 59S1, p. 124). This is no longer true when we have two types of carriers. It was shown by Chambers (52C1) that in this case resistivity as a function of magnetic field is given by:

$$\rho = \frac{(\sigma_1 + \sigma_2) + \sigma_1\sigma_2B^2\,(\sigma_1R_1^2 + \sigma_2R_2^2)}{(\sigma_1 + \sigma_2)^2 + \sigma_1^2\sigma_2^2B^2\,(R_1 + R_2)^2} \qquad \text{II-60}$$

Then $\Delta\rho = \rho - \rho_o$

$$= \frac{\sigma_1\sigma_2B^2(\sigma_1R_1 - \sigma_2R_2)^2}{(\sigma_1 + \sigma_2)\,[(\sigma_1 + \sigma_2)^2 + \sigma_1^2\sigma_2^2B^2\,(R_1 + R_2)^2]} \qquad \text{II-61}$$

Kwan and Woolley (68K2) showed that as in the case of Hall coefficient R, we can express $\frac{\rho_o}{\Delta\rho}$ in the form of a straight line

$$\frac{\rho_o}{\Delta\rho} = tB^{-2} + u \qquad \text{II-62}$$

where

$$t = \frac{\sigma_o - \sigma_1}{\sigma_1\,(R_o\sigma_o - R_1\sigma_1)^2} \qquad \text{II-63}$$

$$u = \frac{\sigma_1(R_o\sigma_o + R_1\sigma_o - 2R_1\sigma_1)^2}{(\sigma_o - \sigma_1)\,(R_o\sigma_o - R_1\sigma_1)^2} \qquad \text{II-64}$$

Using equations II-43, II-63 and II-64, we can again express σ_1, R_1, σ_2 and R_2 in terms of measurable quantities σ_o, R_o and t, u. i.e. σ_1 and σ_2 are again given by equations II-49 and II-50 where c now has the value

$$c = t\left[R_o\sigma_o + \sqrt{\frac{u}{t}}\right]^2 \qquad \text{II-65}$$

and R_1 is then given by:

$$R_1 = \frac{1}{\sigma_1}\left[R_o\sigma_o - \sqrt{\frac{\sigma_2}{t\sigma_1}}\right] \qquad \text{II-66}$$

As before R_2 can then be obtained from equation II-43.

II-7 Limits of Validity of Two Band Picture in the Presence of Non Isotropic Band

Two important assumptions have been made in the above analysis, viz. (a) that the bands can be treated as isotropic and independent and (b) that the variation of R_1, R_2, σ_1 and σ_2 with B can be neglected, i.e. that single band effects are negligible. These assumptions will now be considered.

The materials to which this analysis has mainly been applied are the III-V compounds and their alloys, so that the two bands considered are the Γ_1 conduction band minimum and either the <111> or the <100> minima. It is generally accepted that the energy surfaces at Γ can be taken as spherical, satisfying assumption (a). The energy surfaces at the <111> and <100> minima are ellipsoids of revolution, and are very similar to those of germanium and silicon respectively. The work of Gold and Roth (57G1) shows that in these later cases, the approximation to an isotropic form is satisfactory only if $\mu B \ll 1$. Applying this condition in the case of III-V materials, it is necessary to limit the magnetic field B used in experimental work to a value such that $\mu_2 B \ll 1$ where μ_2 is the mobility of electrons in the <111> or <100> minima. The values of μ_2 obtained for different materials (71K1) show that in most cases a maximum value of B of 3 Wb/m^2 will allow the above analysis to be used.

The question of whether the bands may be considered independent when inter-band scattering can occur has been discussed by Ehrenreich and Overhauser (56E1) and by Beer (63B1), who concluded that the above type of analysis is satisfactory.

With regard to assumption (b), that the single band contributions to the magnetic effects can be neglected, this depends upon the detail of the bands concerned and the temperature in any particular case. However, it has been pointed out by Blatt (68B2), that in the majority of cases such an assumption is valid. As a particular example, here we will consider the case of GaSb. The variation of R_1, R_2,

σ_1 and σ_2 with B can be calculated from standard one band equations (59S1). For the <111> minima, assuming typical conditions, it has been shown (65H1) that the variation in σ_2 due to both ellipsoidal energy surfaces and energy dependent relaxation time is less than 2.5%. In the case of the Hall parameter R_2, provided the condition $\mu_2 B << 1$ discussed above is satisfied, R_2 is effectively independent of B. In the case of the Γ_1 minimum, any single band effects will be due to non-parabolicity of the band and to energy dependent relaxation times. Assuming a Kane model for this band and determining room temperature relaxation time values from a suitable combination of polar optical, interband and ionized impurity scattering (Section IV-332), it is found that $\frac{\Delta R_1}{R_1}$ will be less than 2.0% and $\frac{\Delta \sigma_1}{\sigma_1}$ less than 3.2%

The values are sufficiently small to justify the use of the above method for the analysis of the Hall effect and magnetoresistance data obtained for GaSb at room temperature. This is confirmed by the experimental data in Chapter IV. Thus in figures (IV-5, IV-6) the graphs of $\frac{\rho_o}{\Delta\rho}$ and $-\frac{R_o}{\Delta R}$ versus B^{-2} are straight lines as predicted by equations II-45 and II-62, and also the values of R_1, R_2, σ_1 and σ_2 obtained by the three different methods of analysis are in good agreement. Neither of these results would obtain if the analysis were invalid. Thus in the present work at higher temperature (see Section IV-31), it was found that at temperatures above 120°C the variation of $\frac{\rho_o}{\Delta\rho}$ with B^{-2} was no longer linear, and it can be shown that as the temperature is raised, the variation of R_1, σ_1 and σ_2 with B increases, so that at temperatures above about 120°C, in this case, the single band contributions can not be considered negligible. Thus, it is seen that the applicability of the above analysis must be considered for each individual case. However, to a considerable extent, the analysis provides in itself a check on whether the initial assumptions are valid. This is further illustrated by the results on a GaAs sample doped with

Te (Chapter V) on which magnetoresistance measurements were made at 400°C. The plot of $\frac{\rho_o}{\Delta\rho}$ versus B^{-2} is not linear and has a negative intercept at $B^{-2} = 0$.

II-8 Combined Analysis of Two Band Hall Effect and Magnetoresistance

In practice the accuracy with which the band parameters σ_1, R_1, σ_2 and R_2 can be determined from the analysis of either two band Hall effect or magnetoresistance, depends on the accuracy of the intercept "a" or "u", and is quite sensitive to these factors. Since the values of the intercepts are usually small, of the order of unity, and depend on extrapolation of the straight line to infinite fields, "u" and "a" are less reliable then the slopes s and t. Since only four equations are needed to determine the four band parameters, by combining the results of two band Hall effect and magnetoresistance, more accurate results can be expected using σ_o, R_o, s and t. In this case σ_1 is again given by equation II-49, but now

$$c = t[R_o\sigma_o(1 - (\frac{t}{s})^{\frac{1}{2}})]^2 \qquad \text{II-67}$$

and

$$R_1 = \frac{R_o\sigma_o\,[s\,\sigma_1 - t(\sigma_o - \sigma_1)]}{s(2\sigma_1 - \sigma_o)\sigma_1} \qquad \text{II-68}$$

II-9 Charge Neutrality and Fermi Energy

If we consider a semiconductor in the state of equilibrium, then the net charge within the material must be zero. This is often called the "charge neutrality" condition and may be stated in the form

$$N_d - N_a = \sum_i n_i - \sum_j p_j \qquad \text{II-69}$$

where N_d and N_a are respectively the concentration of ionized donors and acceptors and i and j run over bands containing electrons and holes respectively.

For a simple donor level, the net ionized donor density N_d is given by

$$N_d = \frac{N_D}{1 + g_r \exp\{\frac{-E_D + E_F}{kT}\}} \qquad \text{II-70}$$

where g_r is the "degeneracy" of the donor level, and E_D and E_F are the ionization energy of the donors and Fermi energy respectively. Under suitable conditions of temperature and ionization energy $N_d = N_D$. A similar expression can be written for the acceptors in a p-type semiconductor.

Considering an n-type semiconductor with three conduction bands (1 - 3) with extrema "close" in energy so that under specific conditions all three bands will contain electrons, as is the case for GaSb and GaAs at high temperatures. We shall also consider that the lowest band is at the centre of the Brillouin zone with Γ symmetry, and can be described by the Kane model, the remaining two bands will be assumed to be parabolic. The carrier concentrations will then be given by

$$n_1 = 4\pi(2m^*_{10}\, kT/h^2)^{3/2}[F_{1/2}(\eta) + (5/2 - 5\xi)\beta F_{3/2}(\eta) + (7/2 - 21/2\xi)\beta^2 F_{5/2}(\eta) - (1/4 + 7/2\xi)\beta^3 F_{7/2}(\eta)] \qquad (68T1) \qquad \text{II-71}$$

where

$$\eta = \frac{E_F}{kT}, \quad \xi = \frac{m^*_{10}}{m}, \quad \beta = \frac{kT}{E^*_o}$$

$$m^*_{10}(T) = m^*_{10}(o)\left(\frac{E^*_o}{E_{oo}}\right) \qquad (57E1) \qquad \text{II-72}$$

$$E^*_o = E_{oo} - (E_{oo} - E_o)/2 \qquad (68T1) \qquad \text{II-73}$$

$$E_o = E_{oo} + \alpha_o T^2/(\theta_o + T) \qquad (67V1) \qquad \text{II-74}$$

$F_{1/2}$ etc are standard Fermi integrals. The Fermi energy E_F is measured from the bottom of band 1, m^*_{10} is the effective mass at the bottom of this band, E_{oo} is the absolute zero value of the band gap and α_o and θ_o are constants.

$$n_2 = \nu_2 c \left(\frac{m^*_{2d}}{m} T\right)^{3/2} F_{1/2}(\eta - \delta_2) \qquad \text{II-75}$$

$$n_3 = \nu_3 c \left(\frac{m^*_{3d}}{m} T\right)^{3/2} F_{1/2}(\eta - \delta_3) \qquad \text{II-76}$$

$$p_h = c \left(\frac{m^*_{ph}}{m} T\right)^{3/2} F_{1/2}(\eta - \Delta) \qquad \text{II-77}$$

$$p_\ell = c \left(\frac{m^*_{p\ell}}{m} T\right)^{3/2} F_{1/2}(\eta - \Delta) \qquad \text{II-78}$$

where

$$c = 4\pi \, (2mk/h^2)^{3/2}$$

$$\delta_2 = E_2/kT, \qquad \delta_3 = E_3/kT, \quad \Delta = E_o/kT$$

m^*_{2d}, m^*_{3d}, m^*_{ph} and $m^*_{p\ell}$ are density of states effective masses in bands 2, 3 and valence bands respectively, ν_2 and ν_3 the band multiplicity and E_2, E_3 are the energy separations of 1 to 2 and 1 to 3 conduction band minima respectively.

The temperature variation of E_2 and E_3 can be assumed linear, i.e.

$$E_2 = E_{20} + \alpha_2 T \qquad \text{II-79}$$

$$E_3 = E_{30} + \alpha_3 T \qquad \text{II-80}$$

at temperatures when the more complicated form, such as that given by Varshni (67V1), become linear with temperature. This point will be further discussed in the following chapters dealing with experimental results.

TABLE II-1

	General	Non-parabolic, but spherically symmetric bands	Parabolic bands with ellipsoidal energy surfaces
Band curvature effective mass	$\frac{1}{m^*_{ij}} = \frac{1}{\hbar^2} \frac{\partial^2 E}{\partial k_i \partial k_j}$	$\frac{1}{m^*_e} = \frac{1}{\hbar^2} \frac{\partial^2 E}{\partial k^2}$	$\frac{1}{m^*_e} = \frac{1}{3} \left(\frac{1}{m^*_\ell} + \frac{2}{m^*_t}\right)$
Cyclotron effective mass	$m^*_c = \frac{\hbar^2}{2\pi} \frac{\partial A}{\partial E}$	$m^*_c = \frac{\hbar^2 k}{dE/dk}$	$m^*_c = \frac{\hbar^2}{2\pi} \frac{\partial A}{\partial E}$
Density of states effective mass	$n = \frac{1}{\pi} \int_0^\infty f_0 k^2 \frac{dk}{dE} \, dE$	$n = \frac{1}{\pi} \int_0^\infty f_0 k^2 \frac{dk}{dE} \, dE$	$m^*_d = (m^*_\ell \; m^2_t)^{1/3}$

Table II-1: Definitions of effective masses, m^*_e, m^*_c and m^*_d.

CHAPTER III

EXPERIMENTAL TECHNIQUE AND EQUIPMENT

CHAPTER III EXPERIMENTAL TECHNIQUE AND EQUIPMENT

III-1 High Temperature Furnaces and Sample Holders

Two different furnaces were used in this work, this was necessary since essentially two kinds of experiments were carried out. The measurement of magnetoresistance and Hall coefficient as a function of magnetic field and temperature required long term temperature stability, whereas the measurement of Hall coefficient and conductivity as a function of temperature only, could be carried out rapidly with slow temperature drift. Essential features of the two types of furnace are described below.

III-11 Temperature controlled furnace, (20° - 450°C)

This furnace was originally designed by Dr. G. Dionne (71D1) for the purpose of making Hall effect and magnetoresistance measurements between 77 and 800°K. The principal features of this design are: a) small outside diameter, in order that it would fit between the pole pieces of the Harvey-Wells 15" electromagnet with a gap of $1\frac{1}{4}$"; b) low power consumption and good temperature stability. Schematic drawings of the furnace are shown in Figs. III-1 and III-2. Fig. III-1 shows the overall design and Fig. III-2 shows the region of the heater and sample holder. The manganin heater wire (48Ω/ft.) is wound around a thin copper capsule sealed at the bottom end. The wire is kept in place and insulated from the capsule with Sauereison cement. The capsule fits snugly into a quartz tube which is also sealed at the bottom end and forms the inner wall of a double vacuum jacket which reduces heat losses to the outside. Maximum temperature of the outer stainless steel wall does not exceed 70°C. The two vacuum jackets can be evacuated separately, the inner space can be filled with liquid nitrogen to facilitate measurements below room temperature. The sample holder fits inside the

copper capsule and the whole region can be evacuated, flushed and then filled with helium gas to prevent undue oxidation of the sample and aid in establishing temperature equilibrium. Because the copper capsule is a good conductor and is well insulated, no temperature gradients within the capsule could be observed when a thermocouple probe was used. The design of the sample holder (described below) is therefore critical. It was designed in such a way so as not to introduce excessive thermal leaks which would introduce undesirable gradients at the sample.

There are two (Pt. vs Pt. + 13% Rh.) thermocouples, (not shown in the schematics) one is attached to the copper capsule and responds rapidly to any temperature change of the capsule. The second is part of the sample holder, the junction is placed within 1 mm of the sample. This thermocouple was checked at steam point against N.B.S. 1962 tables. Temperature may be controlled by either thermocouple, although the use of the thermocouple on the sample holder gives a sluggish response due to thermal lag. The advantage of using this thermocouple for control is that it is also used for temperature measurement and hence only one potentiometer is required.

Temperature control is achieved by an electro-optical system shown in Fig. III-3. The signal from the thermocouple is fed into a Rubicon potentiometer set for a given temperature. The galvanometer spot is in off balance position, hence no light falls on the photocell and maximum current is demanded, since the plate current is proportional to photocell resistance. As the temperature rises and the light spot approaches the photocell the current falls reaching equilibrium when the potentiometer is at balance. Temperature control of better than $\pm.01^{o}C$ has been obtained using this system at a maximum temperature of $450^{o}C$. Also long term stability of $\sim.005^{o}C/hr.$ was achieved. The drift problem arises mainly from

two sources, drift of the voltage supply to the potentiometer and secondly the drift of temperature of the reference junction of the thermocouple. These were minimized by placing the potentiometer supply battery in a styrofoam container and keeping it connected continuously. The reference ice bath was stirred periodically to maintain its temperature constant.

III-111 The Sample Holder

The schematic of the sample holder, designed by the author, is shown in Fig. III-4. The sample holder itself was machined out of Pyrophylite and then fired at 1500°C in an inert atmosphere. The sample is held by a stainless steel leaf spring (not shown) which is insulated from the sample by a thin piece of mica. The contacts to the sample are made with .005" platinum wire attached to stainless steel (#304) screws. The copper lead wires are then attached to the other end of the screws at the back of the holder and together with thermocouple wires, are cemented in place in grooves cut for the purpose. The narrow neck of the holder then fits inside a quartz tube which is attached to the upper flange (Fig. III-1). The lead wires are passed through ceramic thermocouple feed-throughs which are placed inside the quartz tube and then pass through covar feed-throughs in the upper flange. In this way the lead and thermocouple wires are continuous from the sample holder to the outside of the furnace reducing possible thermal noise due to junctions.

The use of quartz tube in this construction is not completely satisfactory since it is not mechanically strong. Definite improvement could be made using a ceramic tube of low thermal conductivity.

III-112 Measuring Apparatus and Technique

The leads from the sample were soldered to a Leeds and Northrup eleven position selectron switch which was connected to an Astrodata nanovolt amplifier model 120, the output of which was in turn connected to a 5 figure Dana digital voltmeter model 5330/360. The resolution of the digital voltmeter is 1μV, but in conjunction with the nanovolt amplifier which was used at gains of 10^3 and 5×10^3 gives resolution of 5 nV, limited by the input noise of the instrument.

The current to the sample was supplied by a 12V battery with suitable rheostats in the circuit. Currents of 1 and 10 mA were used depending on sample resistance and magnitude of the signal.

The electro-magnet employed was a Magnion-Harvey-Wells 15 inch model, with a pole gap of $1\frac{1}{4}$" and maximum field of 3.2 Webers/m^2. The accuracy of the field was five parts in 10^5, and stability of one part in 10^6. Uniformity over a 1.0 cm specimen placed in the centre of the pole pieces was one part in 10^5 at maximum field. The calibration and procedure is described by Aubin (69A1) and is given in Fig. III-11.

The advantage of using the Astrodata nanovolt amplifier as a preamplifier is that the input signal can be backed-off to zero on this instrument. When measuring magnetoresistance and Hall effect as a function of magnetic field, this capability of the preamplifier is very necessary and convenient, otherwise external back-off circuitry has to be used. It is due to the use of this amplifier that very accurate measurements were made on n-GaSb.

When the temperature had reached equilibrium, the zero field resistivity voltage was measured, by selecting the appropriate lead wires on the selection switch. This voltage was then backed-off to zero and the magnetic field turned on,

the magnetoresistance voltage was then obtained directly. The procedure was carried out with reversed magnetic field and sample current. The Hall voltage was measured in similar fashion except that in this case only the misalignment voltage was backed-off. With proper care in positioning contacts on the sides of a parallelepiped shaped specimen, the misalignment voltage was small. Time taken to complete the measurements at a given temperature was of the order of 2 hours.

III-12 Temperature Drift Furnace (20 - 800°C)

The design of this furnace was originally made by Coderre (69C2) and is shown in Fig. III-5. The heating element (Nichrome wire 1.26 ohms/ft.) was re-wound in order to improve the temperature profile, giving an essentially flat region at the position of the sample. The profile is shown in Fig. III-6 at two power settings, also the position of the sample in the furnace is shown.

The power to the furnace was supplied by a 2KVA variac. The temperature was continuously changed at a constant low rate by a motor connected by a pulley to the variac. The rate was adjusted by changing the pulley ratio between the motor and the variac. The average rate used was $\sim 3^{\circ}C$/min. The time required to take readings was $\sim$20 sec., hence giving temperature accuracy of $\pm 0.5^{\circ}C$. The temperature was continuously monitored by a Pt. vs Pt. + 13% Rh. thermocouple junction placed within 1 mm. of the sample. The reference junction was maintained at ice point. The thermocouple emf was backed-off by a Tinsley four figure potentiometer and displayed with the aid of a Pye Scalamp light spot galvanometer.

Measurements were taken every $10^{\circ}C$ from room to the highest temperature of $600^{\circ}C$. This temperature limit is set due to the high vapour pressure of As and

the subsequent loss of this element from the surface of GaAs samples at temperatures greater than 600°C, leaving a thin film of highly conducting Ga metal on the sample surface.

III-121 Sample Holder

The sample probe is shown in Fig. III-7 and is again described by Coderre (69C2). One modification was made here: the feed-throughs were changed to hollow type to allow electrical lead copper wires to pass through, maintaining continuity. This served to minimize the possibility of additional thermal emf appearing as voltage noise if all the pins were not at the same temperature.

III-122 Apparatus and Measuring Technique

The measuring circuit was essentially the same as that used by Coderre (69C2) and is shown in Fig. III-8. In order to monitor sample current accurately a 10Ω standard resistance was introduced in series with the sample, also a better constant current power supply (Electronic Measurements Model C612) was introduced in the sample circuit, the ripple was 0.01% or less and drift of less than 0.005% over a day after warm up.

The Hall and conductivity voltages were measured using a Hewlett-Packard model 419A null voltmeter as a preamplifier. The input impedance of this meter was >1MΩ, thus high enough for measurement of low resistivity samples. The output was nominally 1 volt on all scales, and was fed into a Hewlett-Packard 4 figure digital voltmeter.

It was found that the preamplifier gain would always be slightly lower than specified (1% - 2%), hence after each run it was calibrated against a Tinsley

potentiometer and voltage readings were corrected accordingly.

A magnetic field of .800 W/m^2 was used, supplied by an electro-magnet with 4" pole pieces separated by 1.4" gap. The magnetic field was measured using a Rawson-Lush rotating coil gaussmeter.

III-2 Material and Sample Preparation

This thesis is concerned with the determination of some conduction band parameters in GaSb and GaAs. Some of the crystal GaAs used for this work was obtained from Monsanto Chemicals Co., samples prepared from this material will be denoted by the prefix MO. The remaining samples of GaAs were cut from single crystals prepared by Dr. B. Lombos at Northern Electric R & D Laboratories, these will be denoted by the prefix NE.

A number of samples of n-GaSb-Te as well as one p-type sample were measured, these were cut from single crystal ingots prepared by the author and a slice obtained from Dr. Strauss of Lincoln Laboratories. In addition the author attempted to grow good quality alloys of Te doped $Ga_xIn_{1-x}Sb$ in the composition range $.9 < x < 1$, for the purpose of studying interband scattering, Γ_{1c} and L_{1c} band separation and electron effective mass in the Γ_{1c} and L_{1c} bands through magnetoresistance, Hall effect and de Haas Shubnikov measurements at low temperatures. The method of preparation of GaSb and $Ga_xIn_{1-x}Sb$ is described below.

III-21 Preparation of Te doped GaSb and $Ga_xIn_{1-x}Sb$

GaSb single crystals can easily be grown from a stoichiometric melt using the Czochralski (19C1) method.

It was shown by Trumbore et al. (62T1) that single crystals of $Ga_xIn_{1-x}Sb$ also can be grown from the melt using the same method. They report obtaining single crystals in the composition range $0.4 < x < 1$. More recently Robert (69R1) reported in his thesis that only single crystals in the range $0.95 < x < 1$. could be prepared by this method in their laboratory.

(i) The Czochralski method

The melt is contained in a crucible and a seed crystal which dips into it from above is rotated and slowly withdrawn, so that the rate of upward motion is equal to the rate of crystal growth, which is determined by the rate of loss of latent heat through the seed. If the two rates do not balance, the crystal either increases or decreases in diameter as growth proceeds. The purpose of the rotation is to maintain circular symmetry of the crystal, the shape of which would be unstable if the crystal were stationary. An added advantage of the rotation is that it causes the liquid near the interface to flow outwards thus improving mixing of the melt.

The basic vertical Czochralski crystal-pulling furnace is shown schematically in Fig. III-9. The charge is placed in a crucible which in turn fits into a graphite susceptor supported by an insulating pedestal. A seed holder containing a seed at the bottom, is attached to precision motors which withdraw and rotate the seed. In order to be able to grow under controlled atmosphere all is surrounded by a quartz tube which is sealed at both ends by steel flanges with O-rings, and gas inlet and outlet ports. The R-F coil is placed on the outside of the quartz tube surrounding the carbon susceptor.

The Czochralski apparatus used was on loan to the author from the Communications Research Centre at Shirley Bay, by the kind permission of Drs. C. D. Cox and J. Barrie.

(ii) Alloy preparation

In order to prepare heavily Te doped single crystals of GaSb and $Ga_xIn_{1-x}Sb$ in the composition range $0.9 < x < 1$ it was necessary to divide the work in three stages: a) preparation of single crystal GaSb; b) Te doping of GaSb; c) preparation of single crystal $Ga_xIn_{1-x}Sb$.

(a) Polycrystalline GaSb was initially synthesized by sealing off individual elements, in suitable proportions, in an evacuated quartz ampoule and placing it in a furnace at 900°C for thirty minutes and then quenching in air. The ingot obtained in this way was coarsely polycrystalline and was used as a charge in the quartz crucibles in the Czochralski puller. Randomly oriented seed crystals were cut from parts of an ingot obtained from the Monsanto Chemical Co. However, it would have been preferable to use seeds with <111> orientation since this is the preferred growth direction in diamond and zincblende structures, but this was not possible with the available seed material.

It was evident from the start that the use of hydrogen atmosphere was not sufficient to keep the melt surface clean and the melt stoichiometric. Despite its relatively low vapour pressure at the melting point of GaSb, Sb is still lost from the surface. This has two undesirable effects, firstly that the melt becomes Ga rich and secondly that Sb is deposited on the quartz tube making observation of the crystal growth difficult. In order to overcome this, the well known "Liquid Encapsulation" technique was introduced using boric oxide glass. This has the advantage of overcoming the above two problems but also a disadvantage in that the glass is extremely viscous and limits seed rotation to about 10 revolutions per minute. In this way three single crystals of GaSb were pulled, varying in weight from 5 to 11 gms, using a pull rate of ∿5 mm/hr. and a rotation rate of about

7 - 10 revolutions per minute.

Two single crystals of undoped GaSb were grown about 1.5 cm in diameter and 3 cm. long. Undoped GaSb always grows p-type, it is thought (64M1) that lattice defects are responsible for the p-type nature of this material. The p-type GaSb grown was of good quality with uniform carrier distribution. A sample cut from one of the ingots was used by the author for high temperature measurements of Hall coefficient and conductivity. Results of those measurements will be discussed in Chapter IV. This material has also been used by other members of this group for various measurements, e.g. thermoreflectance, electroreflectance and photoconductivity.

(b) Tellurium doping of GaSb. Several crystals of GaSb doped with Te were pulled, none were perfect single crystals, all had at least two or three twin boundaries running from top to bottom or diagonally across the crystal. The twinning was not a consequence of Te doping, but rather of difficulties in obtaining clean melt surfaces. These crystals had room temperature Hall coefficients ranging from 1×10^{-5} to 7×10^{-5} $m^3/^oC$.

In calculating the necessary weight of Te to be added to the melt we initially used the segregation coefficient k_{Te} value of 0.4 given by Madelung (64M1). The results of Hall effect measurements showed that this value was probably high, a value of 0.1 or 0.2 was closer from our results. The Hall effect results also showed that doping uniformity in crystals doped to $>10^{18}$ Te atms/cc was good, but in lighter doped crystals severe gradients could be observed. However, the gradients are not restrictive when measurements with Van der Pauw geometries can be made. This material was therefore used by S. Rosenbaum (72S1) in investigation of the effect of hydrostatic pressure on transport properties of n-GaSb. (Further

discussion of gradient problems is given in Chapter IV which deals with the transport results on n-GaSb).

The pseudo-binary phase diagram of (GaIn)Sb was determined by Woolley et al. (58W1) and is shown in Fig. III-10. It can be seen from this figure that the segregation coefficient is ∿0.2, viz., approximately 50 - 50% melt of (GaIn)Sb corresponds to solidus composition of $Ga_{.9}In_{.1}Sb$. This is the maximum InSb content necessary for the proposed measurements on this system. Hence as a crystal is being pulled from a melt, the melt becomes richer in InSb, causing composition gradients along the growth of the crystal. To overcome this, large melts (100 - 150 gms) were used to pull crystals of up to 10 gms wt.

Several single phase crystals were obtained using melts with InSb content from 20 to 50% using growth rates of between 2 and 3 mm/hr. These crystals were single over the initial 1 to 2 cms. but later, heavy twinning occurred, the reason for this is not understood. The composition of these crystals was analysed using the X-ray powder diffraction method. This requires a knowledge of the lattice parameter variation with composition, which was assumed to be linear to a first approximation. Since this method is accurate to only 1.5% this assumption is not restricting. The composition of three of the crystals grown was determined to be between 2 and 8% of InSb in (GaIn)Sb by the above method.

Although the first one to two cm. were single crystal, difficulties were encountered in increasing the diameter beyond about 0.8 cm. without heavy twinning occurring, this again could in part be ascribed to scum on the melt surface beneath the boric oxide glass and in part to constitutional supercooling.

At this point it was felt that to obtain good quality crystals of the alloy doped with Te by this method would be extremely hard and impractical, since

the growth rates may need to be cut down further to avoid constitutional supercooling extending preparation time to unreasonable limits. Further growth of the alloys was therefore temporarily abandoned. The prepared crystals were not of good enough quality for the purpose of the proposed measurements because of the non uniform impurity distribution. However, this same material can be used for measurements which do not require the use of relatively large samples and hence do not impose such stringent requirements. For example, optical and those electrical measurements for which the Van der Pauw geometries are possible, can be made on this material.

III-22 Sample Preparation and Ohmic Contacts for High Temperature Measurements

All samples measured were parallelepiped shaped with dimensions of the order of 1.5 x 0.2 x 0.1 cm. These were cut from slices using either a carborundum disc or wire saw. They were then boiled in Trichloroethylene, vapour degreased and lapped with #3200 alumina lapping powder.

Ohmic contacts to GaAs samples were obtained by evaporating 0.015" strips of gold through a mask on each side of the specimen, as shown in Fig. III-12. Care was taken to align the strips on each side of the specimen to minimize the Hall voltage offset. The two ends of the specimen were completely covered with gold for current contacts. The gold was then alloyed with GaAs at 530^{o}C in He atmosphere for 2 min. The sample was allowed to cool in the alloying furnace to prevent oxidation. The specimen was placed in the sample holder and 0.005" Pt. wires were then spark welded to the gold areas. This method produced good ohmic contacts which remained ohmic up to the highest temperature reached. Problems were encountered with the mechanical strength of these contacts, when transferring the sample probe into the furnace,

contact was sometimes lost. Also, at elevated temperatures, contacts were lost probably due to expansion of the Pt. wires. Apart from these small problems the method was basically sound.

It was found unnecessary to go through the alloying procedure with contacts to GaSb. Spark welded Pt. wires directly to the specimen produced ohmic contacts of low resistance and good mechnical strength.

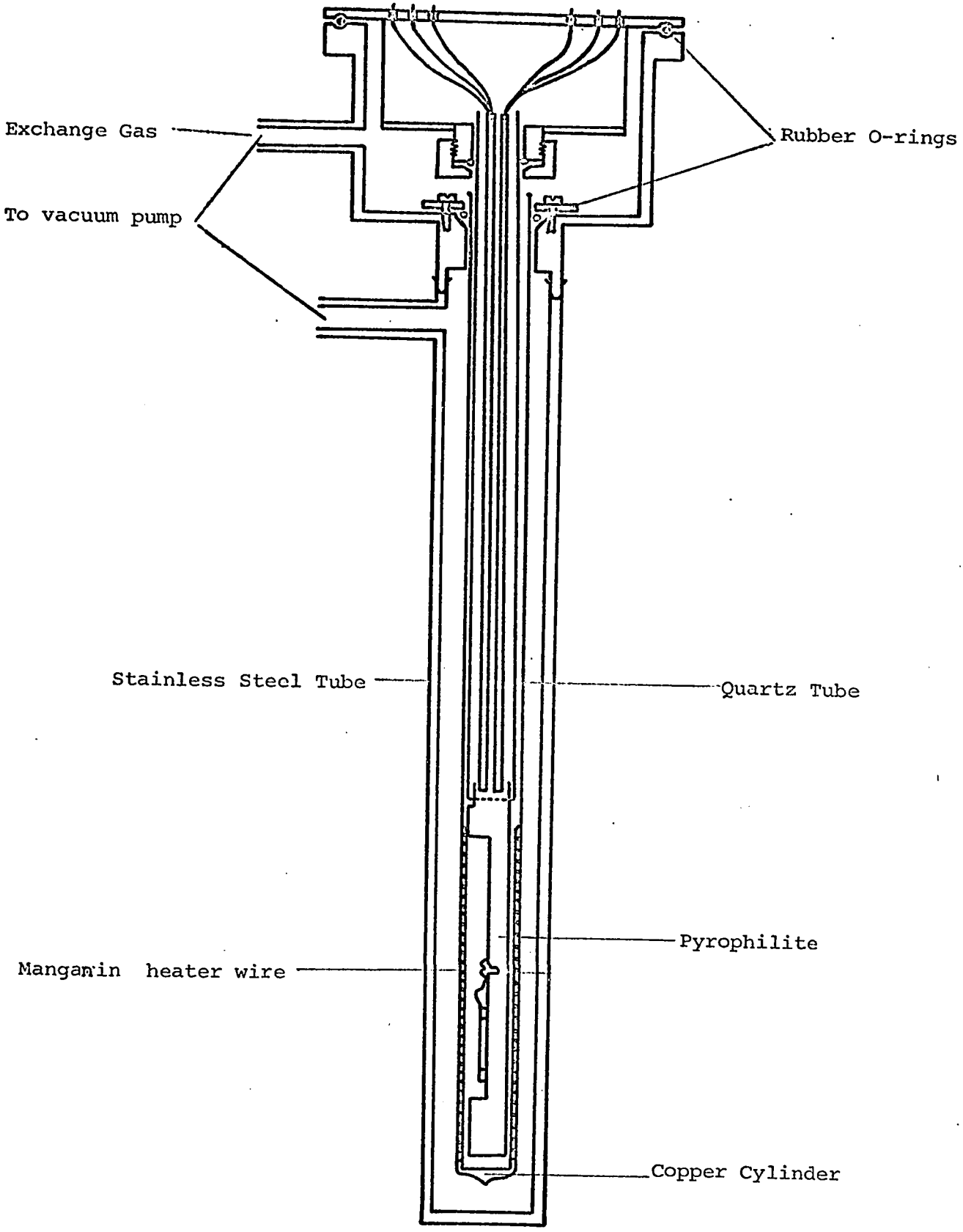

Fig. III-1 Temperature-controlled furnace.

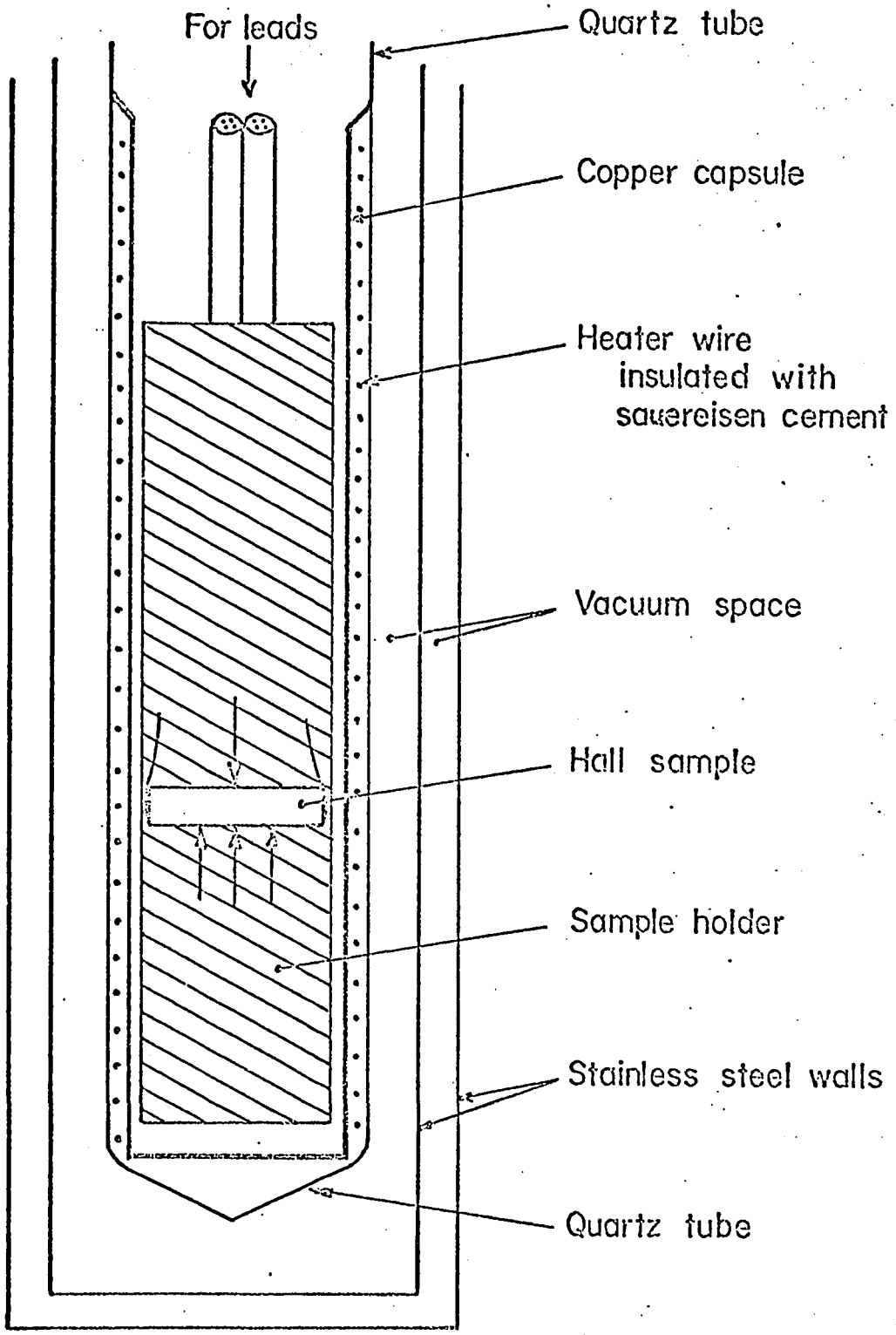

Fig. III-2 Temperature-controlled furnace-sample area. Detail of construction.

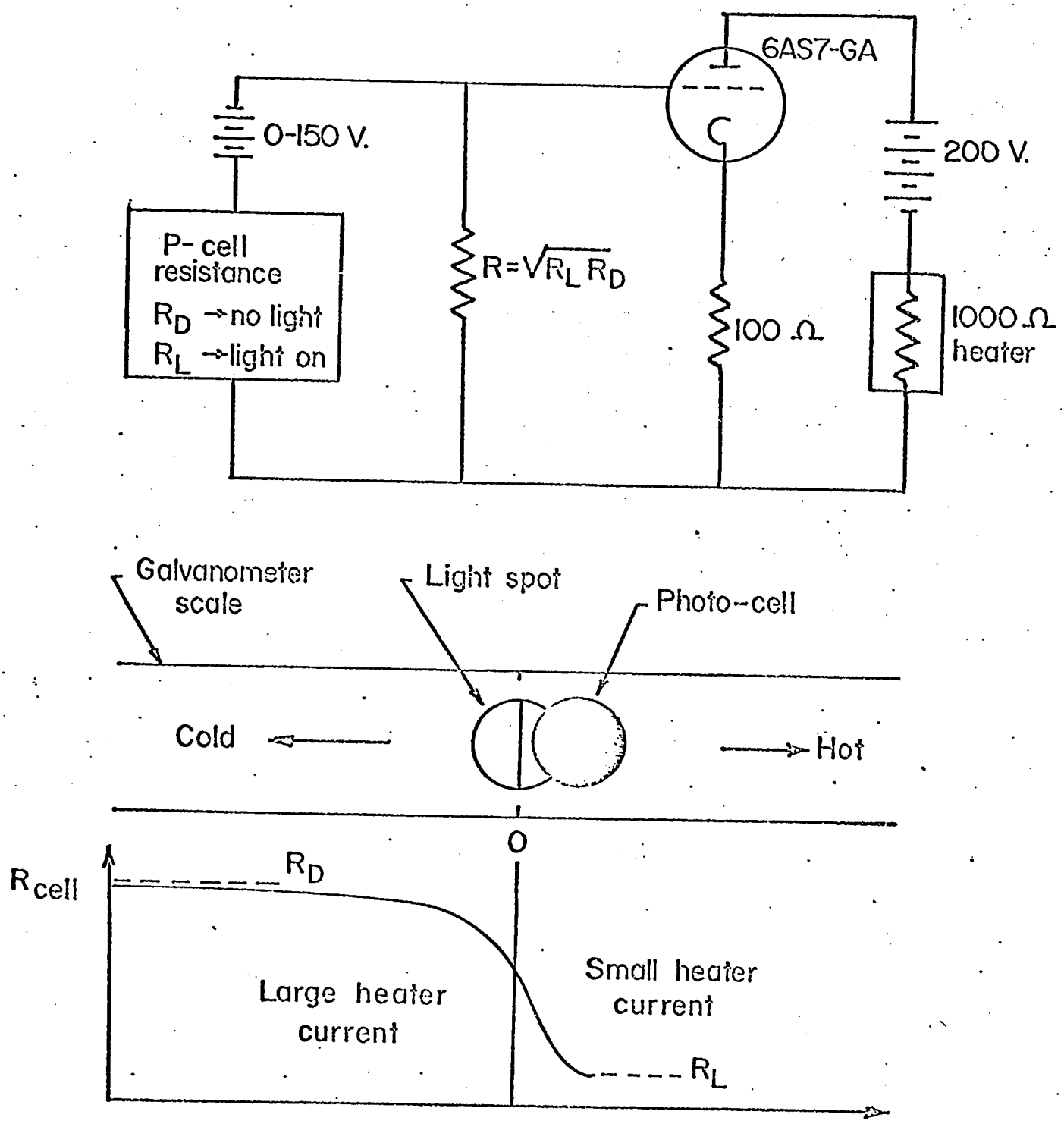

Fig. III-3 Temperature control for controlled furnace.

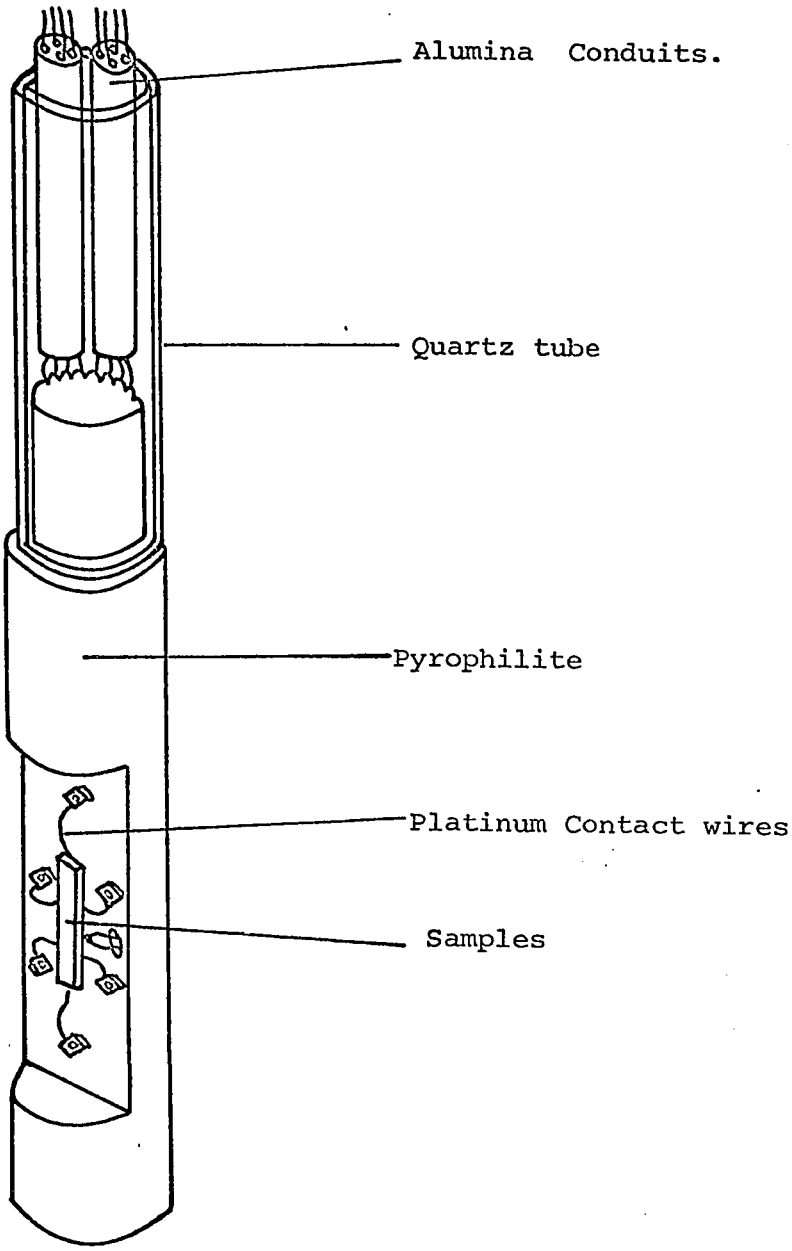

Fig. III-4 Sample holder probe for controlled temperature furnace.

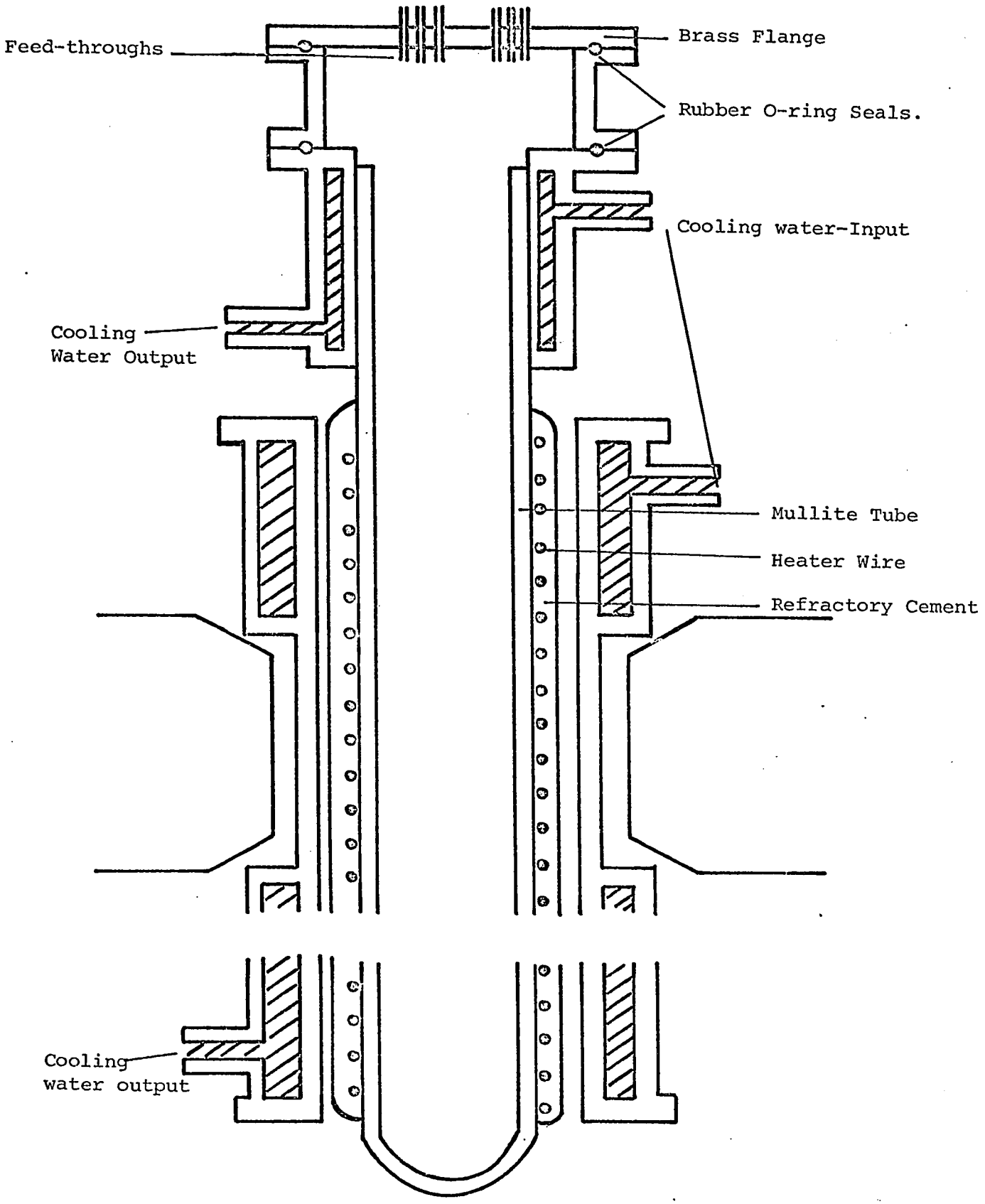

Fig. III-5 Schematic of high temperature drift furnace (20-800°C).

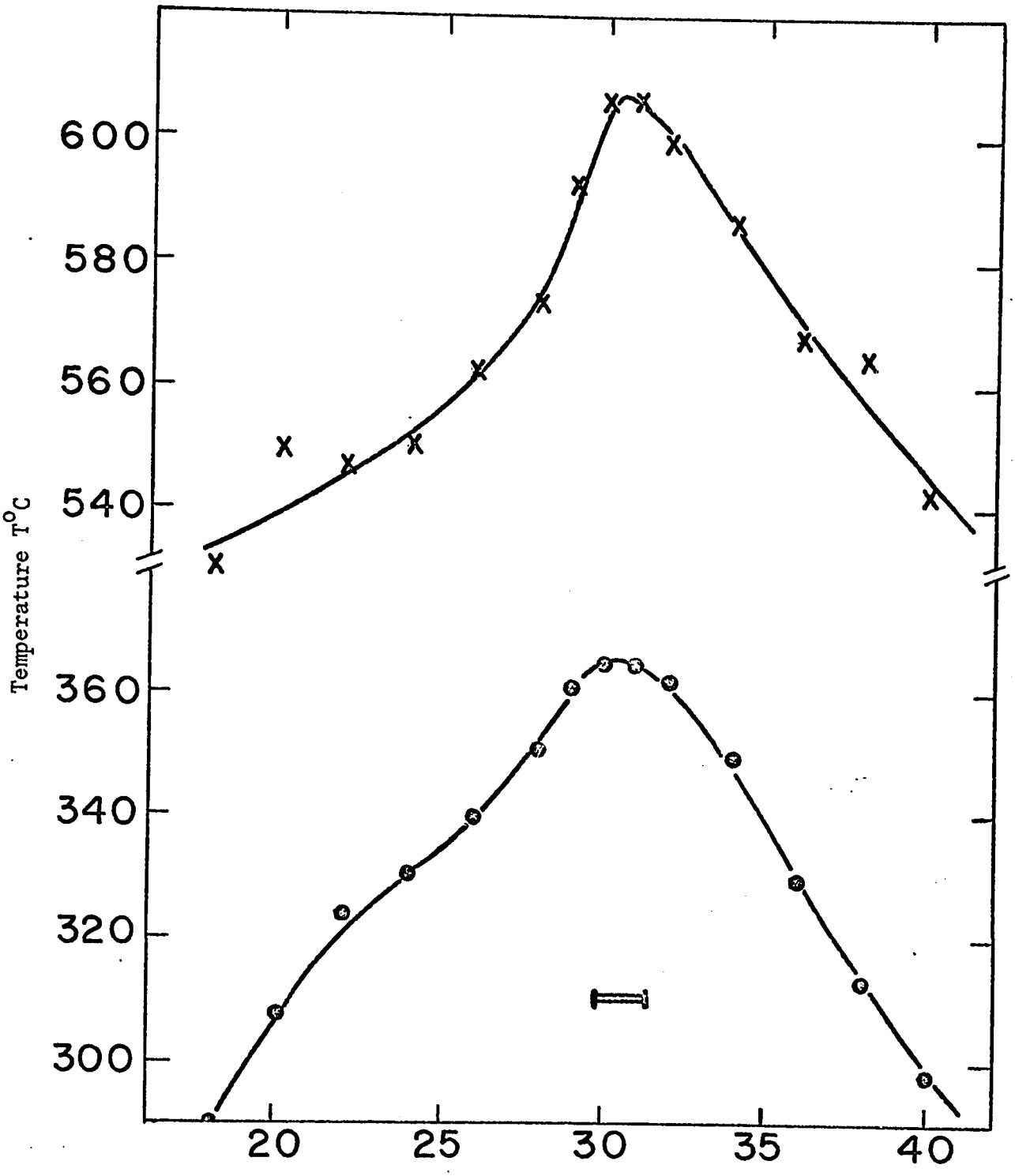

Fig. III-6 Temperature profile in the drift furnace at two rheostat settings.

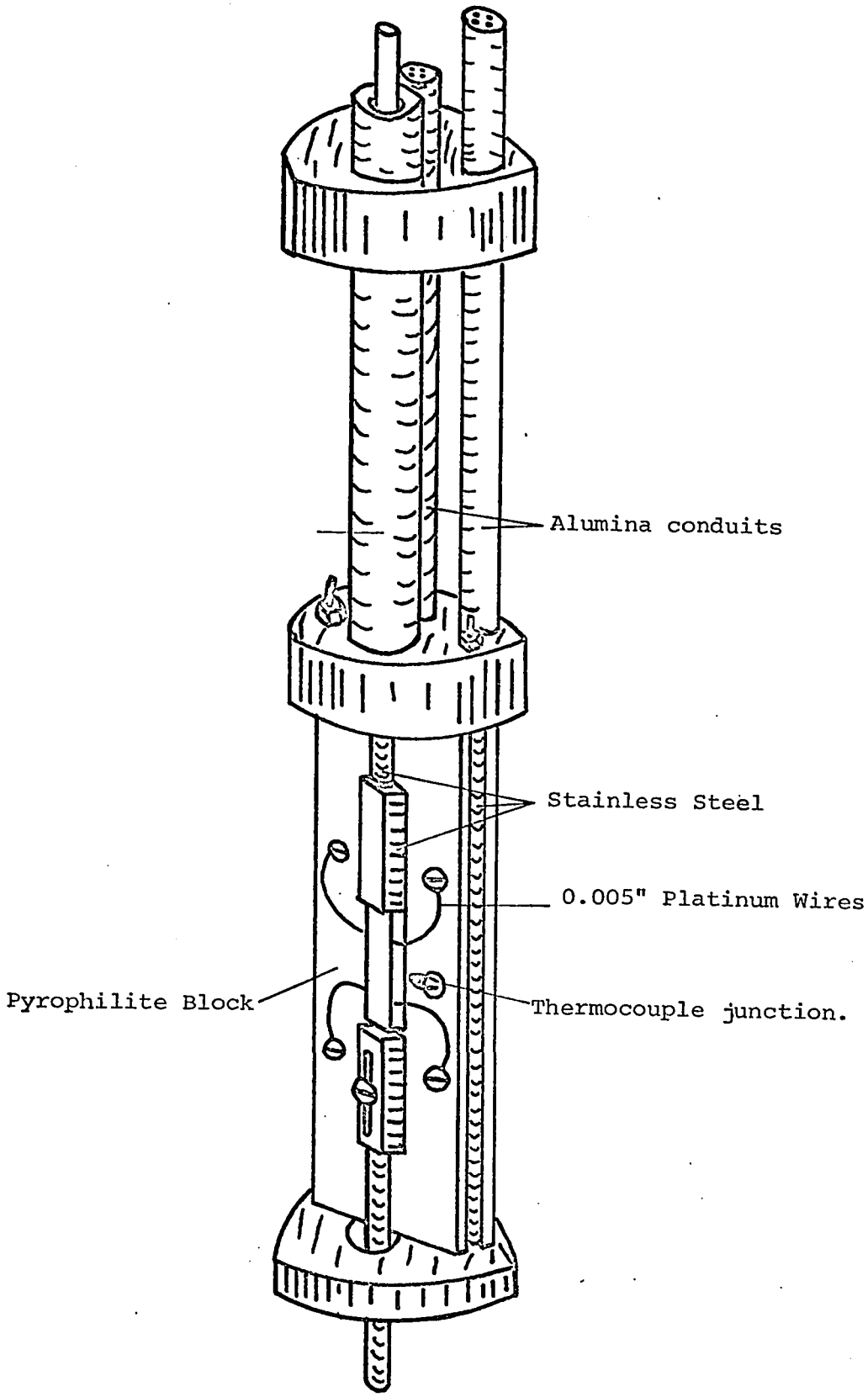

Fig. III-7 Sample holder probe for the high temperature drift furnace.

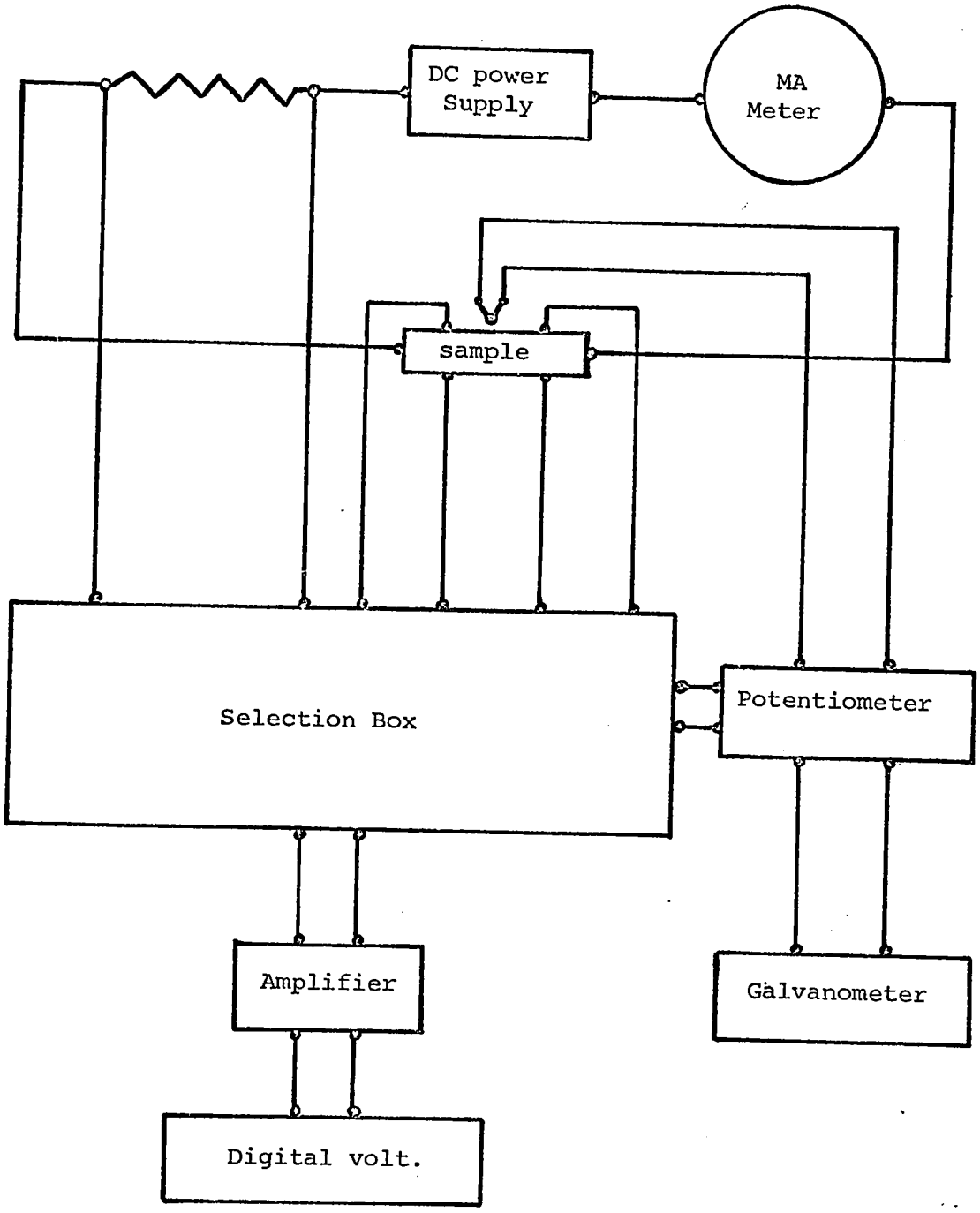

Fig. III-8 Schematic of the measuring circuit.

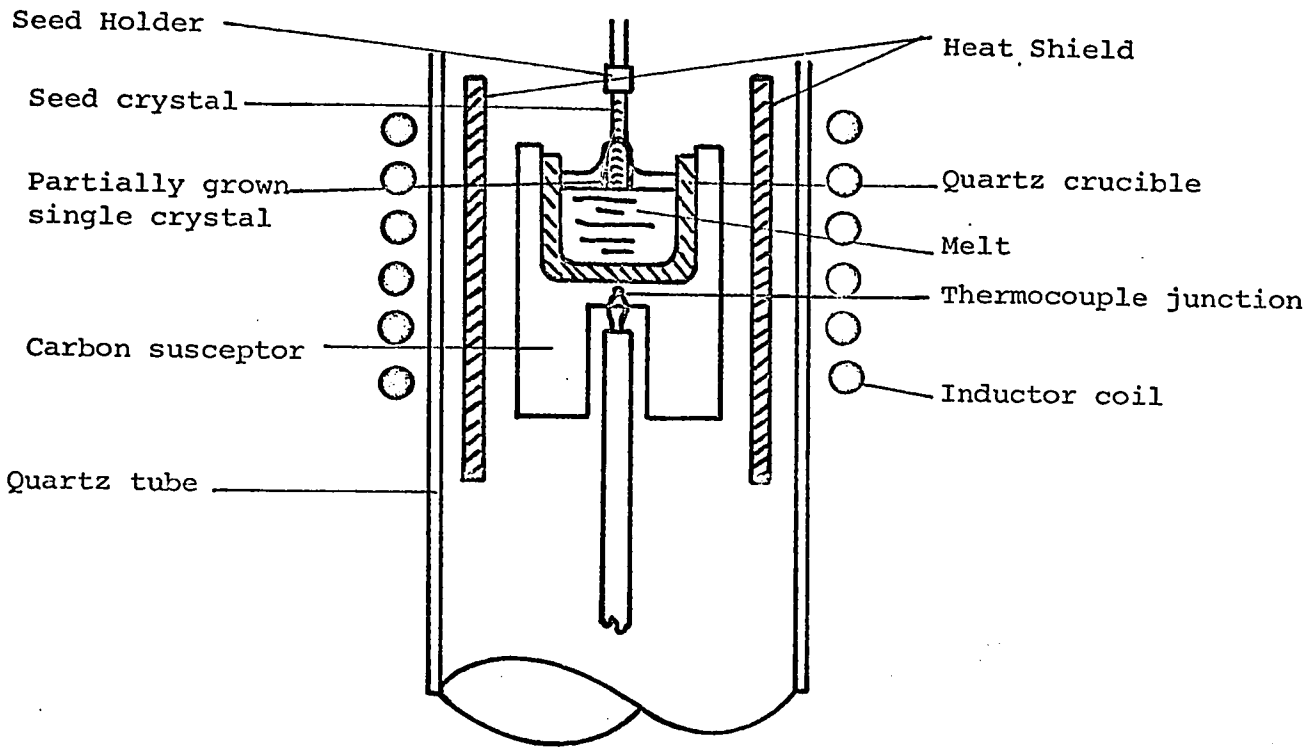

Fig. III-9 Schematic of the Czochralski crystal growth method.

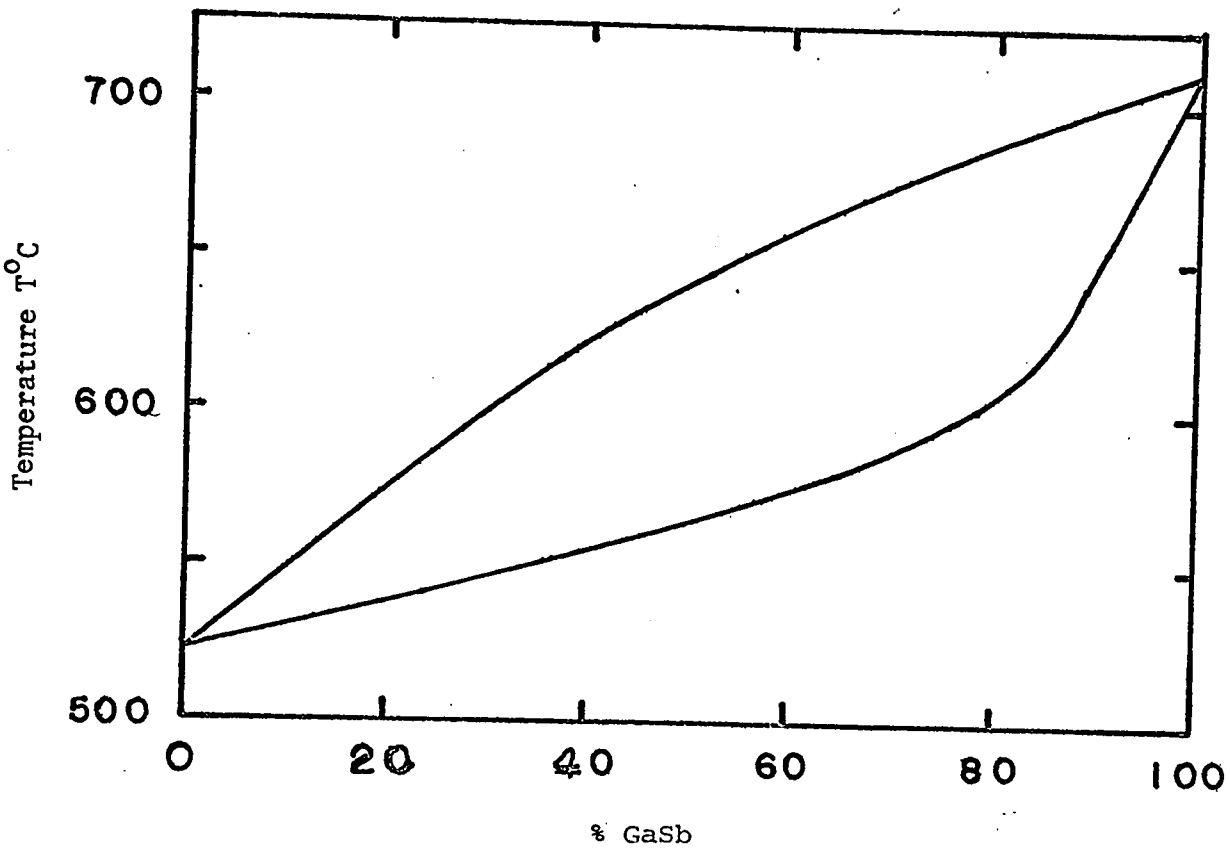

Fig. III-10 Phase diagram of (GaIn)Sb after Woolley and Smith (58W1)

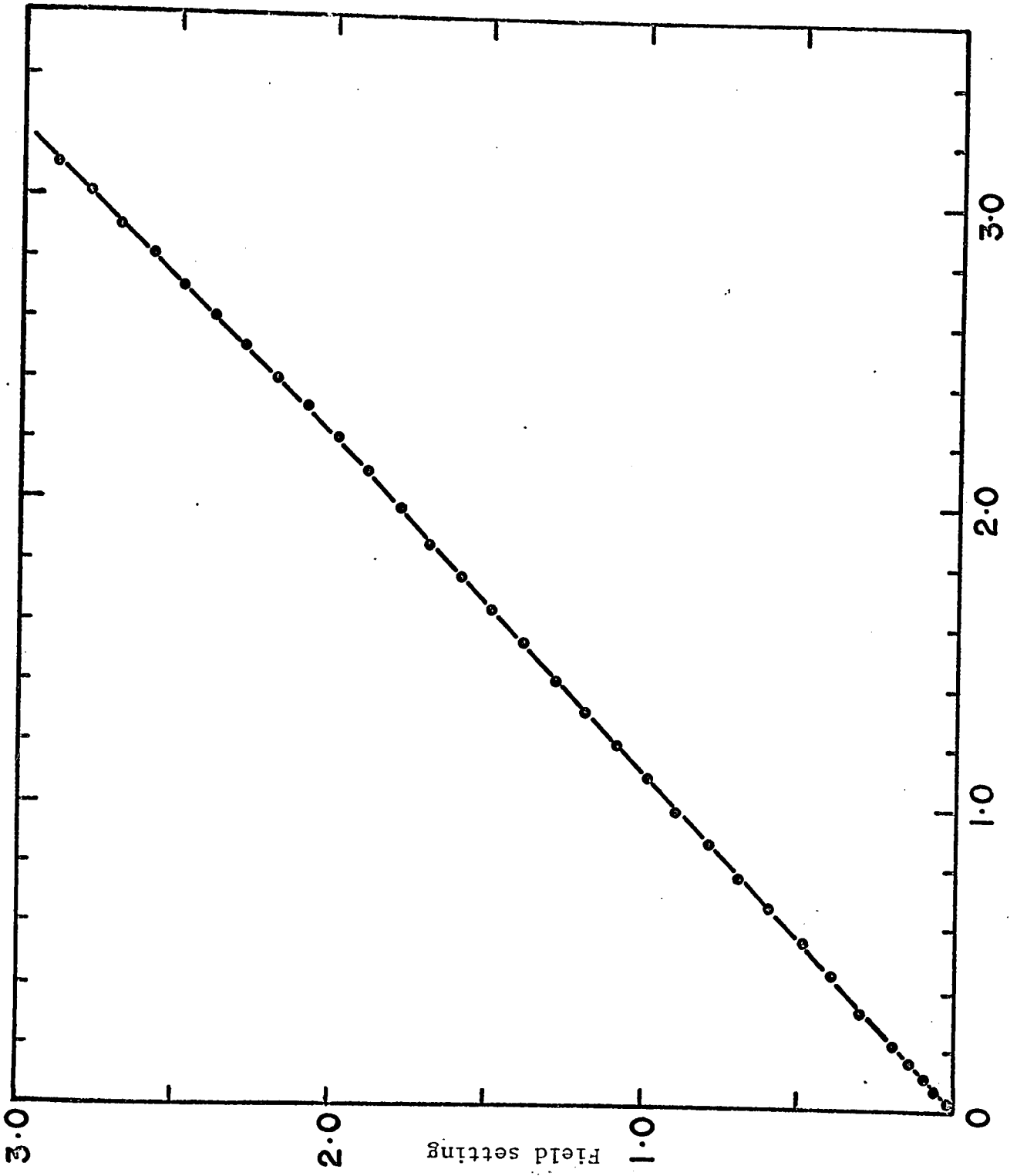

Fig. III-11 Calibration for the 15" electro-magnet.

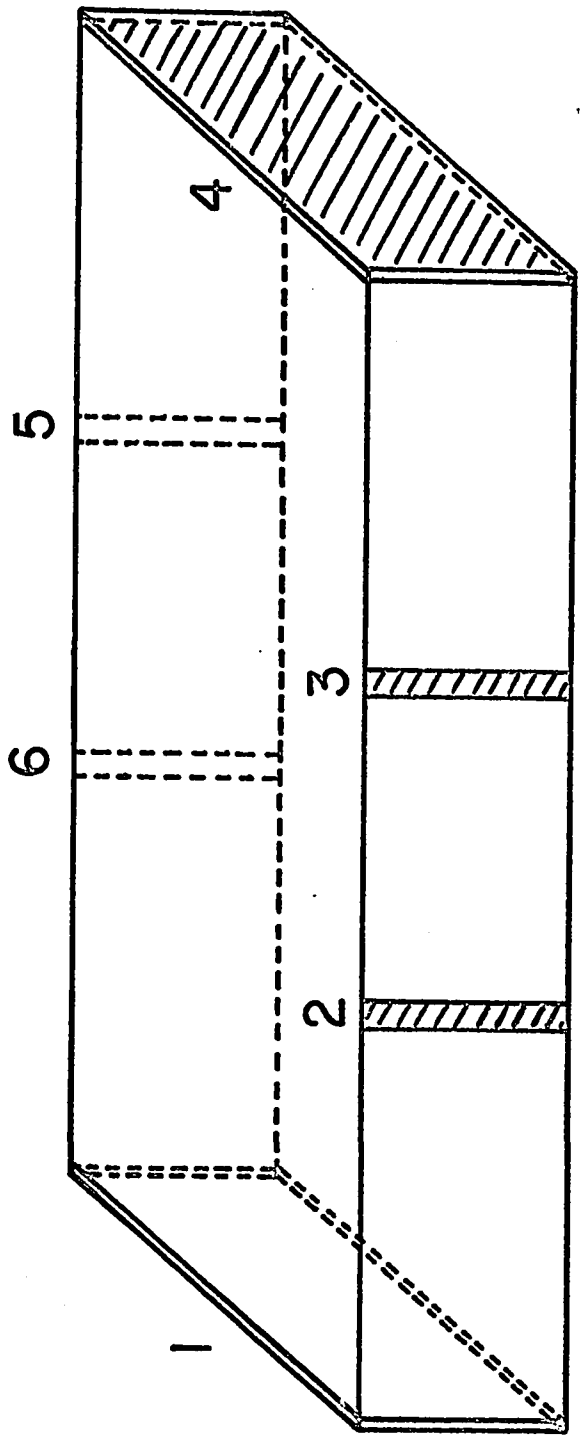

Fig. III-12 Parallelopiped sample showing evaporated gold strips.

CHAPTER IV

CONDUCTION BANDS IN GaSb

CHAPTER IV CONDUCTION BANDS IN GaSb

IV-1 Material and Experimental Conditions

The conduction band structure of GaSb satisfies the two primary conditions required for investigation of the band parameters by the two band model and by measurements of Hall coefficient and conductivity as a function of both magnetic field and temperature. These two conditions are (a) appreciable number of carriers are present in each band and (b) mobilities of the carriers in the two bands are not the same. For optimum conditions, the carrier densities in the two bands should be of the same order of magnitude with a mobility ratio of about 10:1.

Although the above mentioned conditions are satisfied, the range of Tellurium doped n-GaSb on which useful measurements can be made is further restricted. The additional restrictions are imposed by (a) the material and (b) the analysis of experimental data. However, the amount of information on the band structure of GaSb which can be obtained from measurements of Hall coefficient and conductivity as a function of magnetic field and temperature, even within the limits of the above restrictions, make such an investigation of considerable value.

It is well known that grain boundaries and impurity gradients can strongly affect galvanomagnetic measurements and their interpretation (e.g. Beer 63B1, p. 308 and references therein). It is therefore desirable to have single crystal samples with uniform impurity distribution, when galvanomagnetic measurements are used to investigate semiconducting materials.

Single crystal Te doped n-GaSb can be prepared with total electron concentrations of between about 10^{23} m^{-3} and 5 x 10^{24} m^{-3}. The lower limit is imposed by compensating acceptors which are always present in concentrations in the order of 10^{23} m^{-3}., whereas the upper limit is set by Te impurities which strain the lattice so that above this concentration single crystal growth is impossible. Because of the effect of compensation by the acceptors, material doped to $<10^{24}$ m^{-3} tends to have impurity gradients. Although it is not impossible to obtain large samples (required for magnetoresistance measurements) with uniform impurity distribution, nevertheless it is extremely difficult. These considerations therefore, limit the useful material to a doping range from about 10^{24} m^{-3} to 5 x 10^{24} m^{-3}. Additional conditions which restrict the useful range of material are further imposed by the analysis of the data. These further restrictions will now be discussed.

In order to calculate the respective carrier concentrations n_1 and n_2 from R_1 and R_2, the Hall scattering parameters r_1 and r_2 must be known. Since, as will be seen later, the dominant scattering in the Γ_1 band of GaSb near room temperature is by screened Coulomb scattering centres, then, for electron concentrations of $<10^{24}$ m^{-3}, r_1 will have a value of between 1.0 and 1.9 depending on carrier degeneracy. Therefore without prior knowledge of the effective relaxation time for electrons in the Γ_1 band, r_1 can not be calculated and hence the value of n_1 can not be determined accurately from R_1. For this reason it is difficult, if not impossible, to make accurate analyses on n-GaSb with electron density $<10^{24} m^{-3}$.

The above mentioned problems of homogeneity and the difficulty in analyses of galvanomagnetic data, because of uncertainty in r_1, do not apply for material in which the electron concentration is > 10^{24} m^{-3}. However, other factors impose an upper limit of about 2 x 10^{24} m^{-3}. Firstly, the value of r_2 becomes uncertain, at

higher electron concentrations, because of increased impurity scattering. Secondly, the total carrier concentration ($n_t = n_1 + n_2$) no longer remains constant with temperature, which makes the analyses of experimental data more difficult and unreliable. The temperature variation of n_t is due to the presence of the Te impurity states which are associated with the L_1 minima. When the doping increases and the Fermi level approaches the impurity level, some electrons will be trapped by the impurities. Since the ionization energy of the Te impurities associated with the L_1 minima is not well known, this brings in an additional uncertainty into the analyses. In addition, it is not known at what doping concentrations the impurity level becomes a band and overlaps with the L_1 minima. This would have a twofold effect on the L_1 band, i.e. it would distort the band near the minima and would reduce the $\Gamma_1 - L_1$ band separation (69T1). Both effects would further unnecessarily complicate the analyses. The foregoing considerations therefore limit the doping range for useful experiment and analyses to a range of electron concentrations of roughly 1 to 2 x 10^{24} m^{-3}.

It should be made clear that whereas the upper limit is set by the physical properties of heavily doped n-GaSb, the lower limit is principally set by the experimental difficulty of growing homogeneous material. Since, the problem arising from uncertainty in r_1 can be overcome once the electron scattering mechanisms in the Γ_1 band are known, then r_1 can be determined by a "closed loop iteration" procedure.

IV-2 Experimental Results

In view of the discussion of the previous section, the choice of samples for measurements of Hall coefficient, R, and conductivity, σ, as a function of magnetic field, B, was based on two criteria; (a) homogeneity and (b) range of Hall coefficient

satisfying the electron concentration range for accurate analyses. Therefore, preliminary measurements of conductivity and constant field Hall coefficient were made on five n-type samples of GaSb in the temperature range $20^{o} < T^{o}C < 550^{o}$. In addition, for reasons discussed later, a p-type sample of GaSb also was measured in the same temperature range. The n-type samples had room temperature Hall coefficients of between 9 and 70 $x10^{-6}$ m^3/C. Out of these five samples one was chosen for measurements of R and σ as a function of magnetic field and temperature. The remaining four samples were rejected for reasons discussed below.

Typical results of Hall coefficient and conductivity as a function of temperature, for one of the rejected samples, N1, are shown in fig. IV-1 and IV-2. It can be seen from fig. IV-1 that considerable impurity gradient exists in this sample. The two sets of Hall probes (2-6, 3-5; Fig. III-12) were spaced 5.00 mm. apart and gave Hall coefficients differing by about 20% at B = 0.87 Wb/m^2. Fig. IV-1 shows also that the maxima in the separate Hall coefficient curves, corresponding to the two sets of Hall probes, occur at different temperatures. The conductivity, σ_o, over the same temperature range shows an inflection, Fig. IV-2. Since σ_o is a product of the carrier concentration and mobility between the two sets of Hall probes, the inflection in σ_o is therefore due to some average effect of carrier concentration and mobility variation along the sample. On the other hand, the value of R is usually calculated by taking the average of the two Hall coefficients corresponding to the two sets of probes. Therefore the values of R and σ_o are not compatible, since they correspond to different averages.

Three other n-type samples had similar impurity gradients and together with sample N1 were rejected on this basis alone. However, the general shape of the Hall coefficient curves of all of these samples is significant, and will be referred to later.

The remaining n-type sample, N2, with room temperature Hall coefficient of about 1 x 10^{-5} m^3/C, had a gradient of less than 1% between the two sets of Hall probes spaced 5.4 mm. apart. This amount of inhomogeneity was considered acceptable for both magnetoresistance measurements and subsequent analyses based on the two band model discussed in Chapter II. Impurity gradients were further checked in this sample by making contacts at two other positions along the sample and measuring both conductivity and Hall coefficient. The values of σ_o and R calculated for the three sets of positions agreed to better than 1%.

Similar measurements were performed on a p-type sample, P1, which was also found to be homogeneous.

Sample N2 was subsequently used by Demars (72D1) for measurements of magneto-Seebeck coefficient in fields from 0.0 to 3.2 Wb/m^2 at room temperature. A small Van der Pauw type specimen was then cut from sample N2 and was used by Rosenbaum (72R1) for measurements of resistivity and constant field Hall coefficient as a function of pressure up to 12 Kbars at room temperature. Since Van der Pauw samples can be made small (e.g. 2 x 2 mm. in area), in contrast to the much larger samples required for magnetoresistance measurements (e.g. 1 x 15 mm.), Rosenbaum was also able to find large enough areas of uniform impurity distribution for Van der Pauw samples from material which showed severe gradients in the large parallelopiped shaped specimens. He used a specimen with room temperature and zero pressure Hall coefficient of about 28 x 10^{-6} m^3/C for measurements up to 12 Kbars to complement the measurements made on the sample cut from N2. The results of analyses of the data obtained by Demars and Rosenbaum will be discussed in a later section. However, it may be indicated here that the good agreement obtained between the present data on both n and p samples, the magneto-Seebeck data of Demars and both sets of pressure data by Rosenbaum justify the assumption that the present data is representative of GaSb.

IV-21 Measurements of Magnetoresistance and Hall coefficient as a function of magnetic field and temperature on sample N2.

The measurements were made on the apparatus described in Chapter III, at liquid Nitrogen temperature (78°K) and from room temperature (usually between 20° and 25°C) to 360°C in intervals of 20°. Typical results of R vs. B are shown in Fig. IV-3. Similar shaped curves were obtained for σ vs. B, those will not be shown for the sake of brevity. These results are replotted in Figs. IV-4 and IV-5 in the form $-R_o/\Delta R$ and $\rho_o/\Delta\rho$ against B^{-2} for several temperatures. The value of R_o is obtained from a plot of -R vs. B^2 at low fields ($B < .9$ Wb/m^3) extrapolated to B = 0, these plots being shown in Fig. IV-6. To justify this method of obtaining R_o, it is necessary to expand equation II-42 in ascending powers of B^2 as was done by Harland and Woolley (66H1), who showed that the coefficient of B^4 is very small and hence at low fields II-42 approximates to a straight line of the form

$$R = R_o + \alpha B^2 \qquad \text{IV-1}$$

It can be seen from Fig. IV-6 that, within the limits of experimental error, the points do in fact give a straight line, and hence R_o can be found.

Equations II-46 and II-62 predict that plots of $-R_o/\Delta R$ and $\rho_o/\Delta\rho$ vs. B^{-2} should be linear, if the conditions under which these equations were derived are satisfied. Figs. IV-4 and IV-5 do indeed show that straight lines are obtained experimentally, at least below 140° and even at 200°C the deviations from a straight line are found to be small, although at this temperature we would expect the contribution to magnetoresistance from individual bands to become significant. The results of least squares fitting these data to a straight line are tabulated in Table IV-1, together with the values of R_o and σ_o.

IV-22 Measurements of low field Hall coefficient and conductivity as a function of temperature

The results of measurements of low field Hall coefficient ($B < 0.9$ Wb/m^2) and conductivity on samples N2 and P1 are shown in Fig. IV-8 and IV-9 respectively. It is of interest to note that the inflection in R(T) observed for the purer sample N1, Fig. IV-1, is also present in this heavier doped sample.

IV-3 Method of Analysis

IV-31 Determination of Γ - L minima separation and its temperature dependence from magnetoresistance results

The separation of the two minima Γ_1 and L_1 (i.e. E_2) and its temperature dependence (dE_2/dT) can in principle be obtained with the use of the charge neutrality condition, equation II-69, if the carrier distribution between the bands and the band parameters are known.

The carrier distribution can be obtained from the magnetoresistance and Hall coefficient measurements described in section IV-21. The plots of $-R_o/\Delta R$ and $\rho_o/\Delta\rho$ vs. B^{-2} have been shown to be linear, giving slopes s, t and intercepts a, u respectively; these are tabulated in Table IV-1 together with R_o and σ_o. Since we have only four unknowns R_1, R_2, σ_1 and σ_2, to determine these we need to use only four of the experimentally determined quantities. The question arises as to which four should be picked. Obviously, the values of R_o and σ_o will be accurate since σ_o is obtained directly from experiment and R does not vary strongly at low B, hence extrapolation to B = 0 should give an accurate value of R_o. Also the slopes s and t will be accurate as long as straight lines are obtained experimentally. On the other

hand, the values of a and u are obtained by extrapolation to B = ∞ and hence will be the least accurate values. Therefore, best results will be obtained if we use the combination (i) R_o, σ_o, s and t, the other combinations (ii) R_o, σ_o, s, a and (iii) R_o, σ_o, t, u will give less accurate results. We have carried out these calculations with the three sets of values at three different temperatures, using equations II-43; II-49 to II-52; II-65 to II-68, and tabulated the results in Table IV-2. From this Table, it can be seen that the calculated values of R_1, R_2, σ_1 and σ_2 agree well for all three cases, in particular for (i) and (iii). This could be expected, since the value of a is probably the least accurate one, because the relative change of R with B is smaller than that of σ, and hence a will be less accurate than u. We can also conclude that the two band picture is valid in this temperature range. Because of the good agreement between the results using case (i) and (iii), magnetoresistance results above are, in fact, sufficient to determine the quantities R_1, R_2, σ_1 and σ_2, which are tabulated in Table IV-2a. The accuracy of the data is reflected to the largest extent in the value of R_2. From equation II-43, the value of R_2 is determined from the difference of two terms $R_o(\sigma_o/\sigma_2)^2$ and $R_1(\sigma_1/\sigma_2)^2$ which are comparable in magnitude and therefore R_2 is the least accurate value of the four parameters calculated.

Using the values of R_1 and R_2 as a function of temperature, carrier distributions n_1 and n_2 can be calculated when the scattering parameters r_i and the ellipticity K_i are known. No values have been published for either r_1 or r_2 since carrier scattering in neither band is understood. We shall assume that $r_1 = 1.0$ and does not vary with temperature within the experimental range (it will be shown in section IV-333 that this assumption is valid). We shall also assume that the scattering in the L_1 band is dominated by longitudinal acoustic waves and

therefore $r_2 = 1.18$ and is temperature invariant. The value of K_2 was deduced by Piller (64P1) to be 8.6 and this value will be used throughout. The carrier concentrations n_1 and n_2 were then calculated from R_1 and R_2, the mobilities μ_1 and μ_2 were obtained from σ_1 and σ_2, and the results are tabulated in Table IV-3, together with the total carrier density $n_1 + n_2 = n_t$.

The energy level of Te donors was reported by Pitt (69P2) to be about 0.02 eV below the bottom of the L_1 minima, and we therefore expect that for sample N2 the total carrier density should remain constant above room temperature. This, of course, is true only for temperatures below that of intrinsic conduction. Table IV-3 shows that $n_t = 1.45 \times 10^{24}\ m^{-3}$ and does indeed remain constant within the accuracy inherent in the calculation of R_2 and hence of n_2. The charge neutrality can now be expressed in the form:

$$N_D - N_A = n_1 + n_2 = n_t = 1.45 \times 10^{24}\ m^{-3} \qquad \text{IV-2}$$

and thus determines the position of the Fermi level at a given temperature. The condition IV-2 together with equations II-71 and II-75 for n_1 and n_2 were then used to determine E_2 and α_2 by the following procedure. The carrier densities n_1 and n_2 were calculated from equations II-71 and II-75 for a given set of values of E_2 and α_2 together with the parameters given in Table IV-4; the Fermi energy being adjusted so that condition IV-2 was satisfied. The carrier concentrations thus calculated were then compared to the values of n_1 and n_2 obtained from analyses of magnetoresistance data (Table IV-3) over the temperature range $20 < T < 120^{o}C$. E_2 and α_2 were adjusted until satisfactory agreement was obtained between the two sets of results for n_1 and n_2. Since the relative change with temperature of n_1 is much greater than that of n_2, the fit was judged acceptable when $n_1(T)$ was fitted.

The above procedure was then repeated with the X_1 band being included in

the charge neutrality condition, i.e.

$$N_D - N_A = n_1 + n_2 + n_3 = n_t \qquad \text{IV-3}$$

to determine at which temperature an appreciable number of electrons will be excited to the third set of minima. The additional parameters for the X_1 band which were required for the calculations are given in Table IV-4. The density of states effective mass of 1.2 m that was used, was assumed to be the same as that for the <100> band in GaAs (60E1). The band separation, E_{30}, of 0.315 eV was determined at room temperature by Kosicki et al. (68K1) and here its temperature dependence was assumed to be zero. It will be shown later that this assumption is quite reasonable and not very restricting, since only at the highest experimental temperatures are there any appreciable number of electrons in the X_1 band. The results show that at 100°C, n_3 is only 1% of n_1,; at 140°C it is 3% and at 200°C it is 9%. Since the analysis of the magnetoresistance was based on the two band model, the fitting of n_1 is valid up to $\sim$120°C only since, as will be shown in section IV-3, the contribution to magnetoresistance by individual bands could become appreciable above $\sim$120°C. Both these causes of uncertainty combine to make the results (Table IV-3) above 120°C unreliable for use in the determination of E_2 and α_2. Hence, only the values obtained in the temperature range 25° to 120°C were used. The results are shown in Table IV-5 and Fig. IV-7, where we have plotted the fitted carrier density in the Γ_1 band (solid line) and the values of n_1 from Table IV-3 as a function of temperature. The solid line represents the best fit obtained with $E_{20} = 0.099 \pm .002$ eV and $\alpha_2 = -3.4 \pm .01 \times 10^{-5}$ eV/°K. Because a linear form of temperature dependence of E_2 has been used (equation II-79), it is to be expected that the value obtained for E_{20} is slightly higher than the actual band gap at 0°K. Nevertheless, the present value agrees well with that of 0.095 ± .005 eV found by Yep and Becker (67Y1)

at 4.2°K from de Haas-van Alphen measurements, although it is higher than earlier reported values which range from 0.04 - 0.09 eV. The value of α_2 appears quite reasonable, although it is nowhere near the values reported by some authors, which are of the order of $\pm 10^{-4}$ eV, e.g. -2×10^{-4} eV/°K reported by Robert and Barjon (70R1). However, it is close to a value of -5×10^{-5} eV/°K which was estimated from existing experimental data by assuming linear temperature dependences for the two direct energy gaps involved; viz. the $\Lambda_{3v} \rightarrow \Lambda_{1c}$ peak (given by the E_1 reflectance peak) and the principal $\Gamma_{15v} \rightarrow \Gamma_{1c}$ gap (E_o). Bahan (70B1) reported a value of $-5.0 \pm .05 \times 10^{-4}$ eV/°K for the temperature coefficient of the E_1 peak and a value of -4.5×10^{-4} eV/°K was obtained by Woolley and Evans (61W1) for the coefficient of the principal gap, by fitting the optical absorption data. Further discussion and comparison with published values of E_{20} and α_2 is postponed to section IV-42.

Measurements were also made of magnetoresistance, low field Hall coefficient ($B < .9$ Wb/m^2) and conductivity at liquid Nitrogen temperature (78°K), the results being given in Table IV-6. It is clear from these results that even if we use a maximum possible value of $r_2 = 1.93$, i.e. if the carriers in the L_1 band are assumed to be non-degenerate and the scattering wholly due to ionized impurities, the maximum possible total carrier concentration then becomes $n_t = 9.923 \times 10^{23}$ m^{-3}, which is considerably less than $n_t = 1.45 \times 10^{24}$ m^{-3} obtained at room temperature and above. We conclude therefore that the model proposed by Bate (62B1) and used by Pitt (70P2) is correct, that group VI impurities are associated with subsidiary minima and their energies lie above the bottom of the principal minimum. Hence as the temperature drops and the Fermi level approaches the impurity level, "freeze out" of mobile carriers to the impurity level occurs, and therefore the total carrier

concentration drops. For this reason, as was mentioned in the Introduction, the measurements carried out for this thesis were made at T > 300°K on samples which were not too heavily doped. In this way, the exact energy position of the impurity level and their density is not required for the analysis since the impurity states will remain ionized at all the temperatures of the experiment.

IV-32 Determination of carrier mobility in the Γ and L bands from Hall coefficient and conductivity

IV-321 Sample N2

The case of electrons being distributed between two conduction bands, one with high and one with low carrier mobility, is analogous to the case encountered in many semiconductors at low temperature when carriers are distributed between a conduction band and an impurity band, (e.g. Basinski and R. Olivier 67B2). The electron mobility in the impurity band is always considerably lower than in the conduction band. In this case, as the temperature is lowered, the electrons freeze-out into the impurity band, the Hall coefficient starts rising and the conductivity drops. As the temperature is lowered further, provided the mobility ratio remains constant, R will pass through a maximum and will then level off at some still lower temperature. To a first approximation, the position of the maximum is at a temperature where the two conductivities in the conduction and impurity band are equal (67B2).

The analogy with the case of n-GaSb, having a high mobility Γ_1 band and low mobility L_1 minima, is clear, except that in this case the role of temperature is reversed, since we require an increase in temperature for transfer of electrons to the low mobility minima. We would therefore expect for sample N2 that as the temperature is raised, the Hall coefficient would pass through a maximum and then

start to fall. This is not observed, however, (see Fig. IV-8), for the curve starts to level off but then rises again. (N.B. the inflection in R(T) around 150°C is similar to that seen in the Hall coefficient vs. temperature data of sample N1, Fig. IV-1). There are two possible reasons for this, either (a) electrons are lost to the X_1 minima where they will have very low mobility, $\sim$.0045 m/V. sec. at room temperature according to Pitt (69P2), or (b) the mobility ratio (μ_1/μ_2) increases with increasing temperature due to some change in the effective scattering mechanism.

Initially, we tried to fit the results of R(T) vs. T given in Fig. IV-8 assuming case (a) only. To do this, we used the parameters for the Γ_1 and L_1 minima determined from the magnetoresistance data and assumed that the temperature dependences of mobilities μ_1 and μ_2 obtained from magnetoresistance results below 120°C remain the same up to 360°C, and take the following form:

$$\mu = \mu_{300}(\frac{300}{T})^q \qquad \text{IV-4}$$

Values for q_1 and q_2 were determined by least squares fit of the data for $\mu_1(T)$ and $\mu_2(T)$ respectively, (Table IV-3) and the results are shown in Fig. IV-10.

An attempt was then made to fit the Hall coefficient temperature variation, R(T), using equation II-56 by varying α_3 and m_3^*. The contribution of intrinsic carriers was included in the charge neutrality condition in order to take care of any increase in the total electron concentration. The mobility μ_3 was calculated from:

$$\mu_3 = (\sigma_o - \sigma_1 - \sigma_2)/en_3 \qquad \text{IV-5}$$

and E_{30} was given by $E_{30} = 0.315 - 300\ \alpha_3$, the value of $E_3 = 0.315$ at room temperature having been reported by Kosicki et al. (68K1) and by Pitt (70P1). The heavy hole valence band was taken into consideration but not the light holes, the

effective mass of the heavy holes being taken as 0.33 m (68W1) and a hole mobility of 0.14 $m^2/V.$ sec. (64M1) at 300^oK was assumed with a temperature dependence of $T^{-1.5}$. Actually, as can be seen from Table IV-7, even at 360^oC the density of holes is only 4×10^{21} m^{-3}, and hence the fit is very insensitive to the value of the hole mobility or its temperature dependence. In any case, no satisfactory fit could be obtained by varying α_3 and m_3^* within reasonable limits. We concluded therefore that although the third set of minima may indeed contribute to the increase in R above 150^oC, this contribution is small. In view of the above result, an attempt was then made to fit the R(T) vs. T data assuming case (b) only. It was now assumed that all the parameters of the bands were known except $\mu_1(T)$ and $\mu_2(T)$, and these were to be obtained by simultaneously fitting R(T) and $\sigma_o(T)$ data to equations II-56 and II-57. The parameters for the two lowest conduction band minima, Γ_1 and L_1, and the heavy hole valence band were taken as before. In addition the following parameters were assumed for the <100> minima:

$$m_{3d}^* = 0.36 \text{ m}$$

$$\alpha_3 = 0.0$$

$$E_3 = 0.31 \text{ eV}$$

$$\mu_3 = .01 \left(\frac{300}{T}\right)^{1.5}$$

The choice of the parameters for the <100> minima was dictated by the known values of these parameters in Si, GaP and GaAs for minima with the same symmetry. It seems rather unlikely that the <100> band in GaSb would be very different from the band of the same symmetry in these three semiconductors. The values of the parameters of the <100> band in Si, GaP and GaAs are given in Table IV-8. From this Table, we can see that for both III-V compounds the effective mass and mobility in

the <100> minima are roughly the same. In the estimate of the value of α_3 to be used, two results are relevant. It was observed that the Varshni (67V1) expression II-74 holds for direct and indirect gap materials with valence band as reference, and at high temperatures, this expression becomes linear with T. Therefore to estimate α_3, we calculated the difference between the temperature coefficients of the <100> band in GaAs and GaP, and of the Γ_1 band in GaSb, from values at two temperatures, 500 and 700°K. The results are included in Table IV-8 and are denoted by $\alpha_3'(T)$. These values indicate that α_3 should be positive and of the order of $+5 \times 10^{-5}$ eV/°K. (It will be shown in Chapter V that in the case of GaAs $\alpha_3 \sim 1 \times 10^{-5}$ eV/°K.

Since the values of the parameters, m_3^*, α_3 and μ_3, are uncertain, we have varied them to determine what effect, if any, a wrong choice would have on the values of $\mu_1(T)$ and $\mu_2(T)$ obtained from the fit. The following ranges of variations were employed:

$$0.34\ m < m_{3d}^* < 0.38\ m$$

$$-5 \times 10^{-5}\ \text{eV/°K} < \alpha_3 < +5 \times 10^{-5}\ \text{eV/°K}$$

$$.005\ \text{m}^2/\text{V.sec.} < \mu_3(300) < .020\ \text{m}^2/\text{V. sec.}$$

The values of $\mu_1(T)$ and $\mu_2(T)$ determined from the fitting, using the above range of parameters, agreed within 1% and 8% respectively. The final results are shown in Fig. IV-8 as a solid line and are presented in numerical form in Table IV-7.

IV-322 Sample P1

The results of measurements of Hall coefficient and conductivity on the p-type samples are shown in Fig. IV-9 . The curves are typical of a p-type sample in which the Hall coefficient changes sign from positive to negative due to an

increase in the concentration of the highly mobile electrons as they are excited across the band gap with increasing temperature. These data were analysed using the conduction band parameters obtained from the n-type N2 sample, together with known values of the parameters of the valence bands. The method of analysing is described below.

The data were divided into two parts, a low temperature section, below 250°C where purely hole conduction is present, and a high temperature section above 250°C where mixed conduction occurs.

Considering first the low temperature portion of the Hall coefficient curve, the initial drop in the value of R is due to ionization of acceptor impurities with activation energy E_a and density N_a. The curve tends to level off at $\sim$200°C, when the impurity level is practically completely ionized. We shall treat both E_a and N_a as adjustable parameters which can be obtained from the low temperature data. Before this can be done, the values of mobilities in the light and heavy hole valence bands, as well as the Hall scattering parameters, must be known.

It has been pointed out by Blatt (68B1, p. 169), that in Ge and Si, the mobilities in the two valence bands would be expected to be approximately in the ratio of the two effective masses, since the relaxation times of the two bands of holes are approximately equal. This comes about because the scattering probability depends essentially on the density of final states, which in either case is the density of states of the heavy hole band. This follows if it is assumed that the scattering of the light holes is dominated by interband scattering into the heavy hole band and that of the heavy holes by intraband scattering, both of which are directly dependent on the density of states in the heavy hole band. It has been shown by Dresselhaus et al. (55D1) that for Ge the two relaxation times are

$\tau_{p\ell} = 7 \times 10^{-11}$ sec and $\tau_{ph} > 5 \times 10^{-11}$ sec. For convenience, the same assumption will be made about the mobility ratio for the case of the valence bands in GaSb, i.e. the ratio of a light to heavy hole mobilitiy is then given by:

$$\mu_\ell/\mu_h = m^*_{ph}/m^*_{p\ell} = 0.33/.045 = 7.34$$

the values of effective masses of the holes have been determined by Walton and Mishra (68W1) from cyclotron measurements. It will also be assumed that both the Hall scattering parameters are equal to unity and remain constant with temperature.

With the above assumptions the values of N_a and E_a as well as μ_h (and hence μ_ℓ) can be deduced using the following relations,

$$p_h + p_\ell = \frac{N_a}{1 + g_a \exp\left[(E_F - E_o + E_a)/kT\right]} \qquad \text{IV-6}$$

where g_a is the spin degeneracy factor, taken to be 4 for the acceptors, as was also assumed by Compas (69C3),

$$\sigma = e\mu_h(p_h + bp_\ell) \qquad \text{IV-7}$$

$$R = (p_h + b^2 p_\ell)/e(p_h + bp_\ell)^2 \qquad \text{IV-8}$$

where b is the mobility ratio of light to heavy holes.

For a given value of N_a and E_a, the hole densities p_h and p_ℓ can be calculated from the charge balance equation IV-6 together with $p_h/p_\ell = (m^*_h/m^*_\ell)^{3/2}$. By substituting these densities into equation IV-8 and making use of the experimental value of σ, the Hall coefficient is then calculated and compared with the experimental value. N_a and E_a are adjusted so as to give a best fit to the Hall curve below 200°C. The values thus determined were $N_a = 4.44 \times 10^{23}$ m^{-3} and $E_a = 0.042$ eV. The hole mobilities were then determined from the experimental value

of the conductivity using equation IV-7. These display an exponential dependence on temperature of the form

$$\mu_h = \mu_{ho} e^{-T/\phi} \qquad \text{IV-9}$$

The values of μ_{ho} and ϕ were then obtained by fitting the results to equation IV-9, resulting in $\mu_{ho} = .0764\ m^2/V.\ sec.$ and $\phi = 296^oK$.

With the values of N_a, E_a and the magnitude and temperature dependence of the mobility of light and heavy holes determined from the low temperature data, the complete curves of R and σ were then simultaneously fitted, using μ_1 and μ_2 as adjustable parameters. The conduction band parameters used were those obtained from the n-type sample N2. The fitted curves for R and σ are shown in Fig. IV-9, and the values of μ_1 and μ_2 required for the fit are tabulated in Table IV-10.

Below 440^oC the fit is insensitive to the values of μ_1 and μ_2. Thus, considerable scatter in the values of mobilities was obtained in this range and hence these values are not given in Table IV-10, nor are they plotted in Fig. IV-16.

In the transition region of R, from positive to negative sign, ($250 < T < 440^oC$), the fitting is most sensitive to the relative density of holes and electrons and therefore to the temperature dependence of the principal gap, α_o. The value of α_o had to be increased from -5.0×10^{-4} eV/K to -5.4×10^{-4} eV/K in order to obtain a good fit to the experimental results of R and σ. The value of $\theta (=112^oK)$ however was left unchanged. The resulting good agreement with the values of Hall coefficient and conductivity measured as a function of temperature, on the P1 sample, give confidence in the values of conduction band parameters determined from experimental data on the n-type sample N2.

IV-33 Analysis of electron mobility in the Γ and L bands

IV-331 Analysis of the mobility $\mu_2(T)$ in the L_1 band for T < 360°C

Scattering of electrons in the L_1 band of GaSb is not well understood. Although it is possible to make an educated guess at what scattering mechanisms may be important in the temperature range below 360°C, this type of estimate becomes practically worthless at still higher temperatures because of the interaction of the L_1 band with higher lying minimum in the <100> direction. Therefore an attempt will be made here to analyse by an approximate method only the $\mu_2(T)$ data obtained from the n-type sample N2 below 360°C. It was assumed that the scattering in the <111> minima is essentially due to ionized impurities and acoustic phonons only, since these mechanisms are important for heavy carriers. In that case, one can write the total mobility in the approximate form:

$$\frac{1}{\mu_2(T)} = \frac{1}{\mu_a(T)} + \frac{1}{\mu_I(T)} \qquad \text{IV-10}$$

where $\mu_a(T)$ and $\mu_I(T)$ are the mobilities due to scattering by acoustic phonons and ionized impurities respectively. Since the Fermi energy at the lowest temperature is more than 2 kT below the bottom of the L_1 minima (c f. Table IV-7), classical statistics can be used in the integration of equation II-40 to give μ_a and μ_I (equation II-17, II-25) and hence obtain $\mu_a(T)$ and $\mu_I(T)$. The values of μ_a and μ_I so obtained will have the following dependence on temperature:

$$\mu_a = aT^{-3/2} \qquad \text{IV-11}$$

where

$$a = \frac{e\,(8\pi)^{1/2}\,\hbar^4\,c_{\ell\ell}}{3E_1^2\;m_{2d}^{*3/2}\;m_{2e}^{*}\;k^{3/2}} \qquad \text{IV-12}$$

$$c_{\ell\ell} = \rho U^2$$

and $$\mu_I = cT^{3/2} \qquad \text{IV-13}$$

where $$c = \frac{64\pi^{1/2}\,\kappa_o^2\,(2k)^{3/2}\,m_{2d}^{*\,1/2}}{e^3\,m_{2e}^{*}\,N_I\,f(z)} \qquad \text{IV-14}$$

In carrying out the integration for μ_I, f(z) was taken outside the integral, since it is a slowly varying function of energy (59S1). $\mu_2(T)$ can now be written in the form:

$$\frac{1}{\mu_2(T)} = \frac{1}{aT^{-3/2}} + \frac{1}{cT^{3/2}} \qquad \text{IV-15}$$

This expression was fitted to the experimental values of $\mu_2(T)$, Fig. IV-11, a non-linear least squares fitting program (IBM library programme BMDX-85) being used, and the temperature invariant parameters $a = 4.4 \times 10^2$ $m^2/V.\,sec.\,K^{3/2}$ and $c = 2.3 \times 10^{-5}$ $m^2/V.\,sec.\,K^{-3/2}$ were obtained. In doing this, it was assumed that f(z) is independent of temperature, where in fact it is a slowly varying function of temperature. This will cause some error in the value of c. From these values of a and c the deformation potential E_1 and the ionized impurity density N_I were estimated. To calculate E_1 from a, a value for $c_{\ell\ell}$ was required and this was calculated using the Herring and Vogt (56H1) expression:

$$c_{\ell\ell} = c_{12} + 2c_{44} + \frac{3}{5}(c_{11} - c_{12} - 2c_{44}) \qquad \text{IV-16}$$

where c_{ii} are elastic constants, which are given for GaSb by Madelung (64M1). Thus, a value of approximately 9 eV was deduced for E_1, and this compares well with the value of about 10 eV reported by Sherwood (70S4).

In estimating the total ionized impurity concentration N_I from c, we used f(z) = .11 obtained from E = 3kT at T = 300°K, together with $n_t = 1.45 \times 10^{24}$ m^{-3}, resulting in a value of 2×10^{24} m^{-3} for N_I.

Another way of estimating N_I was suggested by Baxter et al. (67B1). They found that in order to explain their measurements of mobility on n-GaSb at 78°K, they required a greater density of acceptors than is usually found in undoped p-GaSb, i.e. 1 - 2 x 10^{23} m^{-3} (67B1). To explain their results, they postulated that the acceptor centres are doubly charged and therefore the effective total ionized impurity concentration N_I^* is given by:

$$N_I^* = n_t + 6N_a^= \qquad \text{IV-17}$$

In that case if the lower limit of 1.0 x 10^{23} m^{-3} is taken for the density of acceptors $N_a^=$, a value of $N_I^* \simeq 2.1 \times 10^{24}$ m^{-3} is obtained. On the other hand, taking the upper limit of 2 x 10^{23} m^{-3} for N_a gives $N_I^* = 2.6 \times 10^{24}$ m^{-3}. The value above from a least squares fit of $n_2(T)$ is closer to the lower limit, therefore somewhat arbitrarily we chose to use $N_I = 2.2 \times 10^{24}$ m^{-3} in the analysis, given below, of the mobility $\mu_1(T)$ of electrons in the principal conduction band.

IV-332 Analysis of the mobility $\mu_1(T)$ in the Γ_1 band

(a) μ_1 mobility deduced from measurements on sample N2 ($T < 360^oC$)

As was pointed out earlier, $\mu_1(T)$ is insensitive to the parameters chosen for the <100> band and therefore was determined to much better accuracy than $\mu_2(T)$. Hence the approximate analysis which we employed for $\mu_2(T)$ is no longer sufficient, and a more accurate approach should be used in analysing the temperature dependence of μ_1.

Conwell and Vassell (68C1) used three scattering mechanisms to analyse their mobility results for the Γ_1 band in GaAs, and all three are appropriate for the Γ_1 band in GaSb. In addition, since we are dealing with a moderately heavily doped sample, ionized impurity scattering must also be included. This is supported by the findings of Baxter et al. (67B1) who found that at room temperature the scattering

of electrons in the Γ_1 band of GaSb by ionized impurities was important.

Initially we tried to simulate the behaviour of $\mu_1(T)$ with the following three scattering modes:

(i) polar optical,

(ii) interband, Γ_1 to L_1,

(iii) ionized impurity.

In this case the net relaxation time τ is given by:

$$\frac{1}{\tau} = \frac{1}{\tau_{po}} + \frac{1}{\tau_{ib}} + \frac{1}{\tau_I} \qquad \text{IV-18}$$

where τ_{po}, τ_{ib}, τ_I are given by equations II-20, II-24 and II-29 respectively. For the purpose of calculations, τ's will be rewritten in a form more adaptable for computer solution.

Using the definition of γ (equation II-23) and equation II-10 for k, it can be shown that the relaxation time due to polar scattering is given by:

$$\frac{1}{\tau_{po}} = 5.716 \times 10^{27} \, P(m_o^*)^{1/2} \, (2N_{q\ell} + 1)/\varepsilon^{1/2} \qquad \text{IV-19}$$

where

$$P = \frac{\frac{m}{m_o^*} - (\frac{m}{m_o^*} - 1)\{1 + \frac{4\varepsilon m_o^*}{\varepsilon_o^* m}(1 - \frac{m_o^*}{m})\}^{-1/2}}{[\frac{m}{m_o^*} + (\frac{m}{m_o^*})^2 \frac{\varepsilon_o^*}{2\varepsilon} - (\frac{m}{m_o^*})^2 \frac{\varepsilon_o^*}{2\varepsilon}\{1 + \frac{4\varepsilon}{\varepsilon_o^*}\frac{m_o^*}{m}(1 - \frac{m_o^*}{m})\}^{1/2}]^{1/2}} \qquad \text{IV-20}$$

$\varepsilon = E/\hbar\omega_\ell$ and $\varepsilon_o^* = E_o^*/\hbar\omega_\ell$, i.e. all the energies are normalized to $\hbar\omega_\ell$[†]. In order to simplify writing these expressions, we have written m_o^* for $m_{10}^*(T)$, i.e. the bottom of the band (Γ_1) effective mass as a function of temperature which is given by equation II-72 in terms of the mass at absolute zero.

[†] For the purpose of calculations we have chosen throughout this section to normalise all the energies to $\hbar\omega_\ell$.

Similarly the expression for the interband relaxation time τ_{ib} (c f. equation II-24) can be written as:

$$\frac{1}{\tau_{ib}} = \frac{6.775 \times 10^{40} (M_d^*)^{3/2} D_{12}^2}{e^{x_{12}} - 1} [(\varepsilon + .8 - \varepsilon_2)^{1/2} + e^{x_{12}} (\varepsilon - .8 - \varepsilon_2)^{1/2}] \quad \text{IV-21}$$

where $M_d^* = 4^{2/3} m_{2d}^*$ is in M.K.S. units and D_{12} in eV/cm. It was also assumed that $\omega_{12} = 0.8\omega_\ell$ (72V1).

Kolodziejczak's equation II-29 for the ionized impurity scattering relaxation time τ_I was derived on the basis of a single non-parabolic band. Therefore the Fermi energy E_F, appearing in the integral $L(\beta, \eta)$ within the expression for the screening radius, describes the distribution of electrons in a single band. Hence it does not correspond to the Fermi energy obtained here in section IV-321 , which is affected by the carriers in the L_1 band. In addition, we have two sets of electrons, light (n_1) and heavy (n_2), and the n_2 electrons will shield the ionized impurities more effectively than the n_1 electrons (67B1). Therefore, the screening correction given by Kolodziejczak can not be applied in this case. It was also shown by Moore and Ehrenreich (66M1, 67M1) that at high doping levels, quantum corrections are important, and both relations II-25 and II-29 are inexact, even when screening is excluded. It was therefore initially thought unnecessary to make corrections to the screening radius due to two band effects without making the more important but very tedious quantum corrections. With these reservations in mind, we used the Brooks-Herring relation for the ionized impurity scattering relaxation time τ_I with only one change, i.e. the inclusion of the non-parabolicity effect through the effective mass, i.e.

$$\tau_I = 277.5 \, (m_c^*)^{1/2} \, \varepsilon^{3/2} / f(z) \quad \text{IV-22}$$

where

$z = 1.61 \times 10^{29} \, m_c^*$, and $N_I = 2.2 \times 10^{24} \, m^{-3}$ was used.

To calculate mobility $\mu = e \langle \frac{\tau}{m_c^*} \rangle$, equation II-39 was used with τ given by IV-18 and m_c^* by II-4. The values of various parameters appearing in the equations for the relaxation times τ_{po}, τ_{ib} and τ_I, which depend on band structure of GaSb, are given in Table IV-9. The numerical integrations required in evaluating the infinite integrals in II-39 were done on an IBM 360 model 65 computer using Simpson's method. It was found that the integrals converged rapidly above $\varepsilon \sim 10$. At $\varepsilon = 35$ the magnitude of the functions in the integrals had values about 10^{-10} smaller than the maximum value, hence integration was cut off at this value of ε. The results of the calculations are shown in Fig. IV-12, the upper curve for $D_{12} = 1 \times 10^8$ eV/cm. It can be seen from Fig. IV-12, that with these three relaxation times, the calculated mobility is roughly twice as large as that obtained from the fitting of R(T) and σ_o(T). Since we do not know the proper magnitude of D_{12}, we can use this as an adjustable parameter and the result for $D_{12} = 4.6 \times 10^8$ ev/cm, is shown as a dashed line, from which it can be seen that by adjusting D_{12} it is possible to fit the high temperature portion of the μ_1(T), but not the low temperature part. This suggests that (a) additional scattering mechanisms are present which are more important at lower temperatures than the interband scattering, i.e. spacecharge scattering, or (b) that the density of scattering centres is higher than that estimated, and that the mobility is governed mainly by τ_I.

Taking the first possibility, and including spacecharge scattering in the analysis, the total relaxation time becomes

$$\frac{1}{\tau} = \frac{1}{\tau_{po}} + \frac{1}{\tau_{ib}} + \frac{1}{\tau_I} + \frac{1}{\tau_{sc}} \qquad \text{IV-23}$$

where

$$\frac{1}{\tau_{sc}} = 9.666 \times 10^{-11} \left(\frac{N_s Q_s}{P}\right) \frac{\varepsilon^{1/2}}{m_o^{*1/2}} \qquad \text{IV-24}$$

The magnitude of $(N_s Q_s)$ is unknown, hence we end up with two adjustable parameters

D_{12} and $(N_s Q_s)$. Fortunately, D_{12} and $(N_s Q_s)$ do not have the same effect on τ over the whole temperature range of measurement. While $(N_s Q_s)$ affects the low temperature portion of the $\mu_1(T)$ curve, D_{12} is more important at higher temperatures. Therefore both these parameters can be estimated by fitting $\mu_1(T)$. Best results were obtained for $D_{12} = 3.2 \times 10^8$ eV/cm and $(N_s Q_s) = 4.8 \times 10^4$ cm^{-1} and are shown as solid lines through the points in Fig. IV-13. These values can be compared with those obtained by Conwell and Vassell (68C1) for GaAs. These authors found the value of the coupling constant D_{12} to be $\sim 10^8$ eV/cm between the Γ_1 and <100> minima, and $(N_s Q_s) \simeq 3.2 \times 10^4$ cm^{-1}. To the best of our knowledge, this is the first estimate of the magnitude of the coupling constant between the Γ_1 and L_1 valleys of GaSb.

In order to see the relative importance of the scattering mechanisms, we have plotted in Fig. IV-14 the calculated relaxation times at room temperature as a function of reduced energy ε $(= \frac{E}{\hbar\omega_\ell})$ with the above mentioned values for D_{12} and $(N_s Q_s)$. It is seen from this graph that polar scattering is the least important mechanism in determining the mobility in the Γ_1 band in this sample. At low energies ionized impurity and spacecharge effects are important, whereas, at higher energies, as expected, the interband scattering takes over.

If we now take the other possibility, and consider N_I as an adjustable parameter together with D_{12}, the relaxation time is:

$$\frac{1}{\tau} = \frac{1}{\tau_{po}} + \frac{1}{\tau_{ib}} + \frac{1}{\tau_I} \qquad \text{IV-25}$$

where

$$\tau_I = 6.11 \times 10^{26} \; (m_c^*)^{1/2} \; \varepsilon^{3/2} / N_I f(z) \qquad \text{IV-26}$$

The resulting fit to $\mu_1(T)$ is shown in Fig. IV-15 for $N_I = 4.2 \times 10^{24}$ m^{-1} and $D_{12} = 3.0 \times 10^8$ eV/cm. It is noticeably worse than the previous fit when spacecharge

scattering was included. However, because of the approximate nature of the ionized impurity relaxation time τ_I which is employed, and the importance of τ_I in determining the mobility when τ_{sc} is neglected, it is not possible to make a positive choice between the two models. With $N_I = 4.2 \times 10^{24}$ m^{-3}, the mobility at room temperature due to ionized impurity scattering alone is calculated to be .54 m^2/V sec. The interband scattering is then responsible for lowering the mobility to the observed value of .38 m^2V sec. This value of N_I seems to be somewhat high when compared with the previously estimated values $\sim 2 \times 10^{24}$ m^{-3} from analysis of $\mu_2(T)$. If, however, the slow n_2 electrons are considered to contribute to the ionized impurity scattering, as has been suggested by Baxter et al. (67B1), this high value of N_I no longer seems so unreasonable.

We have therefore repeated these calculations following the method of Baxter et al. which considers the heavy electrons in the same way as ionized impurities. In that case the effective ionized impurity concentration N_I^* now becomes:

$$N_I^*(T) = n_t + (6N_a^= + n_2(T)) \qquad \text{IV-27}$$

In addition, the effect of the difference in screening between the light and heavy electrons is allowed for through z (in equation II-32). In this case the two adjustable parameters are $N_a^=$ and D_{12}. Good agreement between the calculated and experimental results was obtained for $N_a^=$ of 1.1×10^{23} m^{-3} and D_{12} of 4.1×10^8 eV/cm. The value of 1.1×10^{23} m^{-3} for $N_a^=$ is in excellent agreement with the value of 0.95×10^{23} m^{-3} obtained by Baxter et al. from results of measurements on n-GaSb at 78^oK.

(b) Γ_1 mobility deduced from measurements on sample P1 ($T > 360^oC$)

The temperature variation of electron mobility in the Γ_1 band of GaSb deduced from measurements on the p-type sample are shown in Fig. IV-16, together with calculated results based on the relaxation time approximation. The scattering mechanisms considered in the calculation were:

(i) polar optical,

(ii) interband, Γ_1 to L_1 and Γ_1 to X_1,

(iii) screened Coulomb.

The relaxation time expression for the polar optical and interband (Γ_1 to L_1) scattering have already been given in the previous section, equations IV-19 and IV-21 For scattering between Γ_1 and X_1 bands a density of states mass of 1.2 m was assumed for the X_1 band together with a temperature independent minima separation of 0.315eV. In the screened Coulomb scattering relaxation time, it was assumed that both the heavy electrons in the L_1 and X_1 conduction bands and the heavy holes contribute to the same extent as the ionized impurities. Hence, the effective density of scattering centres is given by:

$$N_I^* = N_a + n_2(T) + n_3(T) + p_h(T) \qquad \text{II-28}$$

This method of accounting for scattering of the light electrons by heavy holes was proposed by Ehrenreich (57E1) and used in calculations of electron mobility in the Γ_1 band of InSb.

With the above assumptions about the total density of effective Coulomb scattering centres, the relaxation time τ_I was calculated using equation II-29 and II-32, together with the Fermi energy determined from fitting R(T) and σ(T) data on the p-type sample. The Fermi energy is required in the calculation of the screening length, from equation IV-33.

It can be seen from Fig. IV-16 that the calculated mobility curve lies about 10% above the values of mobility deduced from the experiment. This is not unexpected since we have neglected in these calculations any effect of electron-electron interaction which would tend to reduce the calculated mobility, as was pointed out by Ehrenreich (59E1) with regard to the electron mobility in the Γ_1 band of InSb at high temperatures. With these considerations in mind, the agreement between the calculated and experimentally deduced temperature dependence of the mobility of electrons in the Γ_1 band of GaSb can be considered satisfactory.

IV-333 Calculation of the scattering parameter r in the Γ band

Having obtained the total relaxation time $\tau(\varepsilon, T)$, taking into account the two scattering models discussed in the last section, it was then possible to calculate the scattering parameter r as a function of temperature T and magnetic field B. It is easily shown that r_1 is given by:

$$r_1(B) = \frac{\left\langle \frac{\tau^2}{m_c^{*2}(1+\omega^2\tau^2)} \right\rangle}{\left\langle \frac{\tau}{m_c^*(1+\omega^2\tau^2)} \right\rangle^2 + \left\langle \frac{\tau^2\omega}{m_c^*(1+\omega^2\tau^2)} \right\rangle^2} \qquad \text{IV-29}$$

where

$$\omega = eB/m_c^*$$

at low fields ($\omega^2\langle\tau^2\rangle << 1$) this reduces to

$$r_1 = \frac{\left\langle \frac{\tau^2}{m_c^{*2}} \right\rangle}{\left\langle \frac{\tau}{m_c^*} \right\rangle^2} \qquad \text{IV-30}$$

With the aid of equation II-39 which defines the average <>, r_1 was calculated for B = 0.2, 0.87, 2.0 and 3.0 Wb/m^2 as a function of temperature ($25^o < T < 360^o$). The results are shown in Figs. IV-17 and IV-18. From these, it can be seen that r_1 is nearly unity over the full range of temperature, the total variation being less than 6% between 25^oC and 360^oC, and <1% over the range (25^oC - 120^oC) where magnetoresistance measurements were analysed. It can also be seen that over the range of magnetic fields used in magnetoresistance measurements, i.e. 1.4 to 3.2 Wb/m^2, the scattering parameter r_1 is only weakly dependent on B. Hence, the assumption that $r_1 = 1.00$, which was used in the analysis of magnetoresistance results, is justified.

IV-334 Calculation of the magnetoresistance coefficient

The analysis of the two band magnetoresistance and Hall coefficient was carried out on the assumption that the magnetoresistance due to individual bands was negligible in comparison with the two band effect. In order to check whether this assumption is valid for the Γ_1 band, in which the magnetoresistance arises because of the energy dependence of the relaxation time, we have calculated the coefficient, ξ, (Smith 59S1, p. 124, eqn. 167), using τ's obtained for the two models in section IV-332. The results are shown in Fig. IV-19. From these, we estimated $\Delta\rho_1/\rho_1$ for three temperatures and B = 3.0 Wb/m^2, using the values of R_1 and σ_1 from Table IV-2a. The following results are obtained:

T^oC	$\Delta\rho_1/\rho_1$
25	3.2%
120	3.5%
200	4.8%

It is seen that the contribution of the Γ_1 band magnetoresistance to the total magneto-

resistance increases with temperature, as expected, but even at 200°C is not very large.

IV-4 Summary, Discussion and Conclusion

IV-41 Summary

Magnetoresistance measurements as a function of field B and temperature T ($25 < T < 120^{o}C$) together with low field ($B < 0.9$ Wb/m^2) Hall coefficient were used to determine n_1, n_2, μ_1 and μ_2. The variation of n_1 and n_2 with temperature was then employed to show that $E_{20} = 0.099 + .02$ eV and $\alpha_2 = -3.4 \pm 0.1 \times 10^{-5}$ eV/°K. The Kane model was used for the Γ_1 band and the L_1 band was assumed to be parabolic. The low field Hall coefficient in the temperature range 25 - 360°C was then analysed taking into account the third set of conduction band minima with X_1 symmetry and the heavy hole valence band, Γ_{15}.

It was found that including these two extra bands (X_1 and Γ_{15}) in the analysis of R(T) and σ_o(T) was insufficient to explain the shape of these curves, whatever parameters were chosen for the X_1 band. The effect of the valence band was found to be negligible. The shape of the R vs. T curve was then explained on the basis of a change in the dominant scattering mechanism in both bands. The parameters for the <100> minima were estimated by comparison with the <100> minima in GaAs and GaP. Using these parameters, together with previously determined parameters for the L_1 and Γ_1 minima, R(T) and σ_o(T) were fitted simultaneously giving μ_1(T) and μ_2(T). The value of μ_2(T) was affected considerably more than μ_1(T) by the choice of parameters for the X_1 band. The mobility μ_2(T) was then fitted using an approximate method which assumed that the two operative scattering mechanisms were ionized impurity and deformation potential, and use being made of Matthiessen's rule for the

addition of mobilities. The fitting gave estimates of the total ionized impurity $N_I \sim 2 \times 10^{24}$ m^{-3} and the deformation potential of ~9 eV.

The mobility of electrons in the Γ_1 band was then fitted assuming two models. The first model included four scattering mechanisms with relaxation times τ_{po}, τ_{ib}, τ_I and τ_{sc}. The assumption of a value of ionized impurity density N_I of 2.2×10^{24} m^{-3}, as estimated above, left two undetermined parameters D_{12} and $(N_s Q_s)$ in the expression for the effective relaxation time τ. These were used as adjustable parameters in fitting $\mu_1(T)$ and a good fit was obtained with $D_{12} = 3.2 \times 10^8$ eV/cm and $(N_s Q_s) = 4.8 \times 10^4$ cm^{-1}. In the second model, spacecharge scattering was not included, and so the mobility was determined by only τ_{po}, τ_{ib} and τ_I. In this case, D_{12} and N_I were used as adjustable parameters, with the best fit being obtained with $D_{12} = 3.0 \times 10^8$ eV/cm and $N_I = 4.2 \times 10^{24}$ m^{-3}. This value of N_I is double that determined from the fitting of the $\mu_2(T)$ data. However, in obtaining the latter value, no account was taken of (a) scattering of the Γ_1 electrons by the heavy electrons in the L_1 minima, (b) the possibility that the acceptors are doubly charged and (c) the difference in the effective screening by the heavy and light electrons. Taking account of these effects in the calculation of τ_I, the $\mu_1(T)$ data were fitted using $N_a^=$ and D_{12} as adjustable parameters, with best fit being obtained for $N_a^= = 1.1 \times 10^{23}$ m^{-3} and $D_{12} = 4.1 \times 10^8$ eV/°K.

Having obtained the relaxation time $\tau(E, T)$ on the basis of the two models the scattering parameter r_1 was then calculated for the Γ_1 band as a function of temperature at four fields, B = 0.2, 0.87, 2 and 3 Wb/m^2. It was found that r_1 was close to unity and varied only slowly with both B and T.

Since the analysis of magnetoresistance measurements against field was based on the assumption that the contributions of the individual bands to the total magnetoresistance were small in comparison with the two band effect, we also calculated the magnetoresistance coefficient ξ for the Γ_1 band. The magnitude of $\Delta\sigma_1/\sigma_1$

was found to be 3.2% at B = 3 Wb/m^2 at 25°C, increasing to 4.8% at 200°C.

The analysis of the data on the p-type sample was made in two stages. First the "low" temperature data were analysed to determine the mobility variation of the light and heavy holes as a function of temperature. Then the complete curves of R and σ_o were analysed using these temperature dependent mobilities for the holes, together with conduction band parameters obtained from analyses of data on sample N2, and using μ_1 and μ_2 as adjustable parameters. These analyses yielded the temperature dependence of mobilities μ_1 and μ_2 at temperatures above 400°C. The electron mobility μ_1 in the Γ_1 band was then calculated from a relaxation time approximation for the same range in temperature, and values obtained were in reasonable agreement with the above experimental values.

IV-42 Discussion

The analysis of the magnetoresistance measurements as a function of magnetic field and temperature were based on the assumption that the observed magnetoresistance is purely a two band effect. The validity of this assumption has already been discussed in section II-7, where we have used the results for the magnetoresistance coefficient of the Γ_1 band given in the previous section. From these considerations alone, we would be justified in using the analysis even above 120°C. However, because of the proximity of the <100> band, and the resulting loss of electrons to this band, the validity of the two band model is questionable at temperatures above this value. Therefore, only the results obtained at temperatures below 120°C were used in determining the energy gap of the Γ_1 and L_1 band and its temperature dependence. To do this, we had to make some further assumptions. Firstly, to obtain n_1 and n_2 from R_1 and R_2 we assumed that the scattering parameters were equal to 1.0

and 1.18 respectively and remained constant with temperature. It was shown that putting r_1 = constant = 1.0 was quite reasonable, its variation (Fig. IV-17) with temperature and magnetic field was a maximum of 8% over the full temperature range. On the other hand, the value of r_2 = 1.18 was used because of a lack of understanding of the scattering processes in the L_1 minima, and although the magnitude may be in error, the fact that the resulting values of $n_1 + n_2 = n_t$ remained constant over the temperature range $25 < T < 120^oC$ indicates that the assumption that r_2 remains constant with T is indeed a valid one.

We also had to assume a linear form for the temperature dependence of E_2. We should have, in principle, used the Varshni (67V1) relation for the temperature dependences of the direct ($\Gamma_{15v} - \Gamma_{1c}$) and the indirect ($\Gamma_{15v} - L_{1c}$) gaps, and taken the difference to obtain E_2. But, although we know the values of α_o and θ_o for the direct, no values are available for the indirect gap. This would leave us with one additional unknown parameter. Since as has already been pointed out in section II-8, the Varshni relation becomes linear at elevated temperatures, it was felt that rather than have one more adjustable parameter, making the fitting more difficult and unreliable, the use of a linear form of $E_2(T)$ would be preferable. As a consequence, the value of E_{20} = 0.099 ± .002 eV which was obtained, is somewhat higher than the actual band gap at 0^oK. The value agrees very well however with the value of E_{20} = 0.095 ± .005 eV obtained by Yep and Becker (67Y1) at 4.2^oK and also with results obtained by re-analysing Harland's (65H1) data of magnetoresistance on GaSb at 4.2^oK, which gave a value of E_{20} = 0.093 ± .003 eV (see Appendix A). It is also in agreement with the value of 0.087 eV at room temperature which was obtained by Rosenbaum (72R1) from pressure measurements on two samples. One of these was cut from our sample N2 and the second also from material doped with Te, but with lower total electron density.

It should be pointed out that the values of E_{20} and α_2 obtained from this analysis are dependent on the effective masses in the two bands. We have used a value of $m^*_{10}(0) = 0.040m$ for the bottom of the band effective mass in the Γ_1 band. This value was determined by Yep and Becker (66Y1) at 4.2°K and was later used by Baxter et al. (67B1) in the analysis of mobility at 78°K on n-GaSb. The choice of this value over other published values, e.g. 0.052 ± 0.002m (61B1) and 0.047 ± 0.003m (59Z1), was made because in the determination of $m^*_{10}(0) = 0.040m$, Yep and Becker (66Y1) took into account the non-parabolicity of the band, and this was not done in the other cases.

The value of the density of states effective mass in the L_1 band, m^*_{2d}, is still less certain. We have used Van Tongerloo's (69T1) value of 0.226m obtained from Faraday rotation measurements at room temperature. It agrees with the result of Piller (63P1, 64P1) who found $m^*_{2d} = 0.228m$ and with the Germanium value of 0.22m (59S1). However, these values are intricately dependent on other assumptions and parameters used in the analysis by which they were obtained, hence can at best be considered to be estimates of the value of m^*_{2d}. The value of E_{20} is quite insensitive to m^*_{2d}, but α_2 is sensitive, and this is the reason, in part, for such large variations in the reported values of α_2.

From consideration of the published values of m^*_{2d}, we estimate that the value of 0.226m is probably the lower limit for the density of states effective mass of the electrons in the L_1 minima. In that case, our value of -3.4×10^{-5} eV/°K^{-1} is also a lower limit. Any increase in m^*_{2d} will make this value more positive. If we double m^*_{2d} (i.e. $m^*_{2d} = .452m$), we obtain a value of $\alpha_2 = +5.4 \times 10^{-5}$eV/°K^{-1}.

Both scattering models gave an essentially good fit to the $\mu_1(T)$ values determined from measurements on the n-type sample N2, and thus on this basis alone, we are unable to reject either model. In fact, we believe that although we obtained

good agreement between the experimental and calculated results when spacecharge scattering was neglected and scattering by heavy electrons included, the correct model can not completely exclude τ_{sc}. We are led to this conclusion for two reasons. Firstly, the scattering cross section of the heavy electrons must be smaller than that of ionized impurities because the former are not stationary. Secondly, the results of measurements by Demars (72D1) of longitudinal and transverse Nernst-Ettingshausen (N-E) coefficients as a function of magnetic field on the same sample at 300°K indicate that some spacecharge scattering must be present. Demars used the relaxation times calculated by the present author for 300°K in the calculation of both longitudinal and transverse N-E coefficients, and found that although good agreement between the calculations and experiment existed for the variation of the longitudinal N-E coefficient as a function of B, less satisfactory agreement was obtained for the transverse N-E coefficient when spacecharge scattering was completely neglected. From our results it is not possible to determine to what extent spacecharge must be included since that would add an extra adjustable parameter ($N_s Q_s$) which has a similar effect on μ_1 at low temperatures as does $N_a^=$.

These calculations have shown that the mobility of $\sim 0.4 m^2/V.$ sec for electrons in the Γ_1 minimum at 300°K is not at all unreasonable when account is taken of Coulomb scattering by both ionized impurities and the heavy L_1 electrons. A further improvement in calculating the mobility in this band can be made by variational calculations, but this type of calculation is beyond the scope of this thesis. Such calculations could take into account quantum mechanical corrections such as those described by Moore (67M1), and any effect of electron-electron interactions of the Γ_1 band electrons which may become important at higher temperatures.

A rough comparison with the electron mobility in the Γ_1 band of GaAs further

shows that a value of $\sim 0.4 m^2/V.sec$ is not unreasonable for the mobility in the Γ_1 band of GaSb. Using the value of $\mu_1(GaAs) \simeq 0.22 m^2/V.sec$ obtained from Moore's (67M1) data for a sample with $N_I^* = 4 \times 10^{24} m^{-3}$ and $\mu_1(GaAs) = 0.93 m^2/V.sec$ for a pure sample (60E1) at room temperature, then the mobility due to ionized impurities scattering alone is estimated to be $\mu_I(GaAs) = 0.288 m^2/V.sec$. If all other effects are assumed to be equal, the ionized impurity mobility is inversely proportional to $(m_c^*)^{1/2}$, and hence:

$$\frac{\mu_I(GaAs)}{\mu_I(GaSb)} \simeq \left(\frac{0.04}{0.07}\right)^{1/2}$$

Thus $\mu_I(GaSb) \simeq 1.3 \times \mu_I(GaAs) = 0.375 m^2/V.sec$. which is close to the value of $0.376 m^2/V.sec$ obtained for sample N2 and is in the range of values quoted in the literature by other authors.

The analyses of the experimental results of R and σ on the P1 sample also lead to an estimate of the temperature dependence of electron mobility μ_1 in the Γ_1 conduction band at $T > 400^oC$. Calculations of the Γ_1 electron mobility from a theoretical model, based on relaxation time approximations and including scattering by optical phonons, Coulomb centres and interband scattering into L_1 and X_1 band, agree reasonably well in magnitude and temperature with the results determined from fitting R and σ. The calculated values lie about 10% above the determined values. This discrepancy can be explained by the neglect of electron-electron interactions in the Γ_1 band which would tend to reduce the calculated mobility still further. However, within the scope of the relaxation time approximation the electron-electron interactions could not be taken into account. The agreement of 10% that was obtained can therefore be regarded as satisfactory.

IV-43 Conclusion

The two band model was used in the analysis of the magnetoresistance data on sample N2. It was then possible to determine the Γ_1 - L_1 band separation (E_{20} = 0.099 eV) and its temperature dependence (α_2 = -3.4 x 10^{-5} eV/^oK). The value of 0.099 eV for E_{20} agrees very well with the value 0.095 ± .005 eV determined by Yep and Becker (66Y1) at liquid helium temperature and with Rosenbaum's (72R1) room temperature value of 0.087 eV.

It was found that screened Coulomb scattering plays an important role in determining the electron mobility in the Γ_1 band. A value for the coupling constant D_{12} of 4.1 x 10^8 eV/cm was also estimated as well as the deformation potential of ∿9 eV for the L_1 band. This estimate of the deformation potential agrees very well with the value of ∿10 eV reported recently by Sherwood (70S1).

The analyses of the data on the p-type sample led to the following conclusions:

(a) scattering in the valence band is dominated by polar optical interactions,

(b) the temperature coefficient of the principal gap, α_o, is -5.4 x 10^{-4} eV/^oK.

In addition, electron mobility in the Γ_1 band of GaSb was estimated at T > 400^{o}C by fitting the experimental results of R(T) and σ(T). These results were then compared with calculated values of mobility based on the relaxation time approximation and an acceptable agreement was obtained.

The overall agreement obtained between our results on GaSb and those of Demars and Rosenbaum supports the claim that the parameters which were determined are in fact representative of GaSb.

TABLE IV-1

T^oC	t Wb^2/m^4	u	s Wb^2/m^4	a	$-R_o \times 10^6$ $Coul/m^3$	$\sigma_o \times 10^{-4}$ $\Omega^{-1}m^{-1}$
25	47.09	0.806	101.5	2.58	9.249	3.103
40	48.35	0.929	97.55	2.50	9.370	2.881
60	49.28	1.042			9.521	2.633
80	51.75	1.154			9.660	2.388
100	53.87	1.253	69.17	2.80	9.764	2.191
120	57.18	1.427			9.836	2.016
140	60.33	1.531			9.899	1.854
160	64.79	1.846			10.018	1.653
200	70.77	2.066			10.121	1.466

Table IV-1: The slopes (t, s) and intercepts (u, a) obtained from $\sigma_o/\Delta\sigma$ and $-R_o/\Delta R$ vs. B^{-2} plots and the zero field Hall coefficient R_o and σ_o for sample N2 of n-GaSb.

TABLE IV-2

$T^{o}C$		(i)	(ii)	(iii)
25	$\sigma_1 \times 10^{-4}$	2.275	2.221	2.284
	$\sigma_2 \times 10^{-4}$	0.827	0.882	0.819
	$-R_1 \times 10^{5}$	1.648	1.670	1.638
	$-R_2 \times 10^{6}$	5.48	6.73	5.33
40	$\sigma_1 \times 10^{-4}$	2.057	1.995	2.039
	$\sigma_2 \times 10^{-4}$	0.824	0.886	0.842
	$-R_1 \times 10^{5}$	1.755	1.791	1.777
	$-R_2 \times 10^{6}$	5.20	8.23	5.48
100	$\sigma_1 \times 10^{-4}$	1.283	1.152	1.336
	$\sigma_2 \times 10^{-4}$	0.908	1.039	0.855
	$-R_1 \times 10^{5}$	2.561	2.877	2.416
	$-R_2 \times 10^{6}$	5.72	8.06	5.13

Table IV-2: Comparison of calculated values of R_1, R_2, σ_1 and σ_2 using the three combinations of experimental parameters (i) R_o, σ_o, s and t, (ii) R_o, σ_o, s and a, (iii) R_o, σ_o, t and u.

TABLE IV-2a

T^oC	$-R_o m^3/Coul$ x 10^6	$\sigma_o (\Omega.m.)^{-1}$ x 10^{-4}	$\sigma_1 (\Omega.m.)^{-1}$ x 10^{-4}	$\sigma_2 (\Omega.m.)^{-1}$ x 10^{-4}	$-R_1 m^3/Coul$ x 10^5	$-R_2 m^3/Coul$ x 10^6
25	9.249	3.103	2.260	.843	1.664	5.33
40	9.370	2.881	2.039	.842	1.777	5.48
60	9.521	2.633	1.773	.860	1.974	5.37
80	9.660	2.388	1.530	.858	2.189	5.26
100	9.764	2.191	1.336	.855	2.416	5.13
120	9.836	2.016	1.160	.856	2.689	5.19
140	9.899	1.854	1.013	.841	2.967	5.01
160	9.956	1.714	.872	.842	3.376	5.03
170	10.018	1.652	.815	.837	3.574	5.13
200	10.121	1.466	.662	.804	4.224	4.98

Table IV-2a: Calculated values of R_1, R_2, σ_1 and σ_2 using magnetoresistance results together with zero field values of Hall coefficient. (R_o) and conductivity (σ_o), i.e. combination (iii) R_o, σ_o, t and u.

TABLE IV-3

T^oC	n_1 m^{-3} x 10^{-23}	n_2 m^{-3} x 10^{-24}	n_t m^{-3} x 10^{-24}	μ_1 $m^2/V.sec$	μ_2 $m^2/V.sec$
25	3.757	1.07	1.45	.3760	.0491
40	3.517	1.11	1.46	.3623	.0475
60	3.167	1.13	1.45	.3500	.0474
80	2.855	1.16	1.44	.3348	.0464
100	2.587	1.19	1.45	.3229	.0448
120	2.106	1.22	1.43	.3007	.0432
160	1.852	1.22	1.40	.2944	.0432
170	1.749	1.19	1.36	.2914	.0441
200	1.480	1.22	1.37	.2797	.0411

Table IV-3: Calculated values of n_1, n_2, μ_1 and μ_2 using the values of Table IV-2a for R_1, R_2, σ_1 and σ_2 and assuming that $r_1 = 1.00$ and $r_2 = 1.18$, both constant with temperature. The value of n_t is obtained by adding n_1 and n_2.

TABLE IV-4

m^*_{10}	=	0.0402m	(66Y1)
m^*_{2d}	=	0.226m	(69T1)
ν_2	=	4	(69P1)
m^*_{3d}	=	0.36m	(60E1)
ν_3	=	6	(60E1)
m^*_h	=	.33m	(68W1)
E_{oo}	=	0.813 eV	(64M1)
$*\alpha_o$	=	-5.0×10^{-4} eV/^oK	
$*\theta_o$	=	112 ^oK	
E_2	=	Variable	
α_2	=	Variable	
E_3	=	0.315 eV	(68K1)
α_3	=	0.0	
K_2	=	8.6	(64P1)
K_3	=	3.6	(60E1)

Table IV-4: Band parameters used in fitting the GaSb data on sample N2. The list of references on the right give the source from which the parameters were obtained.

* Values obtained by fitting the absorption data as a function of temperature of Woolley and Evans (61W1) for GaSb.

TABLE IV-5

T^0C	$n_1 m^{-3}$ x 10^{-23}	$n_2 m^{-3}$ x 10^{-24}	$n_3 m^{-3}$ x 10^{-22}	E_F eV
25	3.81	1.066	-	.0315
40	3.52	1.096	-	.0268
60	2.17	1.131	.1	.0203
80	2.86	1.162	.2	.0136
100	2.59	1.187	.3	.0067
120	2.35	1.209	.5	-.0004
140	2.15	1.230	.6	-.0076
160	1.97	1.246	.9	-.0150
170	1.88	1.252	1.0	-.0188
200	1.66	1.268	1.4	-.0304

Table IV-5: Results of fitting the temperature variation of n_1 given in Table IV-3 and using the band parameters given in Table IV-4, together with E_{20} = 0.099 eV, α_2 = -3.4 x 10^{-5} eV/^oK, and n_t = 1.45 x $10^{24} m^{-3}$.

TABLE IV-6

T	=	$78^{o}C$
R_o	=	6.483×10^{-6} m^{-3}/Coul.
σ_o	=	8.525×10^{4} $(\Omega.m.)^{-1}$
s	=	119.3
a	=	0.744
σ_1	=	8.239×10^{4} $(\Omega.m.)^{-1}$
σ_2	=	0.286×10^{4} $(\Omega.m.)^{-1}$
R_1	=	-6.683×10^{-6} m^{3}/Coul.
R_2	=	-2.13×10^{-4} m^{3}/Coul.
n_1	=	9.356×10^{23} m^{-3} for $r_1 = 1.00$
n_2	=	0.570×10^{23} m^{-3} for $r_2 = 1.93$
n_t	=	9.926×10^{23} m^{-3}

Table IV-6: The results from analysis of measurements at $78^{o}K$

TABLE IV-7

T°C	$n_1 m^{-3}$ x 10^{-23}	$n_2 X\ m^{-3}$ x 10^{-24}	$n_3 X\ m^{-3}$ x 10^{-22}	$\mu_1 m^2$/V.sec	$\mu_2 m^2$/V.sec	E_F eV
25	3.806	1.066	0.03035	0.3738	0.04822	0.0315
40	3.518	1.096	0.04656	0.3621	0.04784	0.0268
60	3.170	1.131	0.07733	0.3496	0.04737	0.0203
80	2.863	1.162	0.1211	0.3343	0.04595	0.0136
100	2.591	1.187	0.1805	0.3224	0.04488	0.0067
120	2.558	1.213	0.2585	0.3104	0.04342	-0.0003
140	2.147	1.230	0.3559	0.2984	0.04196	-0.0076
160	1.965	1.246	0.4761	0.2876	0.04045	-0.0150
170	1.886	1.255	0.546	0.2831	0.03960	-0.0187
200	1.670	1.274	0.7906	0.2667	0.03679	-0.0302
220	1.544	1.284	0.9846	0.2570	0.03507	-0.0381
240	1.349	1.294	1.208	0.2476	0.03328	-0.0460
260	1.339	1.300	1.454	0.2385	0.03162	-0.0542
280	1.254	1.306	1.730	0.2297	0.02985	-0.0624
300	1.179	1.313	2.033	0.2212	0.02815	-0.0707
320	1.110	1.316	2.359	0.2131	0.0266	-0.0792
340	1.048	1.319	2.709	0.2056	0.02513	-0.0878
360	0.9934	1.323	3.089	0.1982	0.02363	-0.0964

Table IV-7: The values of carrier concentrations n_1, n_2, n_3 and mobility μ_1 and μ_2, obtained from fitting R(T) at 0.87 Wb/m^2 and $\sigma_o(T)$ with μ_1 and μ_2 adjustable. Remaining parameters were those of Table IV-4 in addition to E_{20} = 0.099 eV, $\alpha_2 = -3.4 \times 10^{-5}$ eV/°K and $n_t = 1.45 \times 10^{24} m^{-3}$.

TABLE IV-8

	Si	GaP	GaAs
m_3^*	$0.33m^{(a)}$	$0.34m^{(b)}$	$0.36m^{(c)}$
$\mu_{300}(m^2/V.sec.)$	$.130^{(a)}$	$\sim.010^{(d)}$	$.0155^{(c)}$
α_3 eV/°K x 10^4	$-7.0^{(e)}$	$-6.2^{(f)}$	$-5.4^{(g)}$
θ_3 °K	$1110^{(e)}$	$460^{(f)}$	$208^{(g)}$
α_3' (500) x 10^5		+9	+3
α_3' (700) x 10^5		+6	+1

(a) Smith (59S1), (b) Madelung (64M1), (c) Conwell and Vassell (68C1), (d) Montgomery (68M1), (e) Varshni (67V1), (f) Panish and Casey (69P1), (g) This thesis-Chapter V.

Table IV-8: Parameters of the <100> minima in three semiconductors Si, GaP and GaAs and estimates of the temperature dependence $\alpha_3(\equiv\alpha_3')$ using these values together with α_o = -5.0 x 10^{-4} eV/°K., θ_o = 112°K for the fundamental gap temperature variation (c.f. Table IV-4).

TABLE IV-9

$m^*_{10}(0)$	=	0.040m	(67Y1)
m^*_{2d}	=	0.226m	(69T1)
$h\omega_\ell$	=	0.0292 eV	(64M1)
ω_{12}	=	$0.8\omega_\ell$ sec^{-1}	
N_I	=	$2.2 \times 10^{24} m^{-3}$	

Table IV-9: The conduction band parameters of the Γ_1 band used in calculations of electron mobility μ_1 in this band.

TABLE IV-10

$T^{o}C$	n_1 m^{-3} $\times 10^{22}$	n_2 m^{-3} $\times 10^{23}$	n_3 m^{-3} $\times 10^{22}$	p_h m^{-3} $\times 10^{24}$	p_ℓ m^{-3} $\times 10^{22}$	μ_1 $m^2/V.sec.$	μ_2 $m^2/V.sec.$
23.5				.2668	1.344		
40				.2790	1.405		
80				.3028	1.525		
120				.3224	1.623		
160				.3342	1.683		
200				.3506	1.765		
240				.3608	1.817		
280	.0132	.0127	.0028	.3698	1.862		
320	.0528	.0585	.0174	.3808	1.915		
360	.1742	.2191	.0853	.414	2.022		
400	.4721	.6632	.3278	.4502	2.267		
420	.7198	1.065	.5864	.4924	2.480	.2169	.0211
440	1.046	1.625	.9921	.5499	2.769	.2039	.0192
460	1.451	2.364	1.590	.6279	3.162	.1909	.0169
480	1.945	3.311	2.441	.7262	3.657	.1789	.0155
500	2.522	4.473	3.605	.8496	4.278	.1679	.0150
520	3.188	5.893	5.156	1.000	5.037	.1549	.0137
540	3.945	7.580	7.181	1.181	5.949	.1409	.0127

Table IV-10 Results of analyses of the Hall coefficient and conductivity data on sample P1.

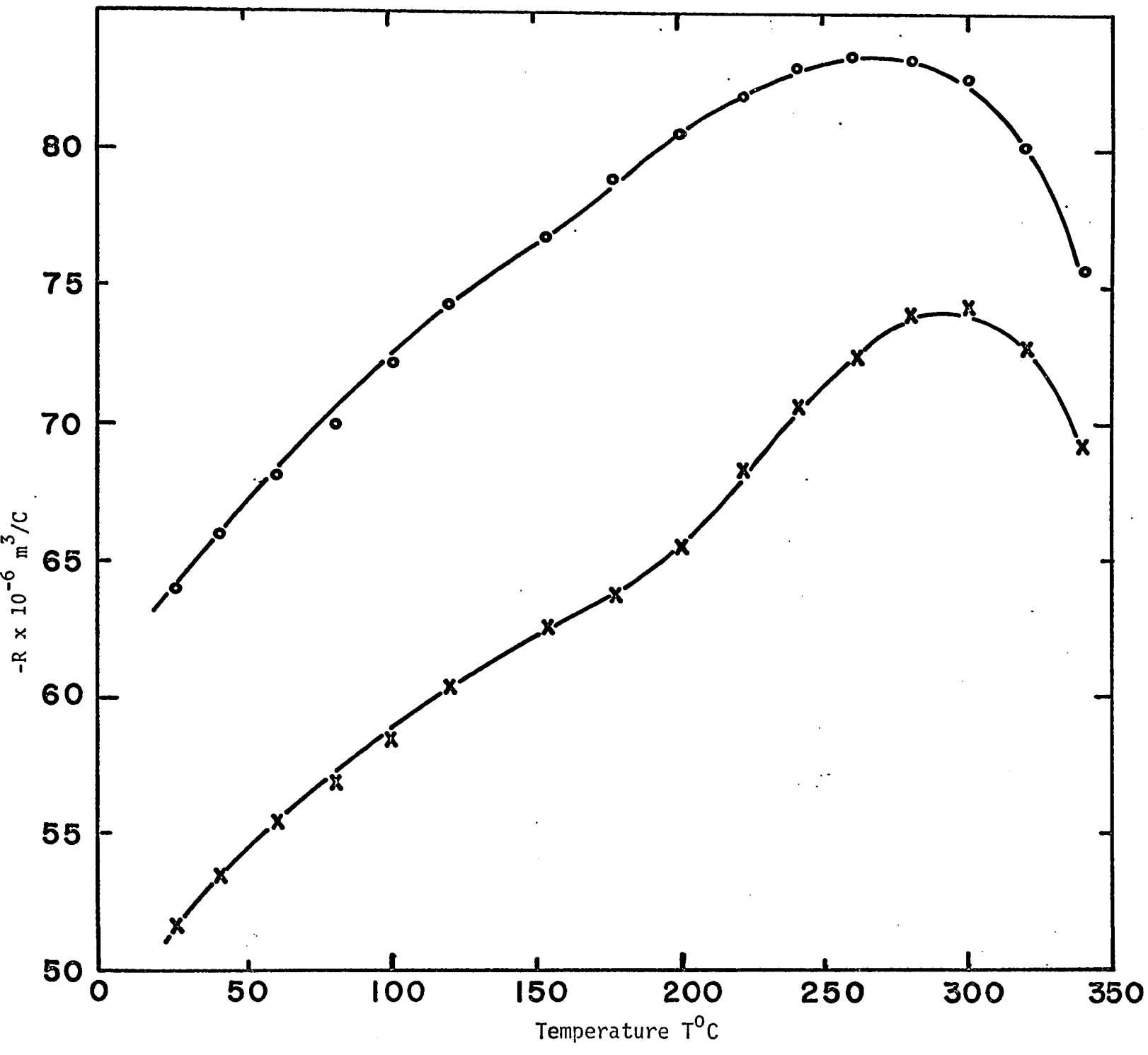

Fig. IV-1 Hall coefficient R vs. Temperature T°C for two sets of Hall probes (2-6) and (3-5), GaSb sample N1.

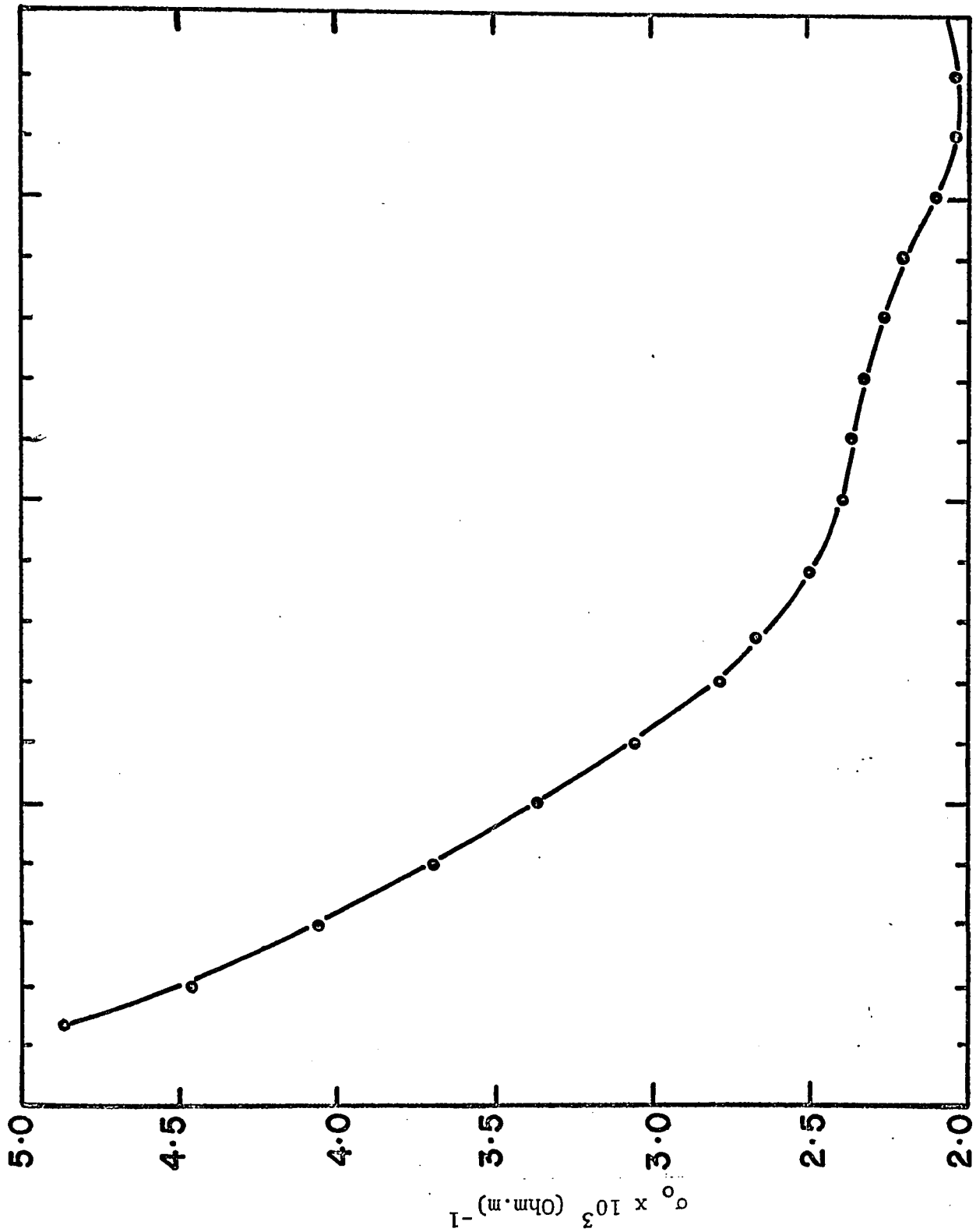

Fig. IV-2 Average conductivity σ_o vs. temperature T°C for GaSb sample N1.

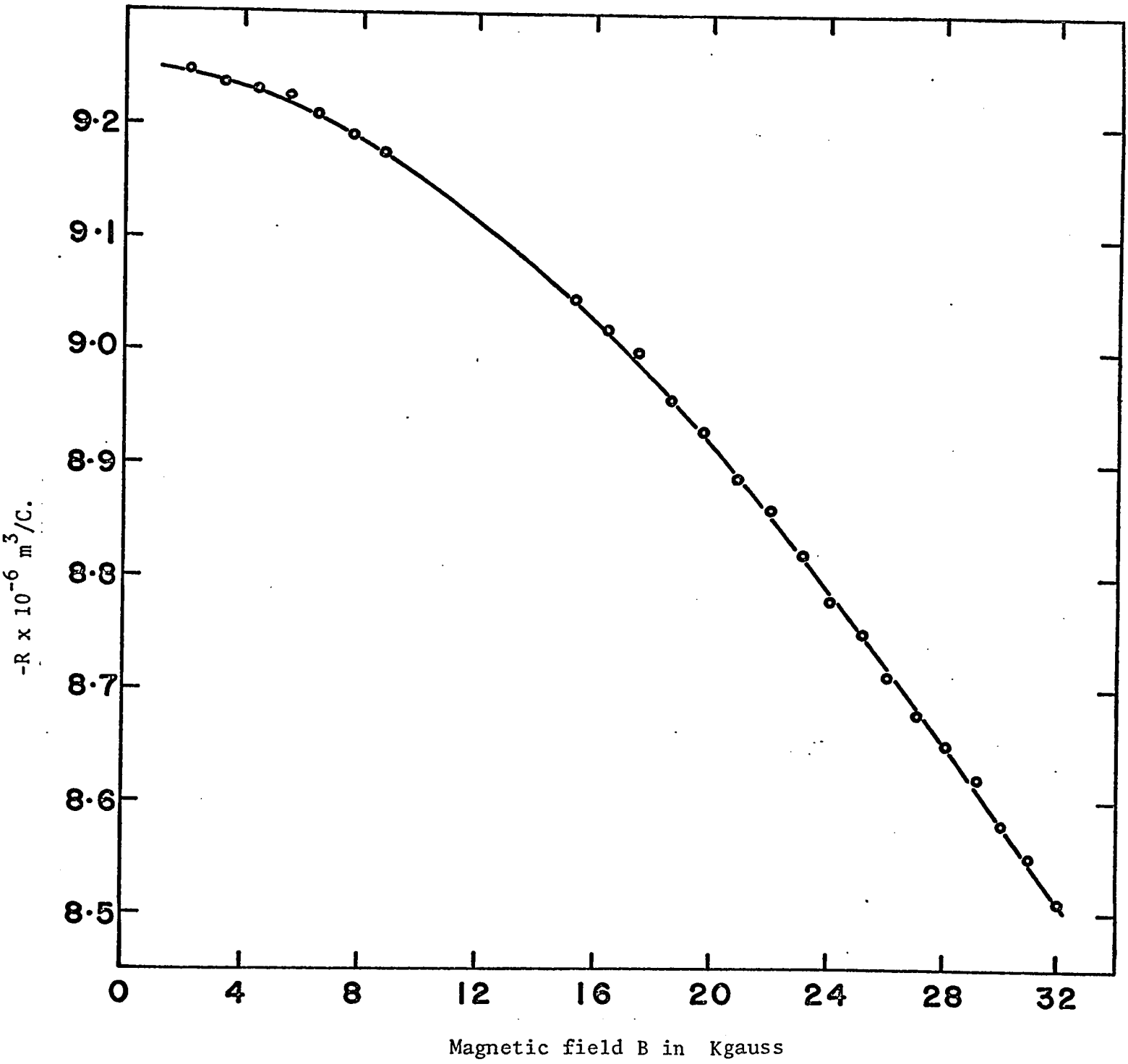

Fig. IV-3 Measured Hall coefficient R vs. B at 25°C for GaSb sample N2.

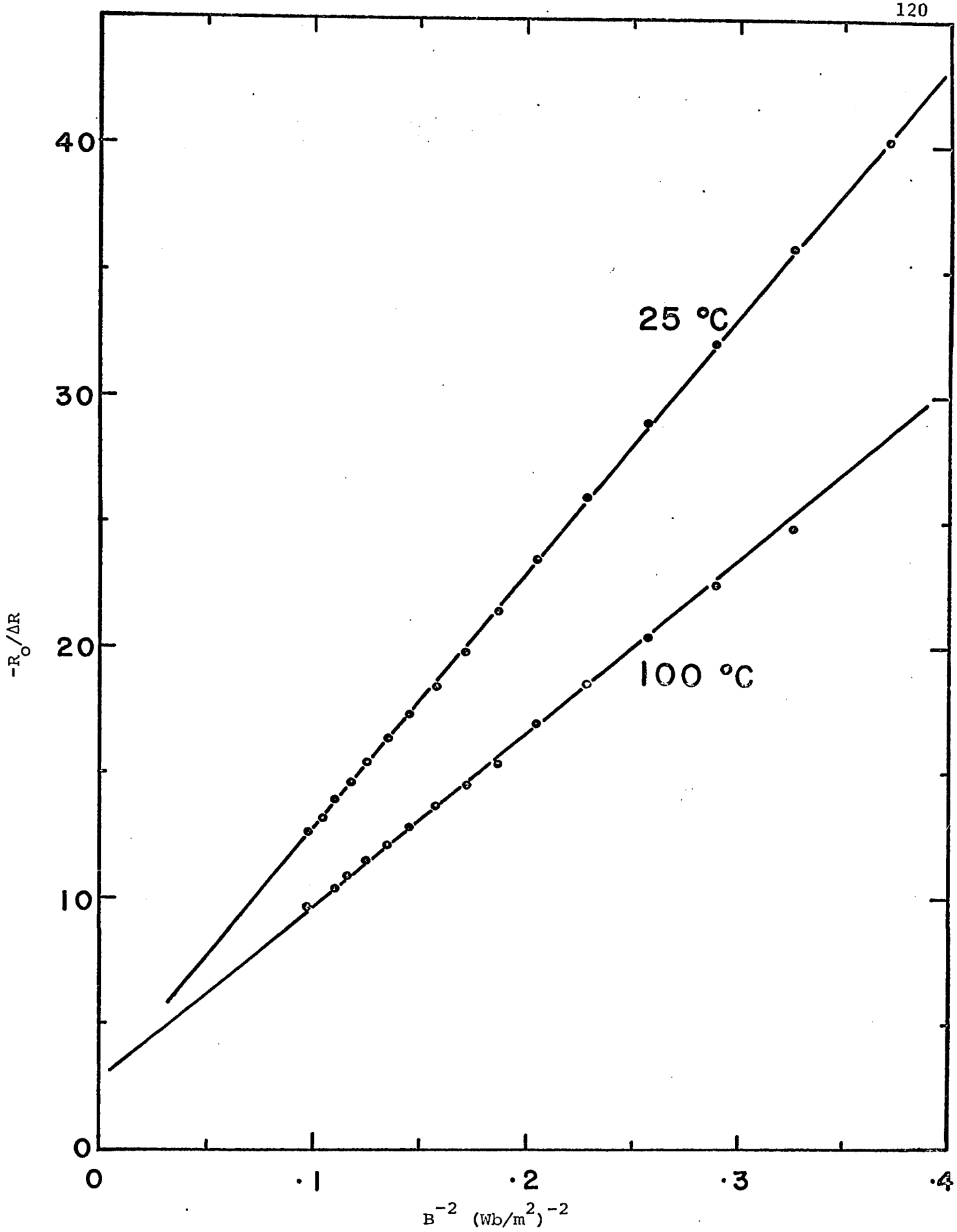

Fig. IV-4 Plots of $-R_o/\Delta R$ vs B^{-2} at two temperatures for GaSb sample N2.

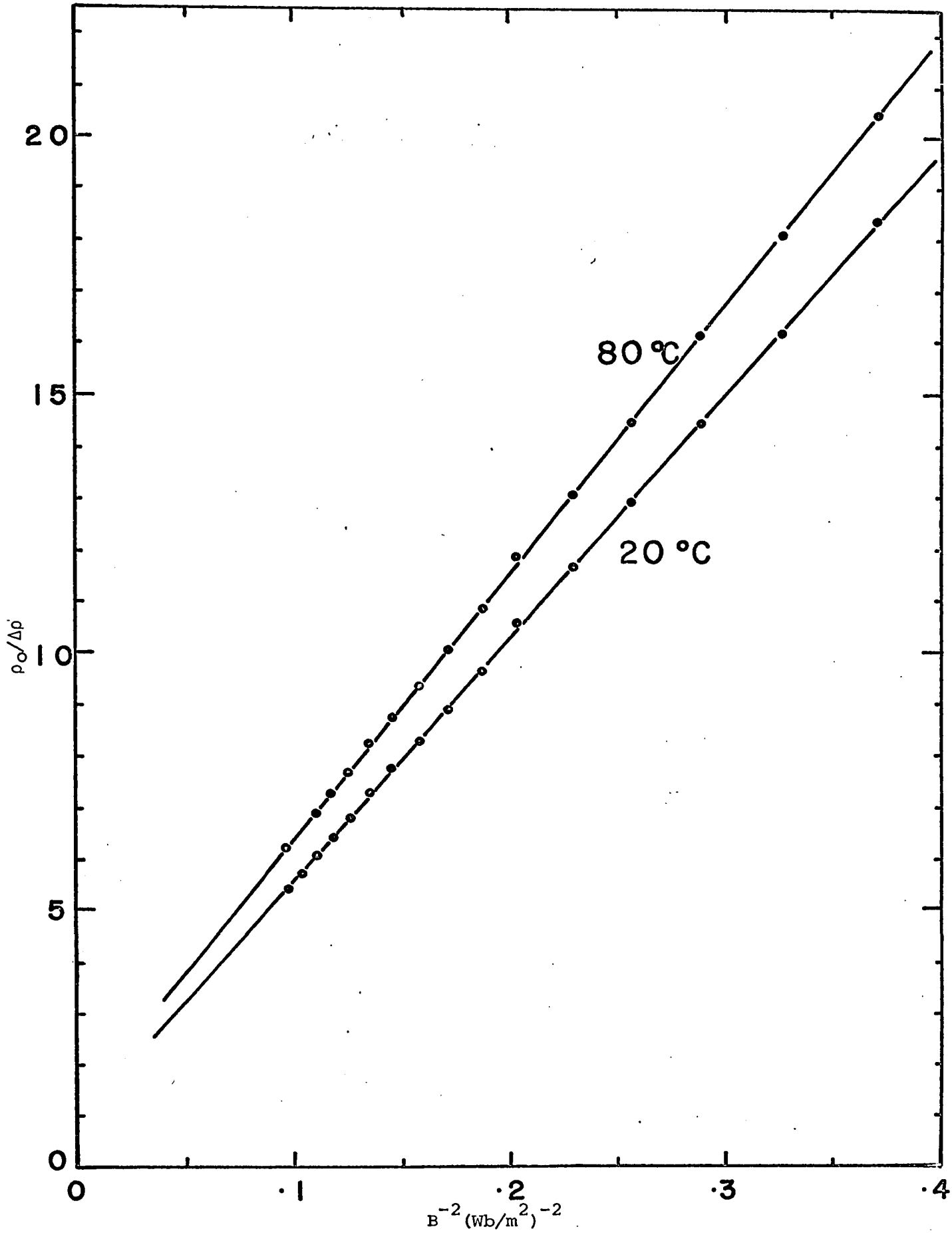

Fig. IV-5 Plots of $\rho_o/\Delta\rho$ vs B^{-2} at two temperatures for GaSb sample N2

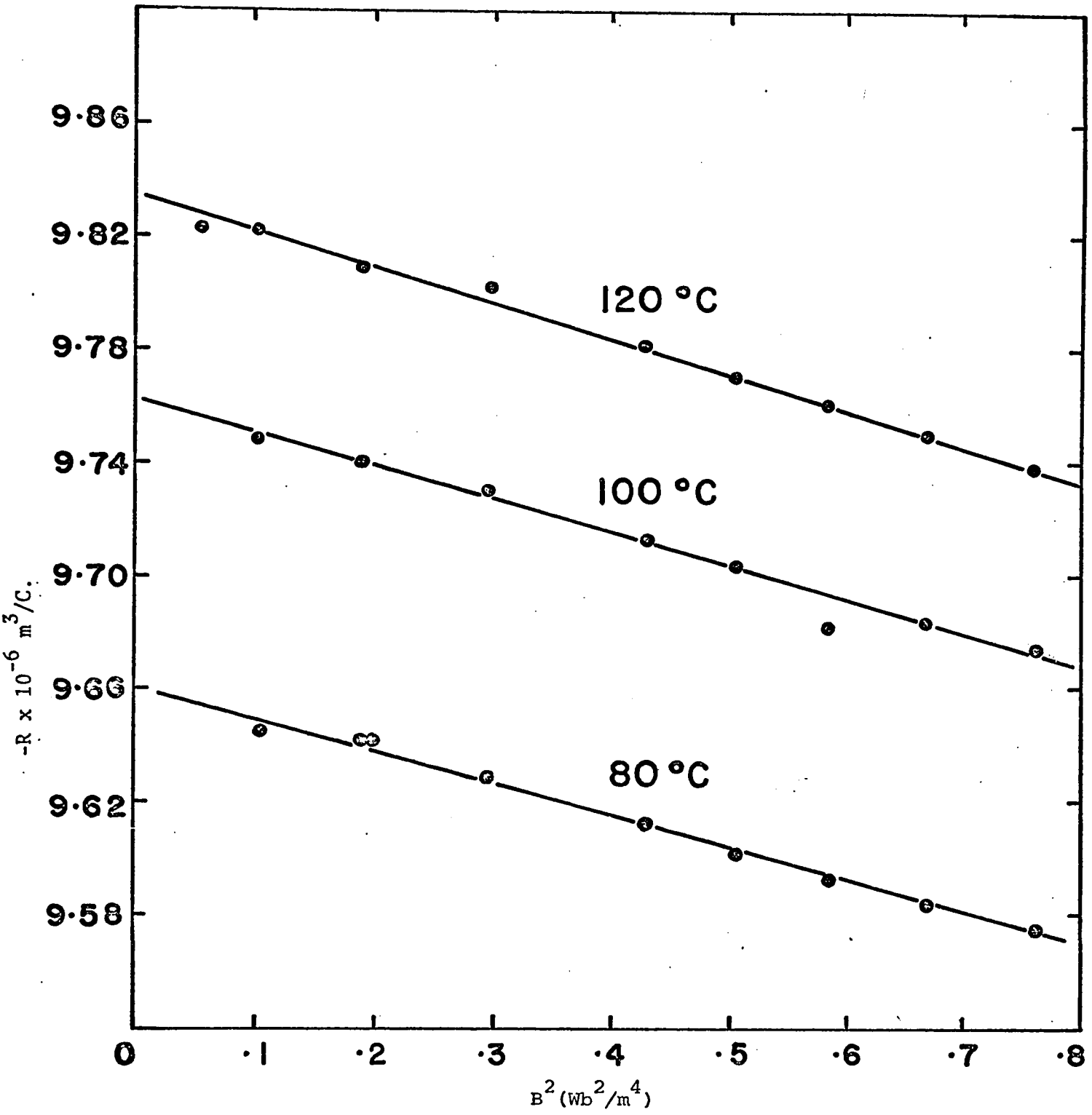

Fig. IV-6 -R vs. B^2 at low magnetic field for the determination of R_o.

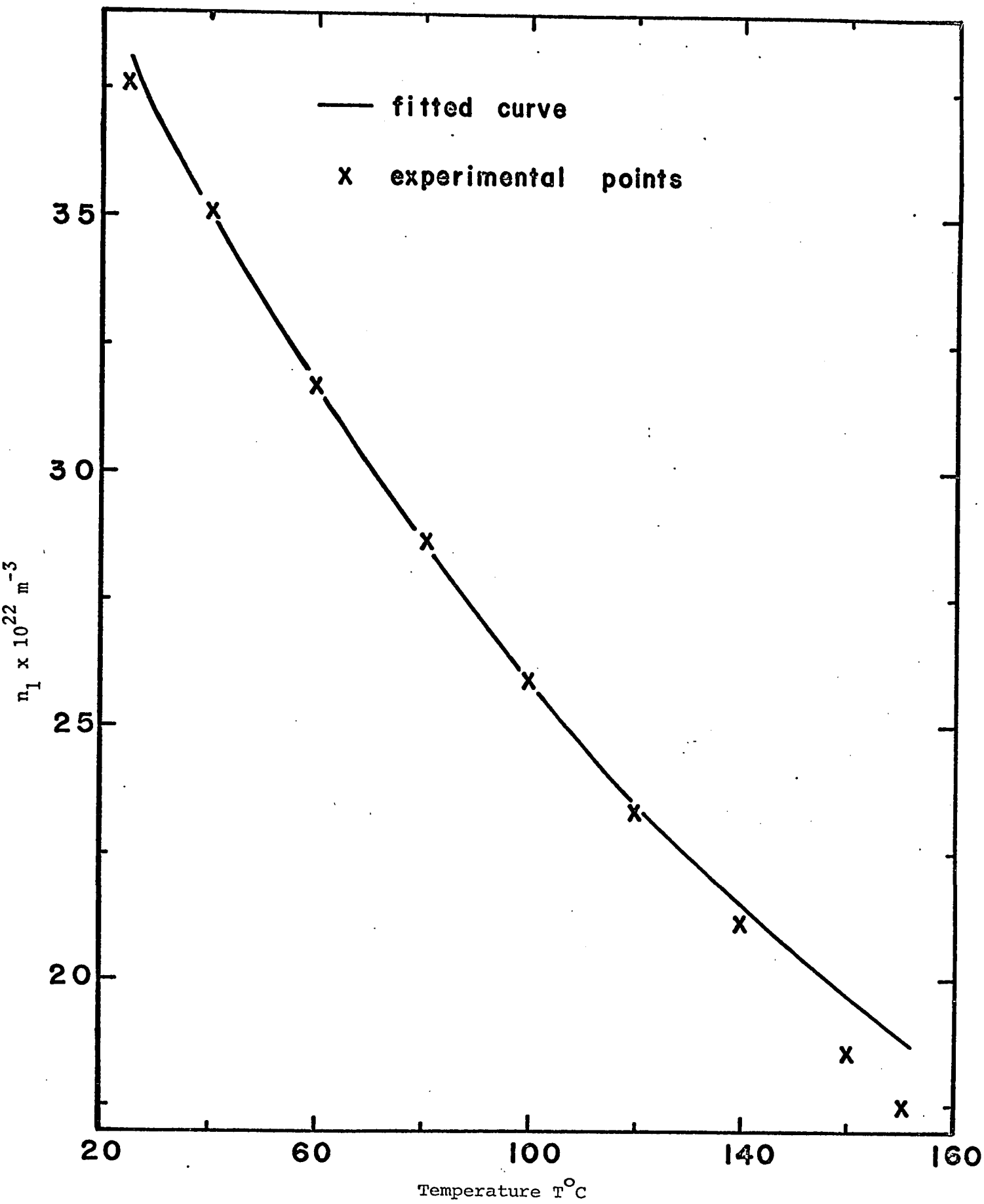

Fig. IV-7 Plot of the fitted curve (solid line) of n_1 vs T^oC and experimental points (X) for E_{20} = 0.099 eV, α_2 = -3.4 X 10^{-5} eV/°K.

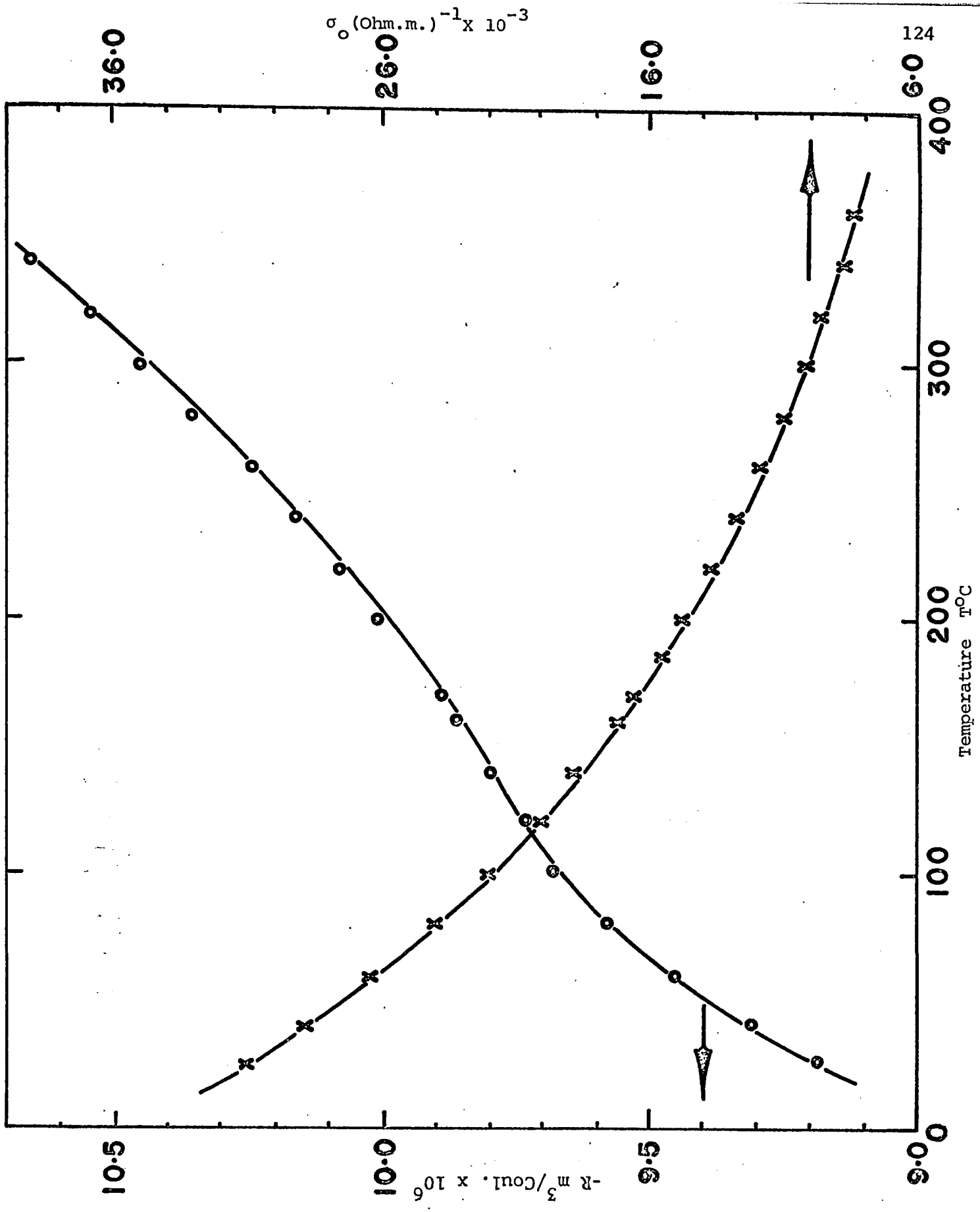

Fig. IV-8 Hall coefficient -R at 0.87 Wb/m^2 and conductivity σ_o vs temperature in °C. GaSb sample N2

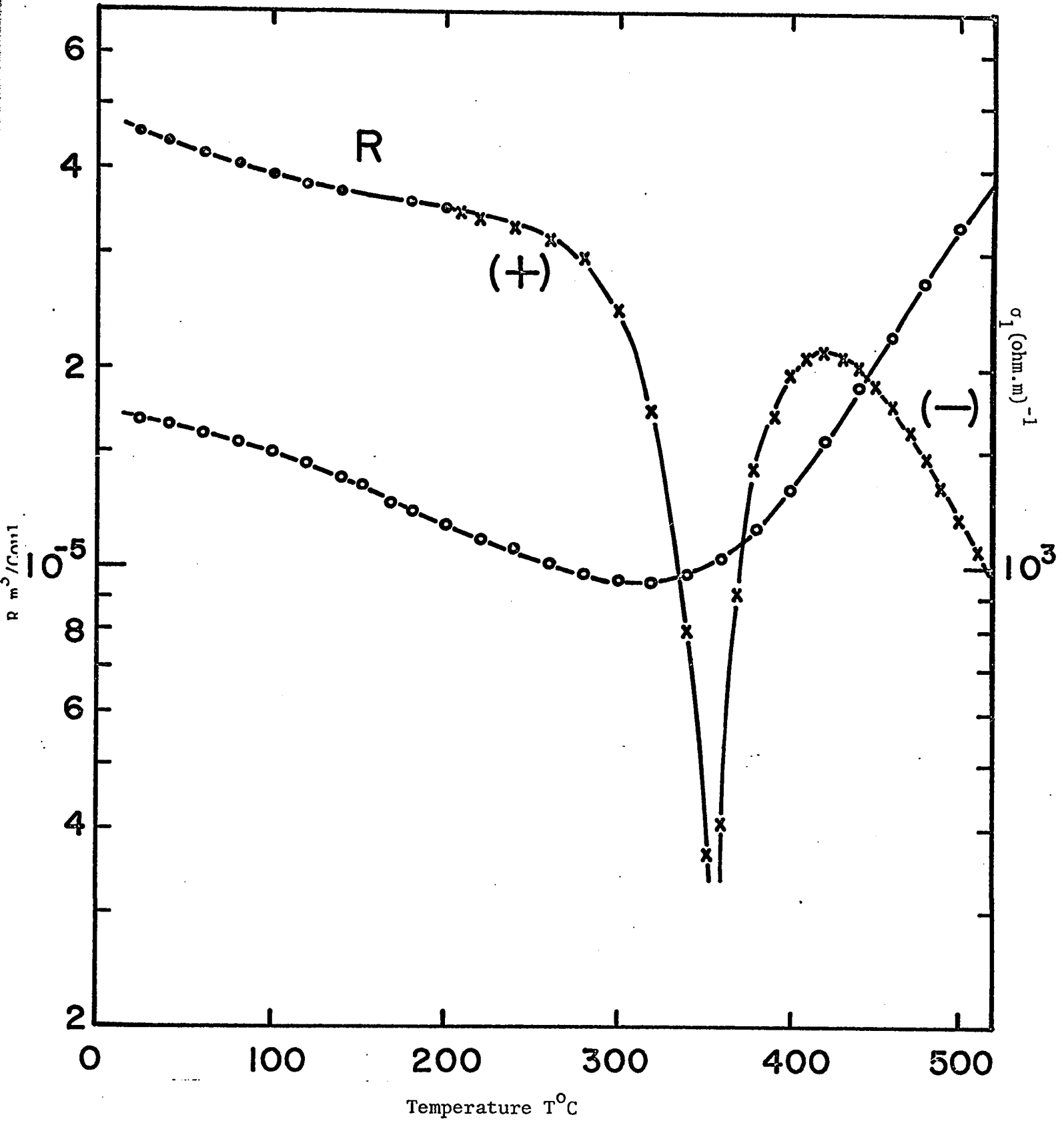

Fig. IV-9 Hall coefficient (B = 0.8 Wb/m^2) and conductivity for p-type sample P1. The fitted curve is shown as solid line.

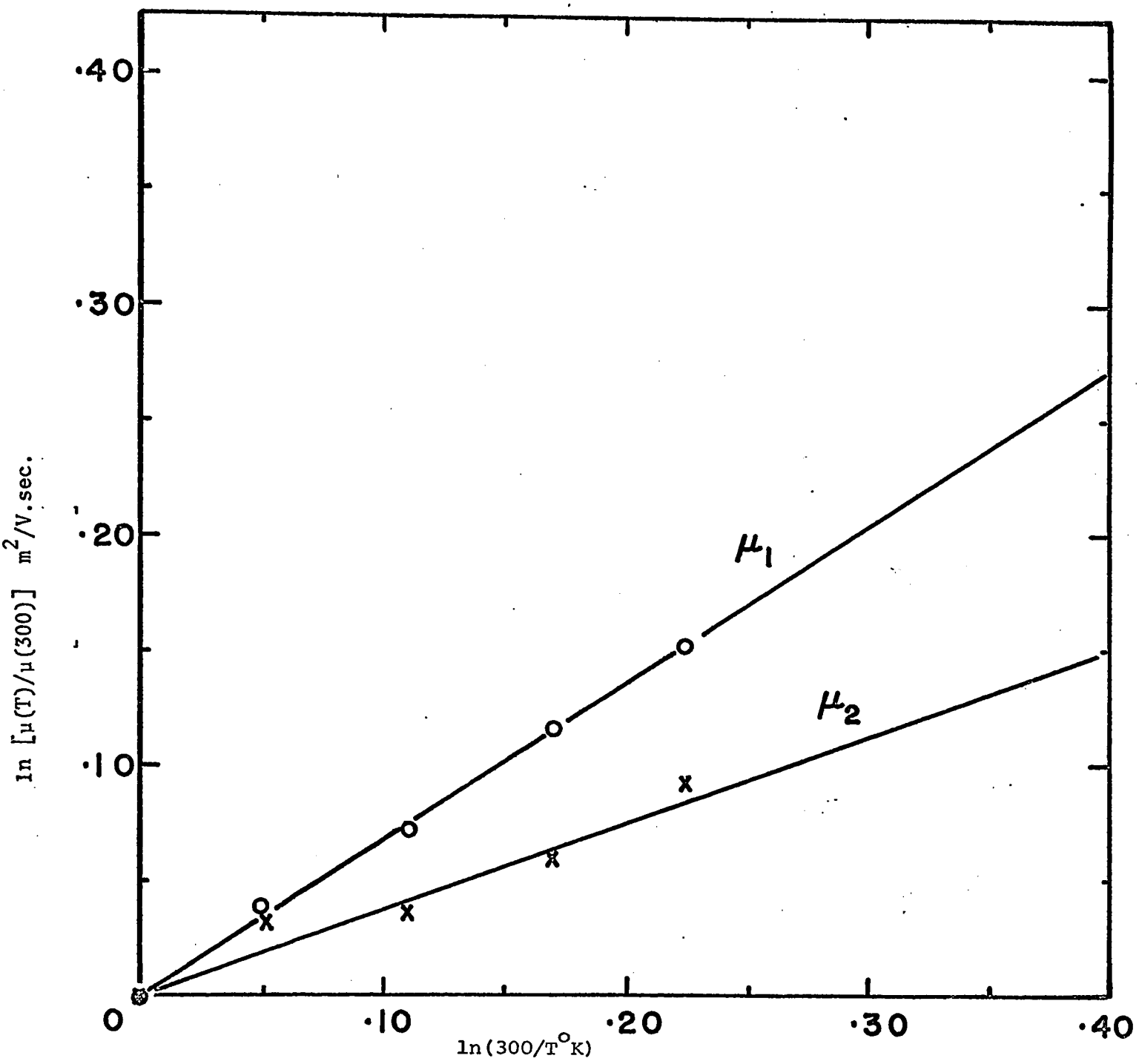

Fig. IV-10 Plots of $\ln[\mu(T)/\mu(300)]$ vs. $\ln(300/T^{\circ}K)$ below 120°C for the estimate of the temperature dependence of the mobilities μ_1 and μ_2 for GaSb sample N2. The slopes n_1 and n_2 are 0.67 and 0.38 respectively.

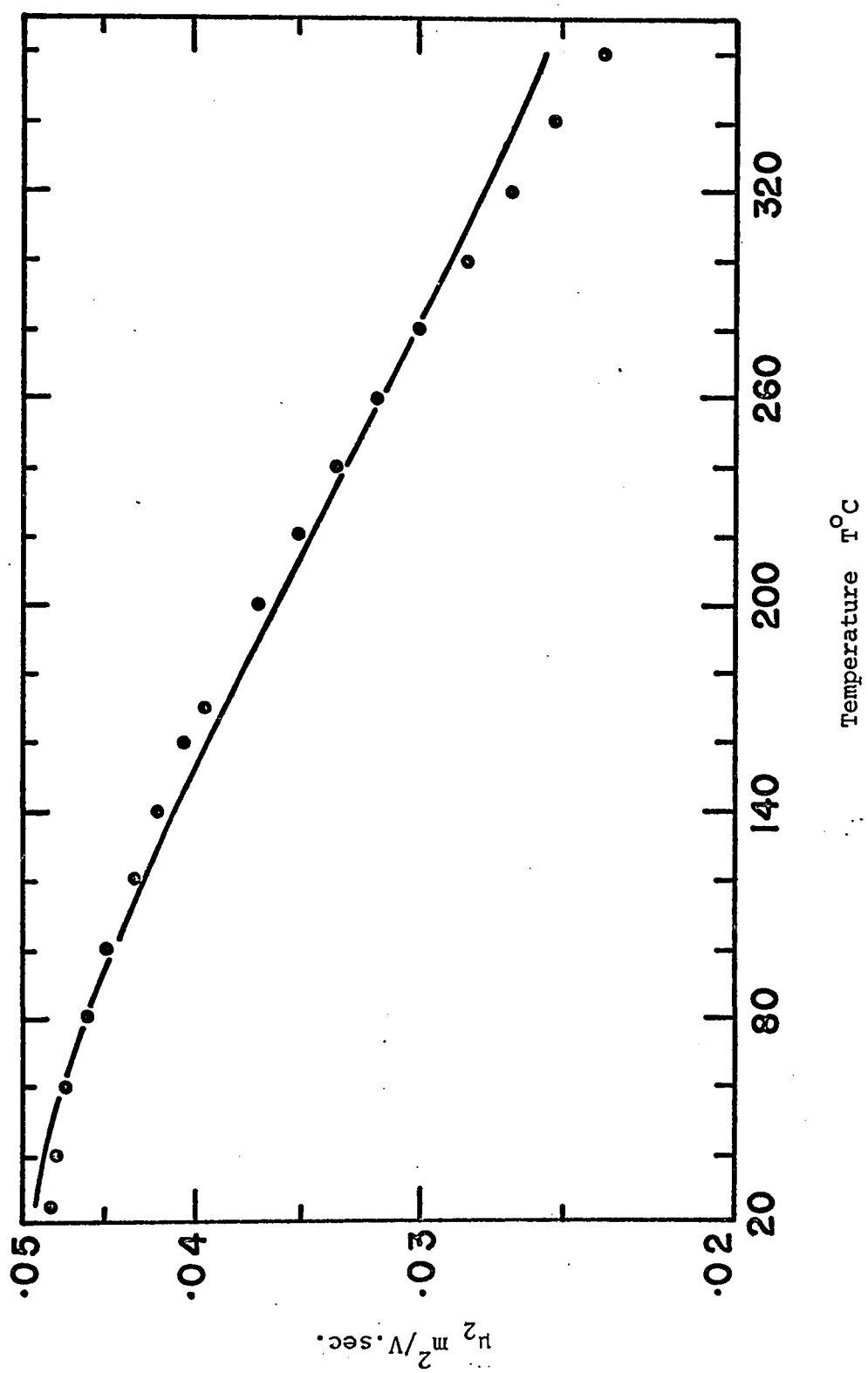

Fig. IV-11 Fitted mobility $\mu_2(T)$ assuming acoustic and ionized impurity scattering and reciprocal addition of mobilities. The dots are the values of mobility μ_2 obtained by the method of Section IV-331

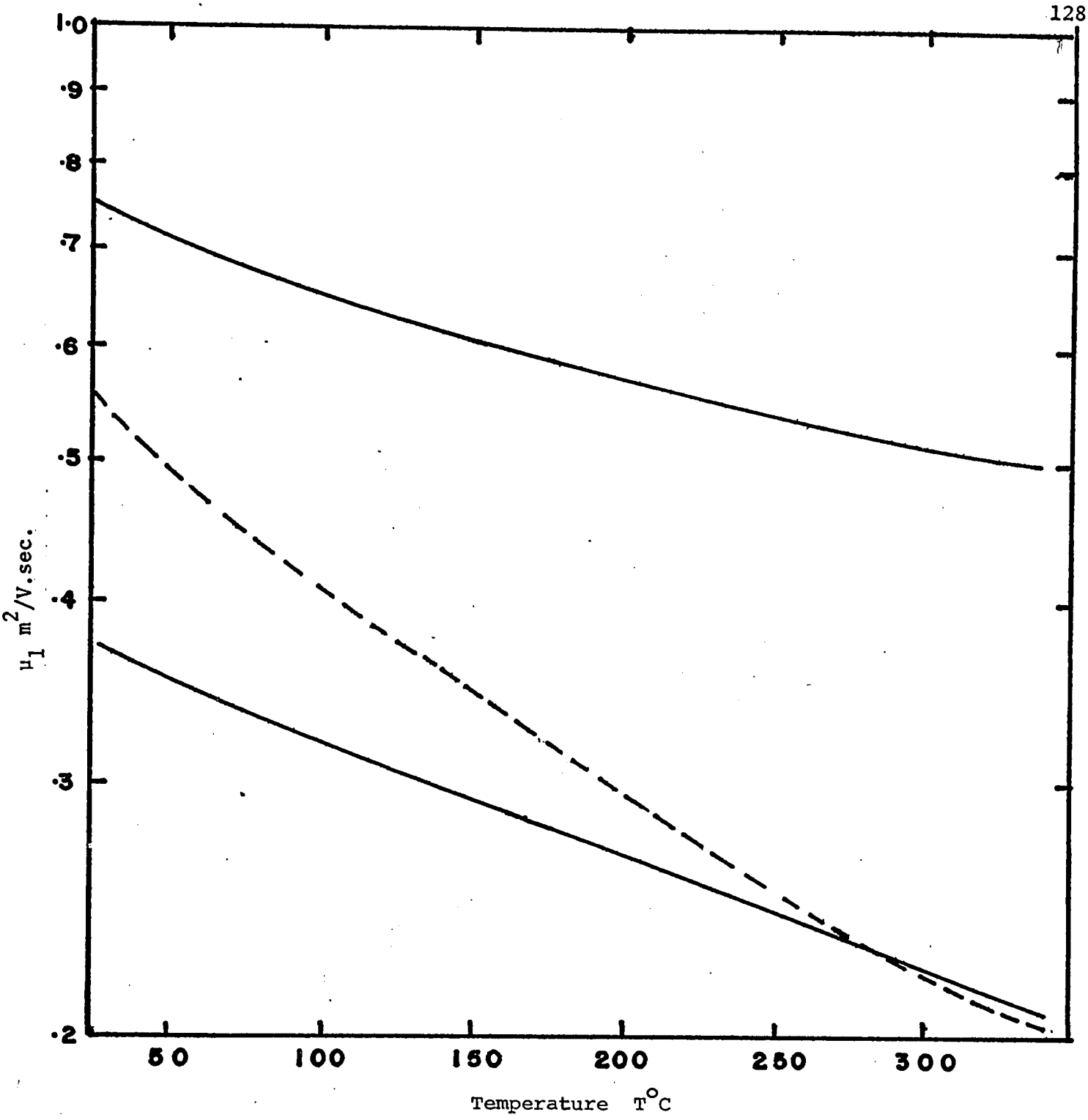

Fig. IV-12 Plots of μ_1 vs. T showing the effect of varying the coupling constant D_{12}. Top curve, calculated $\mu_1(T)$ using τ_{po}, τ_I, τ_{ib} and $D_{12} = 1 \times 10^8$ eV/cm. Dashed curve shows the effect of adjusting D_{12} to fit the high temperature results of $\mu_1(T)$; (bottom curve) obtained by fitting R(T) and $\sigma(T)$ with μ_1 and μ_2 as adjustable parameters, sample N2.

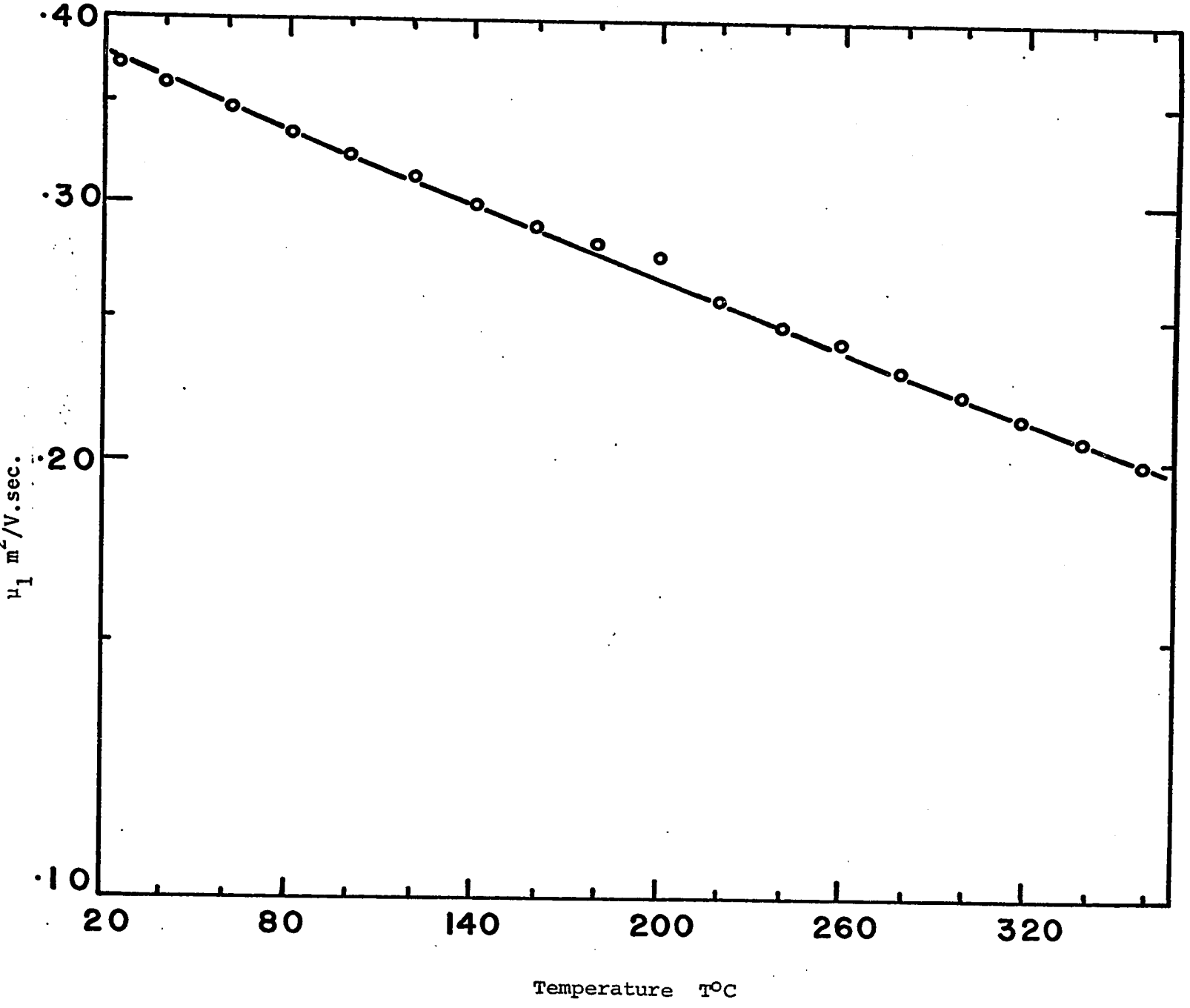

Fig. IV-13 Semi-log plot of $\mu_1(T)$ (circles) as obtained in Section IV-332. The solid line was derived by fitting these points using four relaxation times, i.e. τ_{po}, τ_I, τ_{ib} and τ_{sc}.

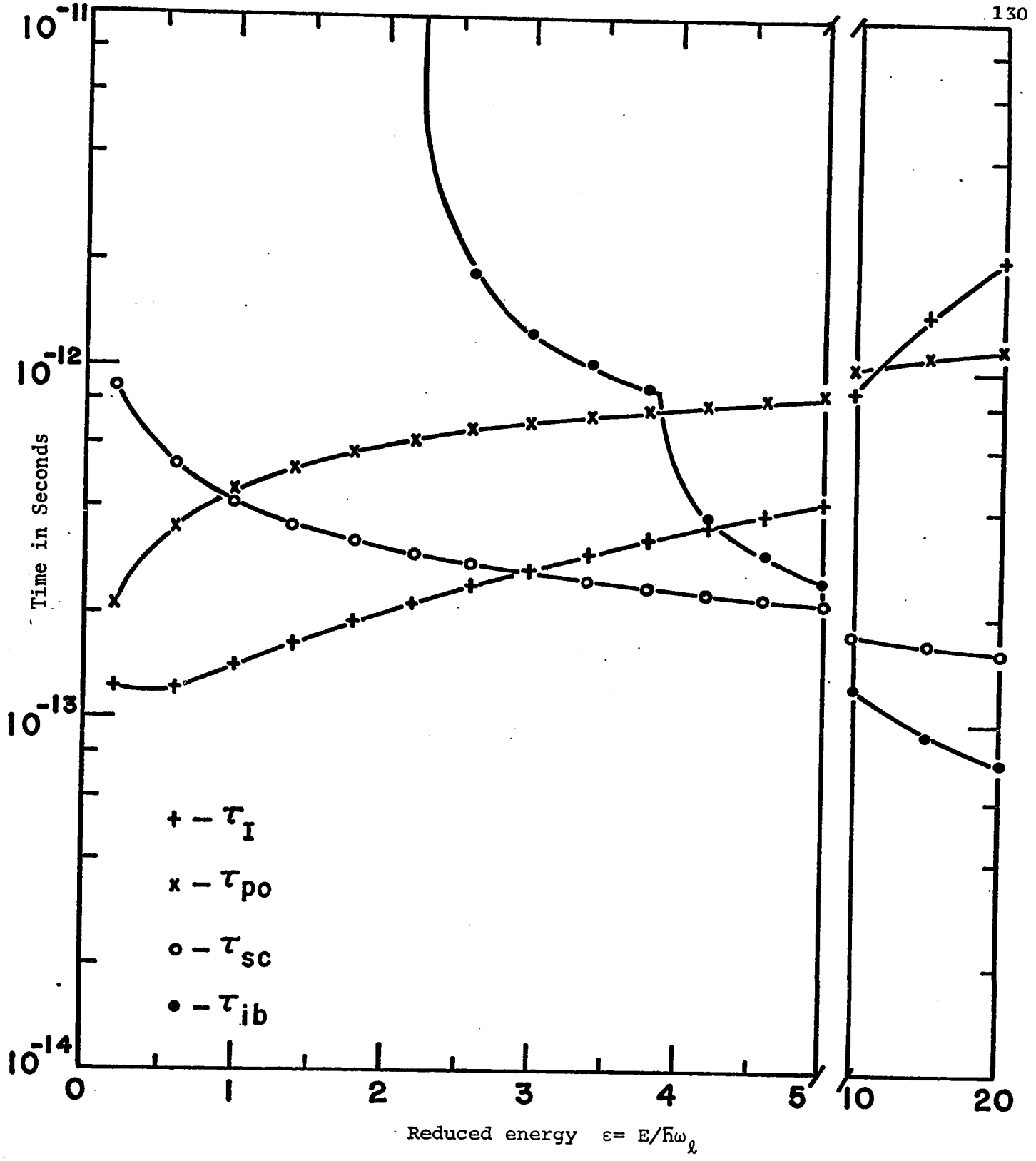

Fig. IV-14 The four relaxation times as a function of reduced energy $\varepsilon = E/h\omega_\ell$ for $N_I = 2.2 \times 10^{24}$ m^{-3}, $D_{12} = 3.2 \times 10^8$ eV/cm. and $(Q_s N_s) = 4.8 \times 10^4$ cm^{-1}.

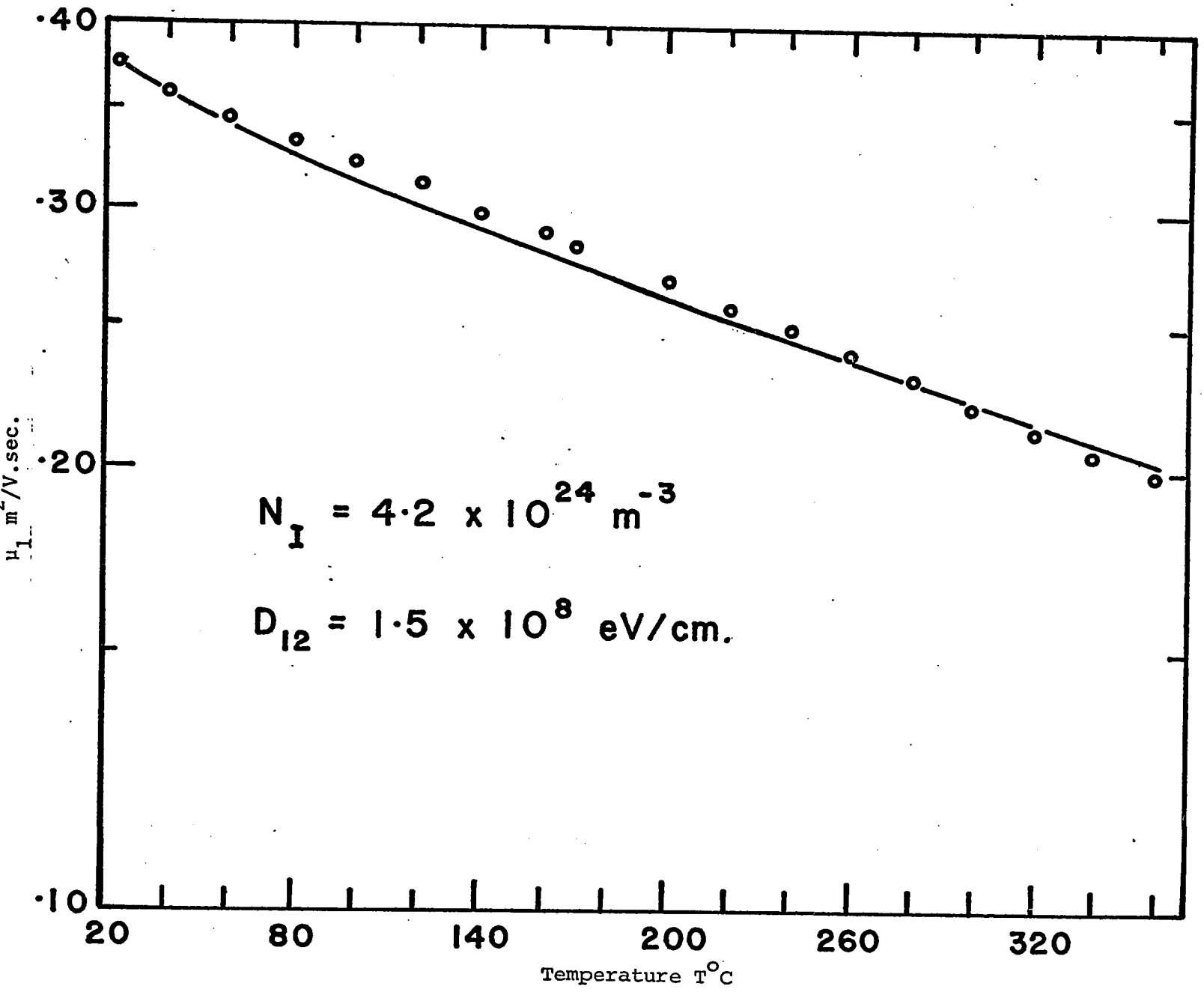

Fig. IV-15 The fitted mobility $\mu_1(T)$ calculated using τ_{po}, τ_{ib} and τ_I with $D_{12} = 3.0 \times 10^8$ eV/cm and $N_I = 4.2 \times 10^{24} m^{-3}$.

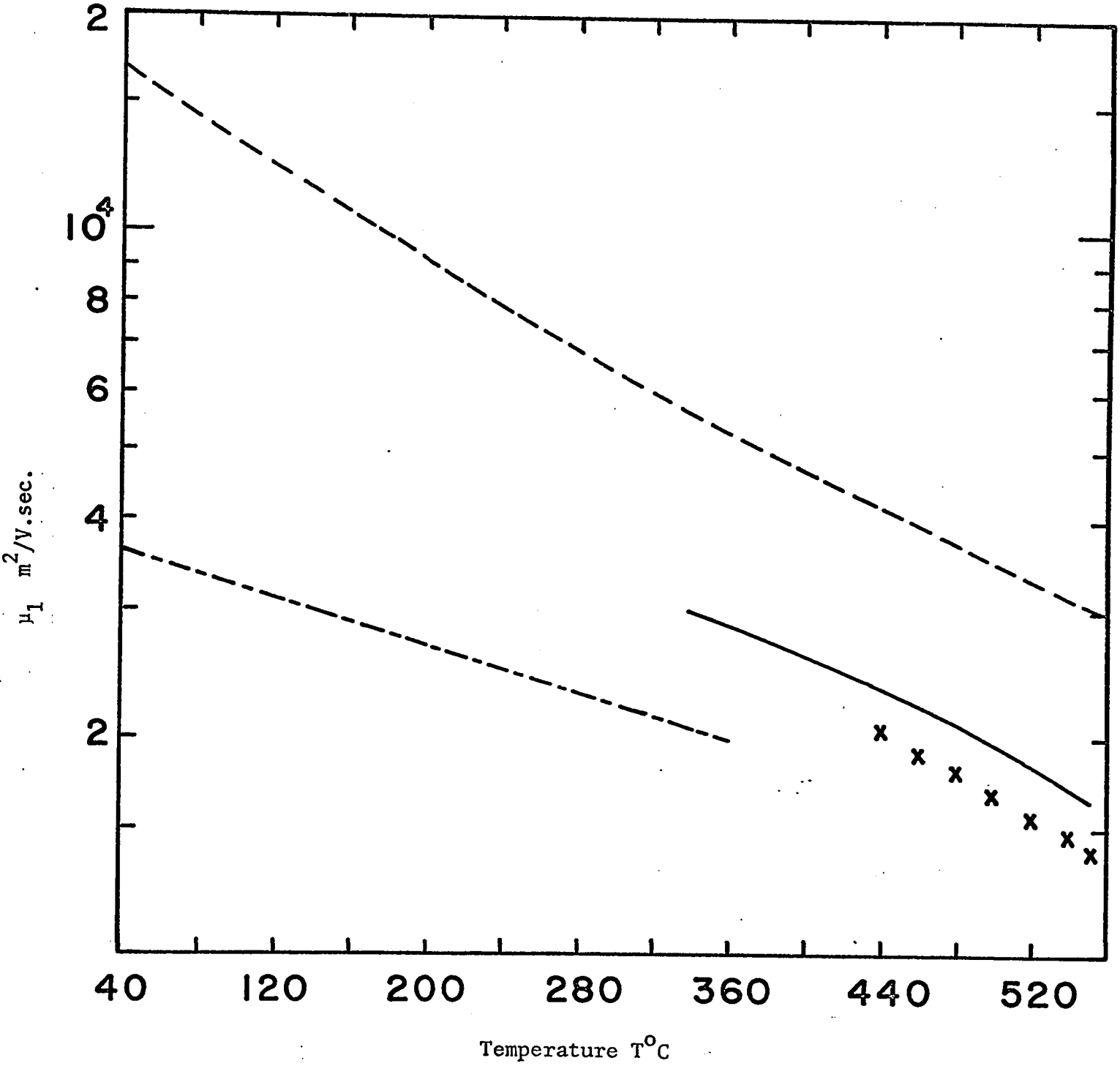

Fig. IV-16 Mobility μ_1 vs. T^oC .---- for $\tau^{-1} = \tau_{po}^{-1} + \tau_{ib}^{-1}$, - . - . - Calculated for sample N2, ——— calculated for sample P1 and (X) are points determined from fitting experimental data from sample P1.

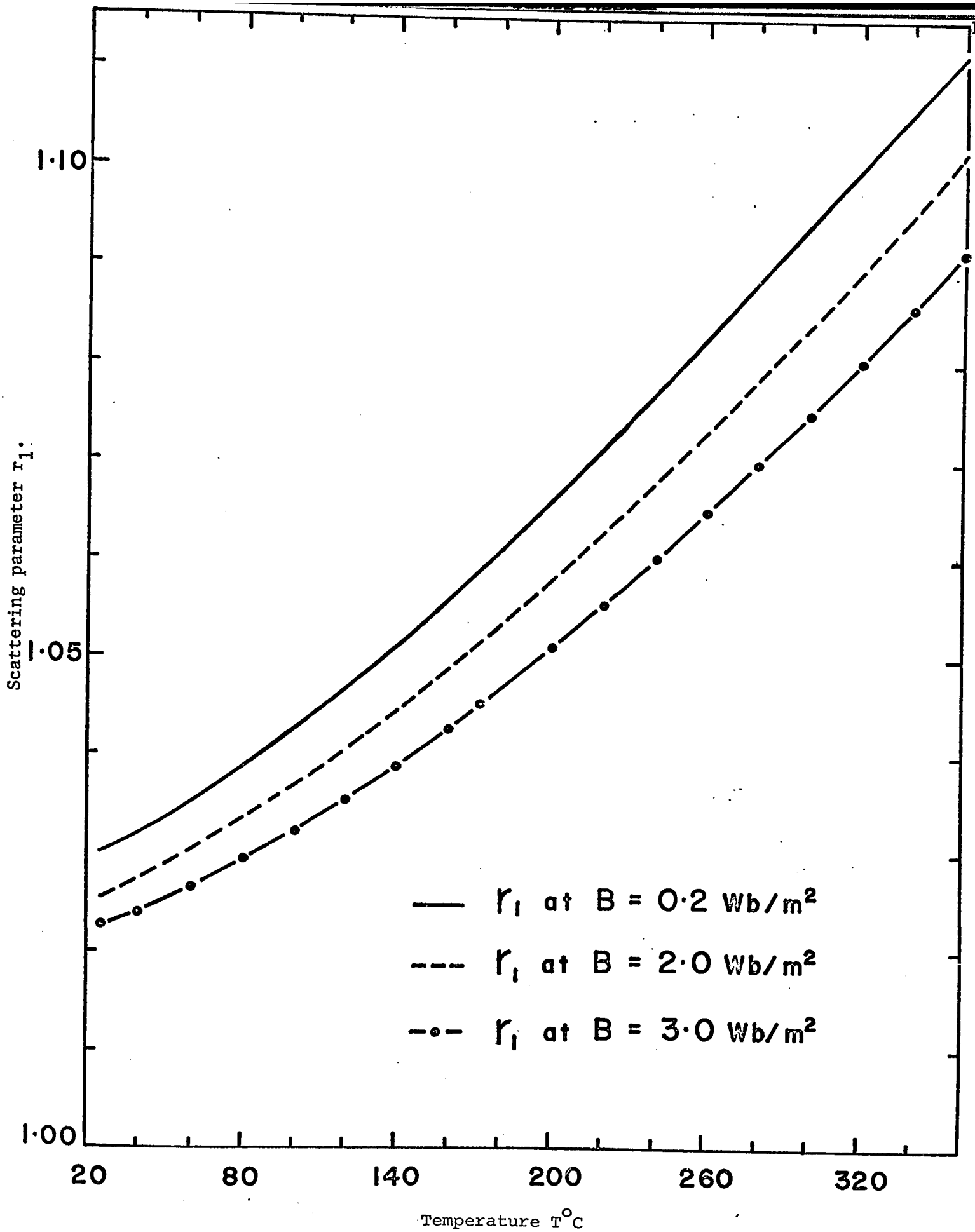

Fig. IV-17 The scattering parameter r_1 as a function of T°C, at three magnetic fields.

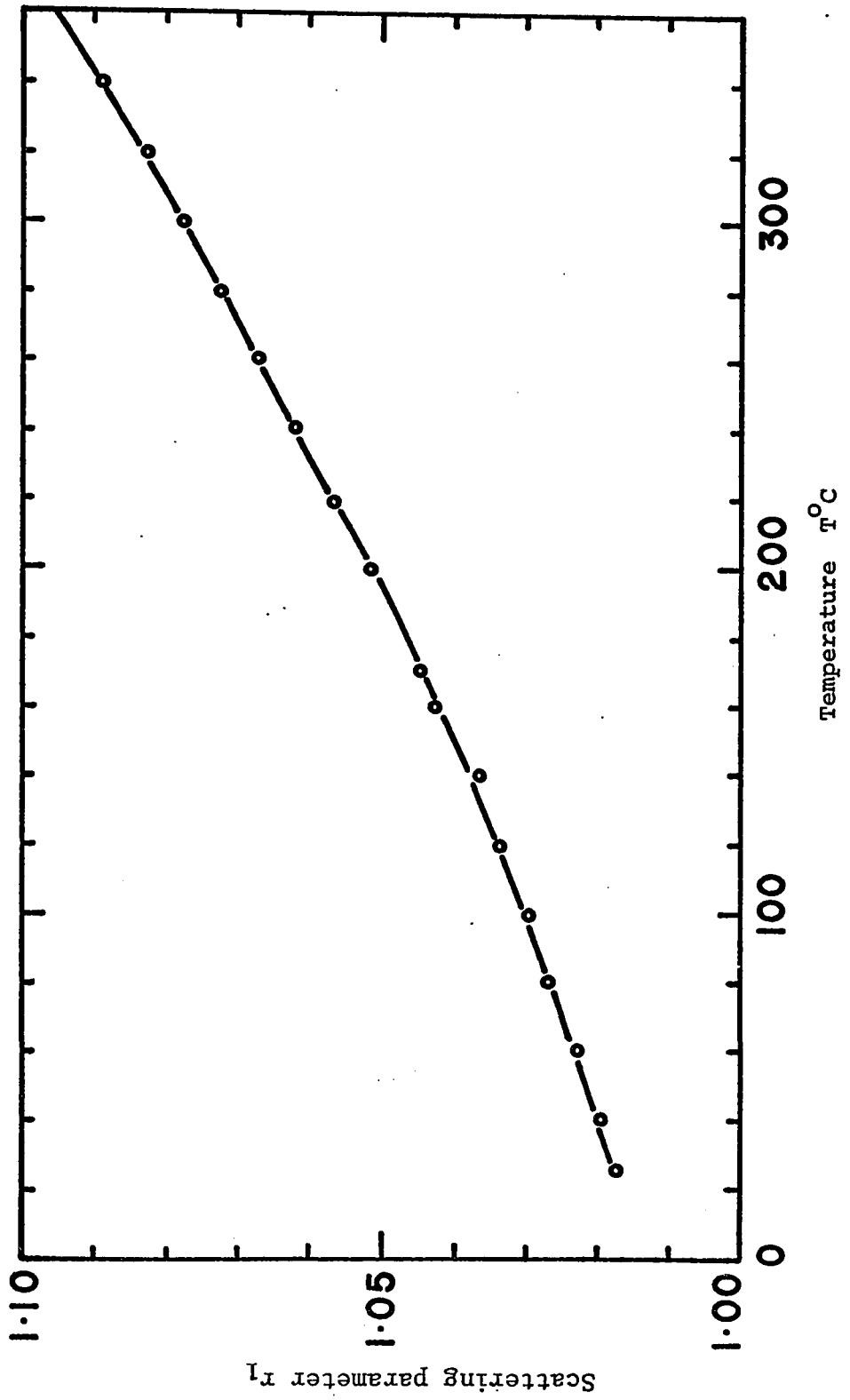

Fig. IV-18 The scattering parameter r_1 as a function of temperature, at B = 0.87 Wb/m^2.

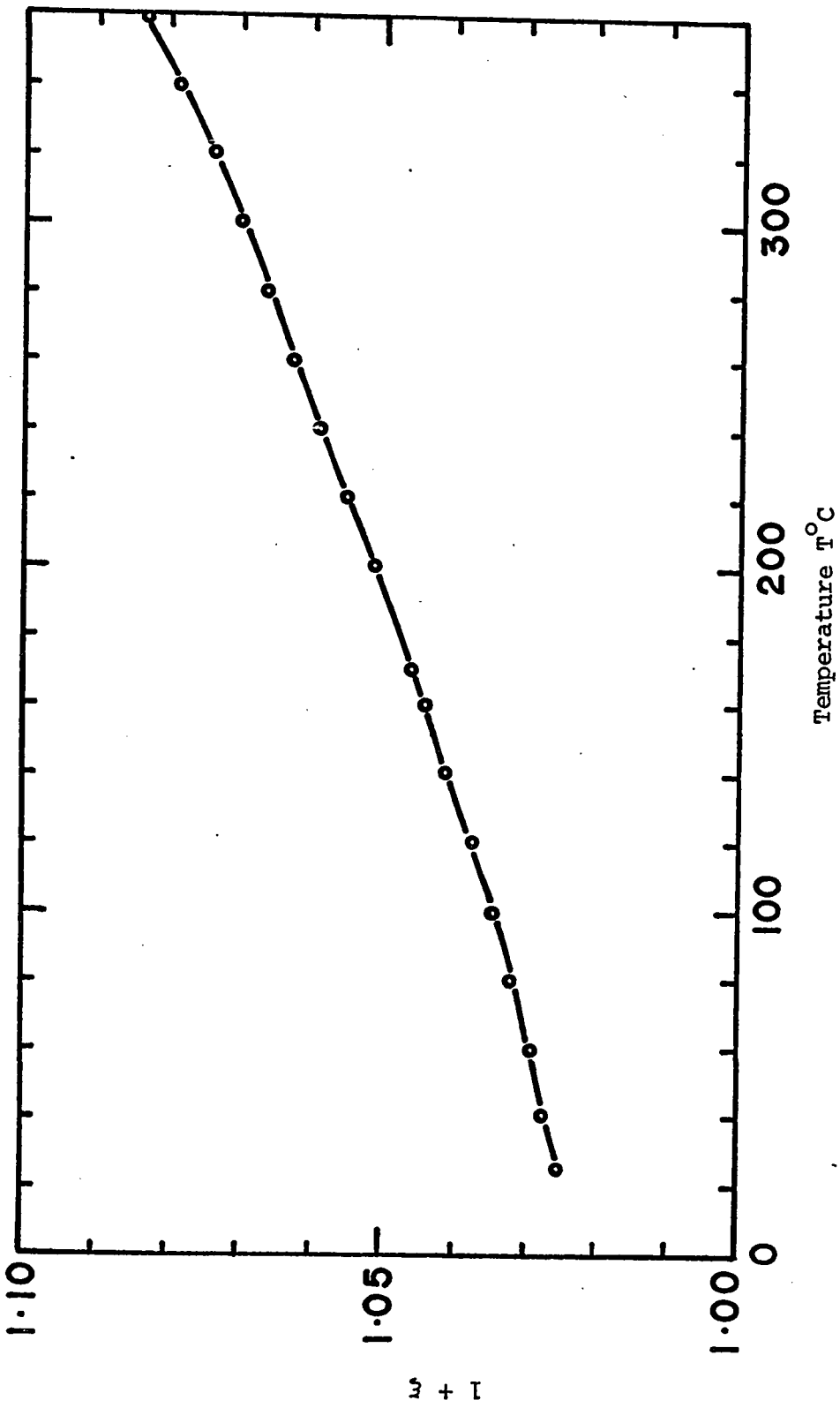

Fig. IV-19 The magnetoresistance coefficient as a function of temperature at B = 3.0 Wb/m^2.

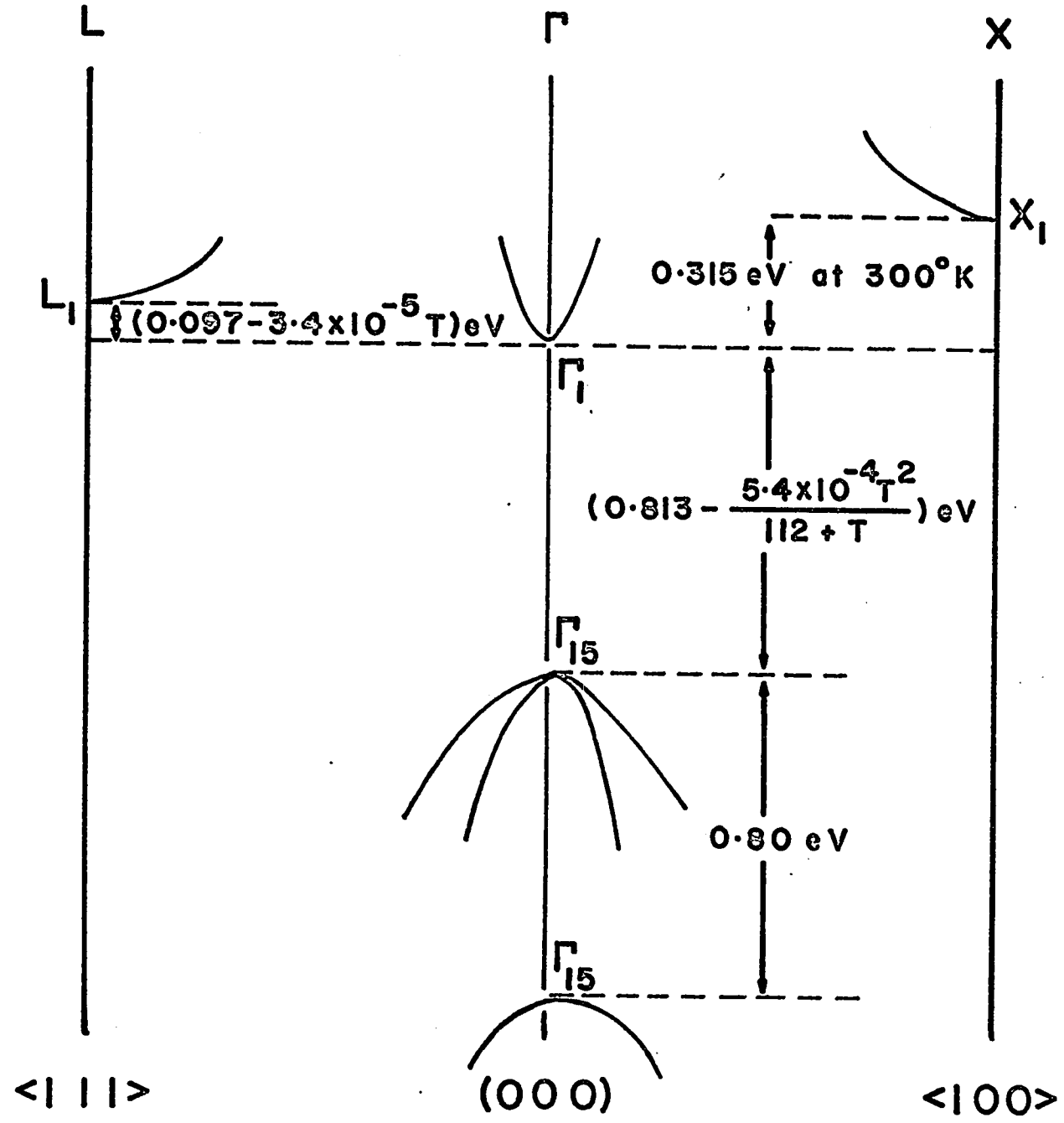

Fig. IV-20 Schematic of the band structure of GaSb. Includes the previously established parameters together with those determined in this thesis.

CHAPTER V

CONDUCTION BAND IN GaAs.

CHAPTER V CONDUCTION BAND IN GaAs

V-1 Preliminary Considerations

In contrast to GaSb where the as-grown crystals are always p-type, bulk GaAs always grows in the n-type form when no intentional dopant is added. The n-type nature of such GaAs crystals is thought to be due to Si impurities, which enter into solid solution from surrounding growth apparatus (e.g. Cochran and Foster 62C1), and not due to non-stoichiometry as is the case for p-type GaSb. It is by now well known that Si behaves as an amphoteric impurity in GaAs (e.g. Kressel and H. von Philipsborn 69K1). Further evidence of the amphoteric behaviour of Si in GaAs has been provided by Hicks and Green (70H2 and references therein). They found that in the growth of layers by the liquid phase epitaxial method, at temperatures between about 700 and 850^{o}C, p-type layers were obtained, because at these temperatures Si shows a preference for the As sites. At higher growth temperatures n-type material is obtained, in which case Si prefers the Ga sites. It was also shown by Hicks and Green that the silicon-doped GaAs layers exhibit a marked degree of compensation. For this reason, Si doped material was considered not suitable for the proposed measurements.

Other well known donor type impurities are Te, Se and S. The latter two are found to give more than one donor level (Pitt and Lees 70P2, Hudson et al. 67H1) and therefore would tend to unduly complicate any analyses of experimental data. Since this work is not concerned with the determination of activation energies of impurities in GaAs, such complications should be avoided. Te doped GaAs was therefore used for

the present work. The doping range used was $5 \times 10^{23} - 5 \times 10^{24}$ m^{-3}. The lower limit is that below which the transfer of carriers into subsidiary bands would not be sufficient at reasonable temperatures. The upper limit is that above which complications due to overlap of the impurity band with subsidiary minima would arise.

Because the separation of the two lowest conduction bands in GaAs is about four times that found for GaSb, essentially no electrons will be in the subsidiary band at room temperature and the highest doping attainable in single crystals. In order therefore to transfer electrons into this band, higher temperatures have to be used. Measurements of constant field Hall coefficient and conductivity show that at around 200°C electron transfer into the subsidiary bands just becomes noticeable. Therefore to get an appreciable effect, temperatures > 200°C must be used.

It has been pointed out in the last chapter which dealt with GaSb, that the conditions required for useful analyses of magnetoresistance and Hall coefficient as a function of magnetic field data are such that the relative density of electrons in the two bands are comparable and that the ratio of mobilities is about 10:1. The mobility ratio condition is satisfied for GaAs, but in order to satisfy the electron density condition high temperatures ($\gtrsim$ 400°C) have to be used. In this case, the conditions under which the equations II-46 and II-62 were derived would no longer be valid, because it is expected that the magnetoresistance of the individual bands would now become comparable with the two band effect. This is borne out by the results of measurements of resistance as a function of magnetic field at 400°C, on a heavily doped sample. Therefore only measurements of constant field Hall coefficient and conductivity were made on GaAs.

V-2 Experimental Results

Measurements of conductivity and Hall coefficient at a field of 0.80 Wb/m^2 were made on six samples of Te doped GaAs in the temperature range from 20°C to 600°C. The samples were doped with Te to concentrations between $4 \times 10^{23} m^{-3}$ and $9 \times 10^{24} m^{-3}$. The results are shown in Figs. V-1 and V-2 where Hall coefficient and conductivity are plotted against temperature. Room temperature values of n_1, μ_1 and σ_1 for the six samples are given in Table V-1.

Two of these samples were also measured up to $\sim$ 800°C. The results were not reproducible on cycling the temperature between 20° and 800°C. Howeyer, as long as the maximum temperature did not exceed $\sim$ 600°C, reproducible results were obtained. This lack of reproducibility above 600°C is ascribed to dissociation of the sample surface due to the loss of As. Various encapsulation techniques were tried to maintain an As overpressure which would prevent As evaporation. However, none were successful. The method of quartz encapsulation used by Roberts (65R1) was considered, but due to obvious practical difficulties was discarded. We therefore limited the measurements to below $\sim$ 600°C. Even with this temperature limitation, the change in Hall coefficient was large enough (Fig. V-1) to allow a meaningful analysis.

Measurements of conductivity as a function of magnetic field (from 0 to 3.2 Wb/m^2) were made at 400°C on the heaviest doped sample ($n \sim 10^{25}\ m^{-3}$). This high temperature was chosen in order that enough carriers would be excited into the first subsidiary band to give a measurable two band effect. The results are shown in Fig. V-14, in the form of $\rho_o/\Delta\rho$ vs. B^{-2} plot.

V-3 Analysis of Results

V-31 The three models of the conduction band structure of GaAs

The uncertainty in the conduction band structure of GaAs has already been fully discussed in Chapter I. It suffices to say in summary here that we have three possible models for the conduction band structure which should be reflected in the experimental results; these are:

(i) Three band model, with band extrema at Γ_1, Δ_1(or X_1) and L_1

The first subsidiary band minima are either in the <100> direction, (i.e. have Δ symmetry), or are at the edge of the Brillouin zone and hence have X_1 symmetry. The next set of minima have L_1 symmetry and are close in energy to the first, i.e. any analysis based on this model must include three sets of minima Γ, Δ(or X_1) and L_1. This model is supported by the theoretical calculations of Cohen and Bergstresser (66C1), Pollak et al. (66P1) and Herman (68H1), and experimentally by James et al. (68J1).

(ii) Two band model with extrema at Γ_1 and Δ_1(or X_1)

The first subsidiary minima are Δ_1 (or X_1) but the L_1 minima are well removed in energy to have no effect on electron distribution. This model was assumed by Ehrenreich (60E1) and is supported by the theoretical calculations of Jones and Lettington (69J1).

(iii) Two band model with extrema at Γ_1 and L_1

The first subsidiary minima have L_1 symmetry, the next highest minima with Δ_1(or X_1) symmetry are well removed and will not affect electron distribution. This model is based on theoretical calculations of band structure by Collins et al. (70C1).

V-32 Analysis based on three conduction band model, Γ_1, Δ_1 (or X_1) and L_1

The experimental results of Hall coefficient and conductivity as a function of temperature were analysed using the three band model. The charge neutrality condition then takes the following form:

$$N_D - N_A = n_1 + n_2 + n_3 - p = n_t \qquad \text{V-1}$$

where again subscripts 1, 2, 3 correspond to the Γ_1, Δ_1(or X_1) and L_1 minima respectively. Since all the samples were doped with Te and it has been shown (70P2) that these impurities are associated with a subsidiary band and have ionization energies $\sim$ .02 eV below the bottom of this band, they will be ionized at all temperatures. Therefore the carrier concentration measured at room temperature is equal to N_D(Te) - N_A, hence the neutrality condition can now be written as:

$$n_t = n_1 + n_2 + n_3 - p \qquad \text{V-2}$$

where n_t = n(300^{o}K). Thus electron distribution in the bands can be calculated provided the necessary band parameters and band shapes are known. Here again, as in GaSb, we shall take account of the non-parabolicity of the Γ_1 conduction band using the Kane model; the other bands will be considered parabolic. The carrier concentrations n_1, n_2, n_3 and p are then calculated using equations II-71 through II-77 with appropriate parameters which are given in Table V-2. Since there are many values reported in the literature for some of the band parameters, the choice of the parameters listed in Table V-2 will now be discussed.

The value of m^*_{10} = .0648m was determined by Chamberlain and Stradling (69C1) through cyclotron resonance measurements on very pure expitaxial n-GaAs. It is therefore preferred over other values, e.g. 0.067m obtained using interband magneto-optical measurements (68V1) or 0.064m determined from Faraday rotation measurements at room

temperature (65M1). The effective mass of electrons in the subsidiary minima are not well established to date, (see Chapter I).

The density of states effective mass in the L_1 band of GaAs has not been experimentally determined, we have therefore used values of $m^*_{2\ell}$ and m^*_{2t} calculated by Pollak et al. (66P1) by the $k.p$ method. These values lead to a density of states effective mass which agrees quite well with the experimental density of states mass for the L_1 band in GaSb and Ge, therefore should be reasonably representative of the density of states mass in the L_1 band of GaAs. The density of states effective mass of 1.2m was determined by Ehrenreich (60E1) for a band with Δ_1 symmetry in GaAs. The most recent determination of the heavy hole effective mass was reported by Walton (68W1) and was determined from cyclotron measurements. Panish and Casey (69P1) derived values of α_o and θ_o by fitting absorption data over a wide temperature range. To do this a value of the principal gap at absolute zero had to be used. They used a value of 1.522 eV determined by Sturge (62S1) which is very close to the latest and most accurate value of 1.5189 eV reported by Bimberg and Scheirer (72B1). Because of the small difference between these two values of E_{oo}, it was not considered necessary to refit the data of Panish and Casey using the more accurate values for E_{oo}. In any case our analyses are not very sensitive to E_{oo}.

The remaining parameters α_2, θ_2, α_3 and θ_3, for the temperature coefficients of the energy gaps in the <111> and <100> directions, were derived using Walter et al. (70W1) data of the shift with temperature of the E_1 and E_2 reflectance peaks. These data were fitted to the Varshni equation II-74 by the least squares method and the results are given in Table V-3. According to Kane (66K1) and Higginbotham et al. (68H2) optical transitions do not occur at band extrema but over a range in k-space, nevertheless the temperature dependence of the peaks should be reasonably represen-

tative of the relative conduction band motion with respect to the valence band. Using these values for the α_2, θ_2, α_3 and θ_3 parameters together with those of α_o and θ_o given by Panish and Casey, the energy separation E_2 and E_3 can be calculated from:

$$E_2 = E_{20} + \left(\frac{\alpha_2}{\theta_2 + T} - \frac{\alpha_o}{\theta_o + T}\right) T^2 \qquad \text{V-3}$$

$$E_3 = E_{30} + \left(\frac{\alpha_3}{\theta_3 + T} - \frac{\alpha_o}{\theta_o + T}\right) T^2 \quad , \qquad \text{V-4}$$

knowing E_{20} and E_{30}. However, neither of these values are known.

Using the value for $E_{23} = E_2 - E_3 = .09$ eV at 300^oK determined by James et al. (68J2), together with equations V-3 and V-4, it is then possible to determine the value of E_{20} as a function of E_{30}. This then, is the only unknown parameter required to calculate the carrier distribution in the bands when use is made of the neutrality condition. Before it is possible to fit the experimental results of the Hall coefficient and conductivity as a function of temperature, it is further necessary to know the mobilities in the bands and their temperature dependences, as well as the respective scattering parameters. Since the valence and the subsidiary bands are only populated at elevated temperatures where ionized impurity scattering is relatively unimportant, the values of room temperature mobility that are required are those measured on pure samples. The magnitude of the mobility in the L_1 band of GaAs at room temperature is not known, it will therefore be used as the second adjustable parameter. For the electron mobility in the Δ_1 band we used the value of $0.015 m^2/V.sec$. This value was determined by Lees et al. (67L1) and is very close to $0.0145 m^2/V.sec$ calculated by Conwell and Vassell (68C1) by combining deformation potential, intraband and interband scattering. The magnitude of hole mobility at

$300^{o}K$ in lightly doped p-type GaAs never exceeds $0.045 m^2/V.sec.$, this value was then employed in our calculation. Since the conductivity will be determined principally by the carriers in the Γ_1 conduction band, use was made of the experimentally measured conductivity σ_o to calculate $\mu_1(T)$ which is given by:

$$\mu_1 = (\frac{\sigma_o}{e} - n_2\mu_2 - n_3\mu_3 - p\,\mu_p)/\, n_1 \qquad \text{V-5}$$

It was assumed that since the carriers in the two subsidiary conduction bands and the valence band have large effective masses, the mobility at elevated temperatures in these bands will be limited by acoustic phonon scattering. Hence, for these three bands, mobility will have $T^{-1.5}$ dependence and the scattering parameters are then all equal to 1.18. The temperature variation of the scattering parameter $r_1(T)$ in the Γ_1 band has been calculated by Ikoma (70I1) and measured by Stillman et al. (70S3) for lightly doped GaAs. Both the calculated and experimental results lead to essentially the same variation of $r_1(T)$ of between 1.03 and 1.10 over the temperature range of interest here. To check these values we made Hall coefficient measurements as a function of magnetic field on sample NE22/1 at about $-50^{o}C$. The results are shown in Fig. V-10; it can be seen that these agree very well with the results of Stillman et al., when account is taken of the experimental temperature. This variation of $r_1(T)$ is small in comparison with $n_1(T)$ and hence to a good approximation it can be assumed that r_1 is constant with temperature and has a value of 1.08. All the mobility parameters discussed above are given in Table V-4.

The two unknowns $\mu_2(300^{o}K)$ and E_{30} were then used as adjustable parameters in fitting the experimental results of the Hall coefficient temperature variation. The method of fitting is the same as that described in the previous chapter on GaSb. The results of the fitting for the five samples are shown in Table V-5. The smallest

increments used were δE_{30} = .001 eV and $\delta\mu_{20}(300^{o}K)$ = 0.005m^2/V.sec. It is of interest to note that the fitting was sensitive only to the value of E_{30} but not to $\mu_2(300^{o}K)$, this was not unexpected since $n_3(T)$ would always be higher than $n_2(T)$ (Fig. V-3) and with $\mu_2(T) > \mu_3(T)$ at all temperatures, the L_1 band would have only a small effect on R(T).

The recent room temperature results of Pitt and Lees (70P2) on Hall effect and conductivity as a function of pressure indicate that the <100> minima lies on the zone boundary and hence have X_1 symmetry. From these measurements they determined the density of states mass M^*_{3d} = 0.85 ± 0.10m, the zero pressure mobility $\mu_3(300)$ = 0.033 ± .005m^2/V.sec. and the band separation E_3 = 0.38 ± .01 eV.

Using Pitt and Lees' values of M^*_{3d} and $\mu_3(300)$, our Hall effect and conductivity data were refitted, with E_{30} as an adjustable parameter. All the other parameters were the same as used for the previous analysis. However, to obtain an acceptable fit it was found necessary to adjust the temperature dependence of the band separation, α_3, in addition to E_{30}, keeping θ_3 constant. To do this and still maintain only two variables (i.e. E_{30} and α_3) we set $\mu_2(300)$ = 0.065m^2/V.sec. This was considered to be justified since it was found in the previous analysis that the fitting was insensitive to the value of μ_2.

The fitted curves are shown in Figs. V-4 through V-8 and the parameters E_3 and α_3 resulting from this fitting procedure are tabulated in Table V-6. The curves apply to both the <100> band symmetries, Δ_1 and X_1, since the agreement between the calculated and experimental curves was good in both cases. For the case of minima with Δ_1 symmetry, we obtained E_{30} = 0.38 ± .004 eV where we used the value of $\alpha_3 = -5.45 \times 10^{-4}$ eV/^{o}K derived from optical experiments. Since this value of α_3 could not be used for the minima with X_1 symmetry, in this case we obtained a value

of $\alpha_3 = -6.0 \times 10^{-4}$ eV/°K and $E_{30} = 0.374$ eV. Comparing the two temperature dependences with that of the principal gap, i.e. $\alpha_o = -5.8 \times 10^{-4}$eV, it can be seen that in the first case the separation increases with temperature, while in the second case it decreases. The band separation at absolute zero is also smaller in the second case. This difference is due to the lower density of states mass and higher mobility in the <100> band for the case of minima with X_1 symmetry.

V-33 The two band model, Γ_1 and Δ_1 (or X_1)

The two band model proposed by Ehrenreich (60E1) will now be considered. In this case there is only one set of subsidiary minima in the <100> direction. Using the parameters for the two bands (Γ_1, Δ_1) from Table V-2 it was again found necessary to adjust α_3 as well as E_{30} to obtain a satisfactory fit to the experimental results of all five samples. We also had to assume a linear temperature dependence for the band separation in order to maintain a maximum of two adjustable parameters. Bearing this in mind we expected that E_{30} obtained from this fit would be slightly larger than the true value. Good agreement was again obtained between the experimental and the calculated Hall coefficient for all five samples; the fitted curves for two of them are shown in Fig. V-9 and the values of the adjustable parameters, corresponding to the best fit, are given in Table V-7. It can be seen that the most consistent values of E_{30} and α_3 are 0.386 eV and -3.6×10^{-5} eV respectively.

It was pointed out in the last section (V-32) that the effect of reducing the density of states effective mass in the subsidiary minima and increasing electron mobility in these minima was to lower the band separation and increase the rate at which the two band minima approach each other with increase in temperature. It was

therefore considered not necessary to repeat the analysis using Pitt and Lees' values of M_{3d} and $\mu_3(300)$ for minima with X_1 symmetry, since the results are predictable.

V-34 The two band model, Γ_1 and L_1

The recent calculations of Collins et al. (70C1) give the following values for the band separations: E_{20} = 0.38 eV and E_{30} = 0.82 eV, and the density of states mass of 1.78m for the lowest subsidiary band, L_1. Since E_{30} is large, no electrons can be excited into the X_1 minima either thermally or by means of applying a high electric field (Gunn effect). Hence all available electrons would be distributed between the two lowest bands with minima at Γ_1 and L_1. In this case the Gunn effect can only involve the L_1 and Γ_1 bands and one would expect that the threshold voltage for oscillations would therefore increase with uniaxial stress in the <111> direction, because the L_1 minima tend to move away from the Γ_1 minimum under applied stress (68C1). However, this is not found experimentally by Harris et al. (70H1), on the contrary, the threshold remains constant up to about 10 Kbars and then decreases by $\sim$ 10% when the stress is increased to 20 Kbars. On the other hand Harris et al. show that with <100> stress applied the threshold voltage decreases appreciably and the oscillations are quenched at just below 10 Kbars. In addition, it can be pointed out that the density of states effective mass of 1.78m seems rather high for a band with L_1 symmetry when compared to the density of states effective masses in the principal conduction band of Ge and the first subsidiary band of GaSb, both of which have the same symmetry and density of states masses of 0.55m and 0.57m respectively. The foregoing arguments rule out this band model as being representative of the conduction band structure of GaAs.

V-4 Mobility in the Γ_1 band of GaAs

The temperature variation of the electron mobility of the Γ_1 band determined from the fitting procedure for the three conduction band model (Γ_1, Δ_1, L_1) is shown in Fig. V-10. This temperature dependence can be explained on the basis of a simple model. As an example, we will take the results for sample M0807/8, Fig. V-11. The compensation in these samples should be negligible, in which case the total ionized impurity concentration will be given by the room temperature carrier concentration, i.e. $N_I = N_D = n_1(300)$. The ionized impurity mobility μ_I can then be approximately calculated using the Brooks-Herring expression obtained by averaging τ_I (equation II-25) over the carrier distribution and then applying the quantum correction factors calculated by Moore (67M1). These are given in Moore's paper in Figs. 2 and 4 as a function of both carrier concentration and temperature. From these figures it can be seen that the total correction factor ($\sigma_B + \sigma_M + \sigma_D$) is about 1.45 and remains fairly constant over the temperature range 20°C - 600°C. The mobility μ_I (equation II-28) is then given by $\mu_I = \mu_I^*/1.45$, and is given for six temperatures in Table V-8, column 2.

The lattice scattering mobility μ_ℓ was calculated by Ikoma (70I1) and included polar optical, two phonon resonant scattering and interband scattering. His results are given in column 3 of Table V-8 and apply for temperatures greater than 500°K. In addition we calculated the mobility due to acoustic scattering, μ_a; this is given in the 4th column of Table V-8. The combined mobilities, using Matthiessen's addition rule, are shown in columns 5 and 6 of Table V-8 for several temperatures. The values given in column 5 include μ_I and μ_ℓ whereas those of column 6 also include μ_a. The last column gives the mobility results derived for sample M0807/8 by fitting the three conduction band model to the experimental results of Hall coefficient and conductivity. These mobilities are plotted in Fig. V-12 against temperature. As can

be seen from Fig. V-12 the magnitude and temperature dependence of mobility based on this rather approximate calculation agree fairly well with the results obtained from curve fitting. It is evident from Fig. V-12 that ionized impurity scattering plays an important role in determining the mobility of electrons in the Γ_1 band. It is therefore important to have a proper expression for the relaxation time due to ionized impurity scattering which must take into consideration both the quantum mechanical correction factors discussed by Moore, and the screening due to both light and heavy electrons. It is understandably a difficult problem to carry out these calculations and perhaps for this reason has not been carried out to date. We have used the Moore correction factor of 1.45, but ignored any effect of screening due to heavy electrons in calculating μ_I^*. It was necessary to include the correction factor to lower μ_I so that reasonable agreement between the calculated values of mobility and those obtained from the fitting procedure could be obtained. Even then, at highest temperatures the calculated μ_I is greater than the fitted value. This discrepancy could be explained by the fact that our approximate calculations ignored interband scattering between Γ_1 and L_1 bands, since Ikoma used only a two band model (Γ_1 and Δ_1) in his calculations. It can also be seen from Fig. V-10 that for the heaviest doped sample, MO241/44, the mobility at high temperatures is considerably lower than for the three more lightly doped samples. This suggests that interband scattering may become stronger at these temperatures and would support the existence of the L_1 band close in energy to the Δ_1 (or X_1) minima. The computer programs written for the calculations of the electron mobility in the Γ_1 band of GaSb could easily be adopted for similar calculations in GaAs. However, such calculations of the mobility in the Γ_1 band of GaAs were considered not worth while until the band structure of GaAs has been settled and more parameters have been experimentally determined for the L_1 band.

V-5 Magnetoresistance measurements at 400°C

The heaviest doped sample available was chosen for these measurements in order to obtain maximum possible electron transfer into the subsidiary band at a reasonable temperature. The sample used (MO18/60) had a room temperature electron concentration of 7.93×10^{24} m^{-3}. It was not employed in the determination of band parameters since, as was pointed out earlier, with such high doping the possibility arises of impurity band overlap with the subsidiary band and thus lowers the energy separation. However, this would only increase the number of carriers excited into the subsidiary band and therefore give better conditions for observation of the two band effect. The results of measurements at 400°C are shown in Fig. V-14 where $\rho_o/\Delta\rho$ is plotted against B^{-2}. Two points are readily apparent from this Figure:

a) systematic deviation from a straight line behaviour is observed and

b) the intercept at $B^{-2} = 0$ is negative.

Neither the non-linearity of the plot nor the negative intercept can be explained by experimental error and are not predicted by the two band model with the assumption employed. It can be seen that the intercept u given by equation II-64 can not be negative.

Calculation of $\Delta\rho/\rho_o$ at 400°C for sample MO241/44 at a field of 3.0 Wb/m^2 gives 0.21% for the two band magnetoresistance. This is less than half the value of the observed magnetoresistance at 3.0 Wb/m^2, i.e. $\Delta\rho/\rho_o = 0.60\%$. Although the carrier density in sample MO18/60 is higher than in MO241/44, hence more carriers will be transfered to the subsidiary band, at the same temperature, which would increase $\Delta\rho/\rho_o$ above 0.21%, this increase will not be large enough to give $\Delta\rho/\rho_o$ of 0.60%. A rough estimate of the magnetoresistance due to the two band effect for sample MO18/60 gives a value of 0.25% at 400°C. The observed magnetoresistance of

0.6% must therefore, to a greater part, be due to a contribution from individual bands. Hence, these types of measurements can not be used to determine band parameters in GaAs as was done for GaSb.

V-6 Summary and Discussion

The results of the analyses for the two models of the conduction bands are summarized in Table V-9. It can be seen that in all cases, E_{30} is $\sim$ 0.38 eV, the lowest value of 0.374 eV is obtained for the three band model (Γ_1, X_1 and L_1). This is reasonable since electron mobility given by Pitt and Lees (70P1) for the subsidiary band with X_1 symmetry is double the value calculated for the Δ_1 band. Hence, to account for the experimentally observed rise in R(T) more electrons have to be present in the subsidiary band in the case of X_1 symmetry.

It is quite evident from the results of the analyses that a clear cut choice can not be made as to the correct conduction band structure of GaAs, based purely on analyses of measurements of the Hall coefficient and conductivity as a function of temperature. However, as can be seen from Tables V-5 through V-7, the most consistent results for the five samples are obtained with the three band model with minima having Γ_1, Δ_1 and L_1 symmetries. The results based on this model are shown schematically in Fig. V-15. It should however be pointed out that since some uncertainty exists in the values of several band parameters used in the analyses, the larger scatter in E_{30} and α_3 obtained in the other cases does not completely rule them out.

V-7 Conclusion

It has been shown that the Hall effect and conductivity measurements on heavily doped GaAs can not, by themselves, conclusively distinguish between the three conduction band models for GaAs. It is felt though, that the investigation reported here has shed more light on the problem at hand and has allowed a more unified understanding of this part of the field. However, there is a need for more work to help in solving some of the points still not fully understood. The position of the L_1 minima is probably the most important of these. This problem can be solved by transport measurements on $GaAs_xSb_{1-x}$ alloys. The <100> bands in the compounds GaAs and GaSb are at about 0.4 and 0.3 eV above the Γ_1 band, these therefore do not move to any extent throughout the alloy system. On the other hand the L_1 band minima in GaSb are about 0.1 eV above the Γ_1 minimum and about 0.5 eV in GaAs (as suggested by the present work). If this is actually the case, then in alloys with x between 0.3 and 0.5, the L_1 minima would lie below the <100> minima, in which case electrons would primarily transfer into these sets of minima when high temperatures, pressures or electric fields are applied. Unfortunately, the problem of growth of these alloys has not been solved to date, therefore, until such time as these alloys are available and measurements of the Hall coefficient and conductivity as a function of temperature are analysed the results of the present work, although not conclusive, give best agreement with available data. Hence, the assignment of the hierarchy of the bands is Γ_1, Δ_1 and L_1.

TABLE V-1

Sample	$T^{o}C$	$n_1 m^{-3}$ x 10^{-23}	$\sigma_1 \Omega^{-1} m^{-1}$ x 10^{-4}	$\mu_1 m^2/V$ sec.
MO572/8	20.1	4.25	2.42	.360
NE22/1	21.5	6.33	3.23	.323
MO807/8	20.0	12.4	5.86	.295
MO370/55	20.4	34.3	9.33	.170
MO241/44	23.0	44.3	15.1	.214
MO18/60	23.2	79.3	21.70	.166

Table V-1 Room temperature values of n_1, σ_1 and μ_1 for the five samples of n-GaAs.

TABLE V-2

	m^*_{1o}	= .0648m	(69C1)
	$m^*_{2\ell}$	= .970m	(66P1)
	m^*_{2t}	= .116m, K_2 = 8.4	(66P1)
†	$m^*_{3\ell}$	= .88m	
	m_{3t}	= .23m, K_3 = 3.8	(66P1)
	M^*_{2d}	= .59m, 4 minima	(66P1)
	M^*_{3d}	= 1.2m, 6 minima	(60E1)
	m^*_h	= 0.50m	(68W1)
	E_{23}	= 0.09 eV at 300°K	(68J2)
	E_3	= Variable	
	E_{oo}	= 1.522 eV	(69P1)
	α_o	= -5.8×10^{-4} eV $^oK^{-1}$	(69P1)
	θ_o	= 300°K	(69K1)
††	α_2	= -6.52×10^{-4} eV $^oK^{-1}$	
††	θ_2	= 214°K	
††	α_2	= -5.45×10^{-4} eV $^oK^{-1}$	
††	θ_3	= 208°K	

† This value was calculated using Ehrenreich's value of M^*_{3d} = 1.2m and Pollak's value of m^*_{3t} = .23m.

†† These values were obtained by least squares fitting of optical data reported by Walter et al. (70W1).

Table V-2: List of band parameters for GaAs together with the references from which these were obtained.

TABLE V-3

E_1 peak	T^oK	E_1(expt)eV	E_1(fit)eV	δ
	0 0	3.015		
	25	3.014	3.013	-.001
	50	3.010	3.009	-.001
	75	3.002	3.002	.000
	100	2.996	2.994	-.002
	125	2.986	2.985	-.001
	150	2.976	2.975	-.001
	175	2.964	2.964	.000
	200	2.952	2.952	.000
	225	2.939	2.940	.001
	250	2.926	2.927	.001
	275	2.914	2.914	.000
	300	2.902	2.901	-.001
		$\alpha_2 = -6.52 \times 10^{-4}$,	$\theta_2 = 214$	
E_2 peak	0	5.114		
	25	5.113	5.113	.000
	50	5.110	5.109	-.001
	75	5.105	5.103	-.002
	100	5.098	5.096	-.002
	125	5.090	5.088	-.002
	150	5.080	5.080	.000
	175	5.070	5.070	.000
	200	5.060	5.061	+.001
	225	5.050	5.050	.000
	250	5.039	5.040	+.001
	275	5.029	5.029	.000
	300	5.018	5.018	.000
		$\alpha_2 = -5.45 \times 10^{-4}$,	$\theta_3 = 208$	

Table V-3: Results of least squares fitting of the optical data for the E_1 and E_2 peaks as a function of temperature from wavelength modulation reflectance data of Walter et al. (70W1).

TABLE V-4

Band	Mobility at $300^{o}K$ $m^2/V.Sec.$	Temperature dependence of μ	Scattering parameter
Γ_{1c} (000)			1.08
L_{1c} <111>	Variable	$T^{-1.5}$	1.18
Δ_{1c} <100>	0.015	$T^{-1.5}$	1.18
Γ_{15V} <000>	0.045	$T^{-1.5}$	1.18

Table V-4: The mobility, its temperature dependence and scattering parameter used in fitting the GaAs data.

TABLE V-5

Sample	E_{30} eV	E_{20} eV	$\mu_2(300^oK)$ $m^2/V.sec.$
M0241/44	0.380	0.487	.065
M0370/55	0.381	0.488	.070
M0807/8	0.380	0.487	.065
NE22/1	0.384	0.491	.065
M0572/8	0.381	0.488	.060

Table V-5: Results of fitting to the three conduction band model, Γ_1, L_1 and Δ_1.

TABLE V-6

Sample	E_{30} eV	α_3 eV^oK^{-1} x 10^4	E_{20} eV
MO241/44	0.373	-6.1	0.472
MO320/55	0.372	-6.1	0.471
MO807/8	0.374	-6.0	0.473
NE22/1	0.376	-5.9	0.475
MO572/8	0.376	-6.0	0.475

Table V-6: Results of fitting to the three conduction band model, Γ_1, L_1 and X_1.

TABLE V-7

Sample	E_{30} eV	α_3 eV^oK^{-1} x 10^5
MO241/44	.385	-3.5
MO370/55	.388	-3.8
MO807/8	.386	-3.4
NE22/1	.386	-3.6
MO572/8	.384	-3.2

Table V-7: Results of fitting to the two conduction band model Γ_1 and Δ_1.

1	2	3	4	5	6	7
T^oK	$\mu_I^* m^2$/V.sec.	μ_ℓ m^2/V.sec.	$\mu_a m^2$/V.sec.	$\mu_1 m^2$/V.sec. (μ_I, μ_ℓ)	$\mu_1 m^2$/V.sec. (μ_I, μ_ℓ, μ_a)	$\mu_1 m^2$/V.sec. $(\Gamma_1, \Delta_1, L_1)$
293	.462	.930	13.5	.309	.302	.295
503	.582	.362	5.98	.223	.215	.235
603	.645	.294	4.56	.202	.193	.203
693	.693	.255	3.70	.186	.177	.176
773	.728	.220	3.14	.169	.160	.153
813	.744	.210	2.91	.164	.155	.143

TABLE V-8

Table V-8: Approximate calculations of mobility $\mu_1(T)$ of the electrons in the Γ_1 band, for sample M0807/8 of GaAs. The ionized impurity scattering mobility μ_I^* was calculated using $N_I = 1.24 \times 10^{24} m^{-3}$ and Ehrenreich-Moore correction factor of 1.45. The lattice mobility μ_ℓ was taken from Ikoma (70I1) and acoustic mobility was calculated assuming the deformation potential of 7 eV.

			$\Gamma_1 - L_1$			$\Gamma_1 - X_1$		L_1	Δ_1, X_1
Model	Conduction bands	E_{20} eV	α_2 eV $^oK^{-1}$ x 10^{-4}	θ_2 ^oK	E_{30} eV	α_3 eV $^oK^{-1}$ x 10^{-4}	θ_3 ^oK	$\mu_2(300)$ $m^2/V.sec.$	$\mu_3(300)$ $m^2/V.sec.$
1	Γ_1, Δ_1 and L_1	0.488	-6.52	214	.381	-5.45	208	.065	.015
	Γ_1, X_1 and L_1	0.473	-6.52	214	.374	-6.00	208	.065	.035
2	Γ_1 and Δ_1	-	-	-	.386	-.35	-	-	.015

Table V-9 : Summary of results for the two models of the conduction band structure of GaAs.

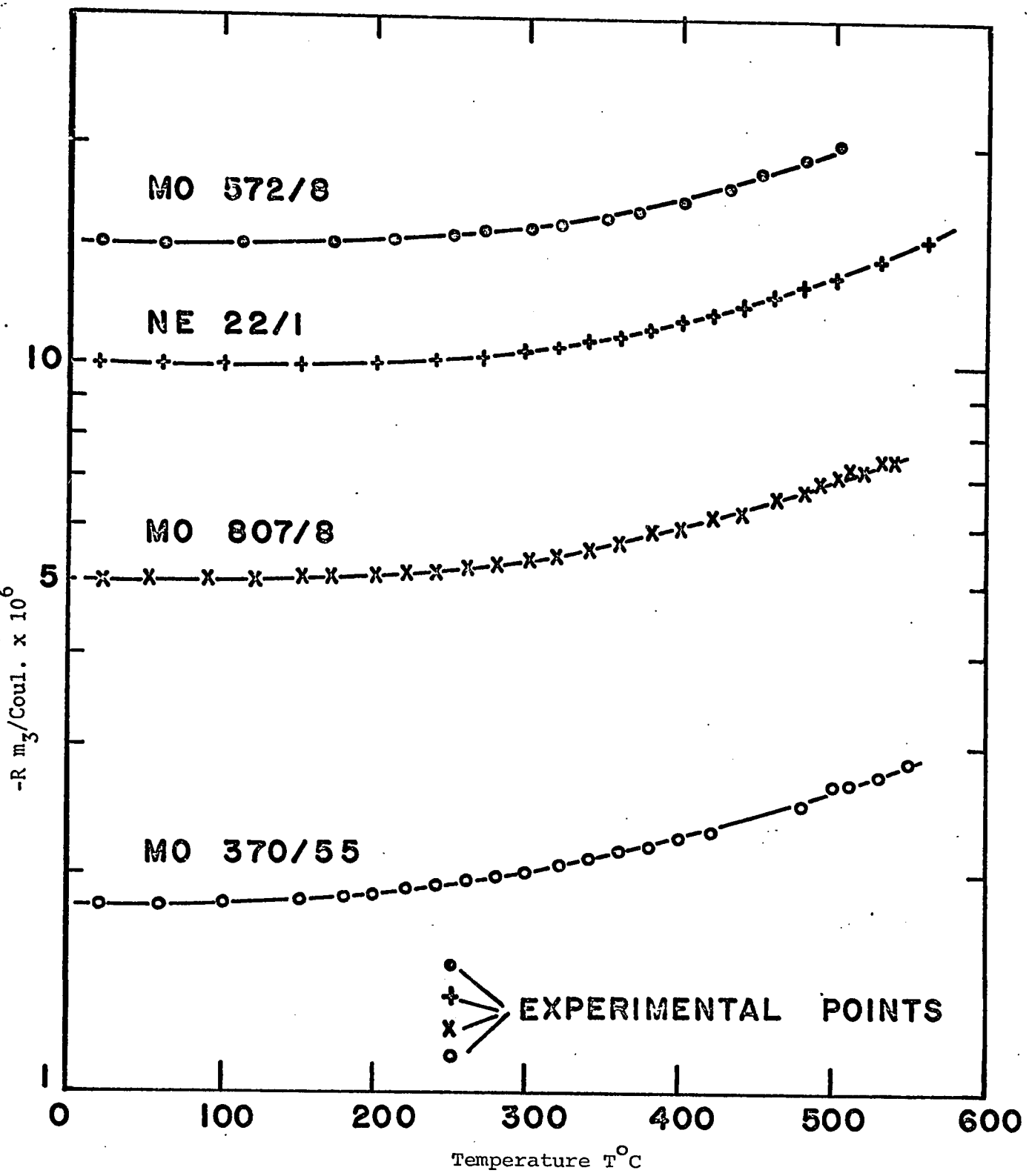

Fig. V-1 A semi-log plot of the experimental Hall coefficient vs temperature for four samples of n-GaAs.

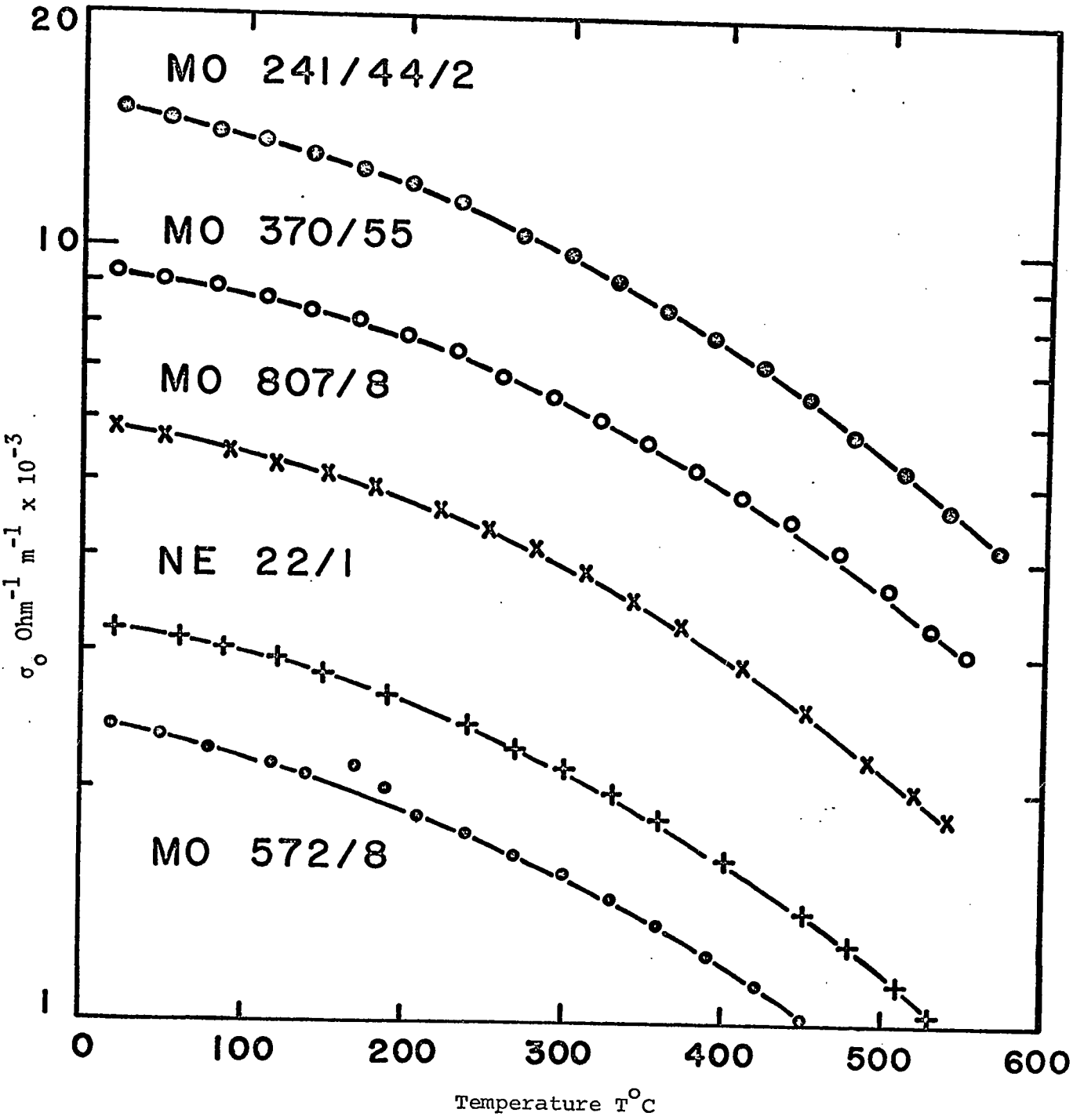

Fig. V-2 A semi-log plot of the experimental conductivity vs temperature for five samples of n-GaAs.

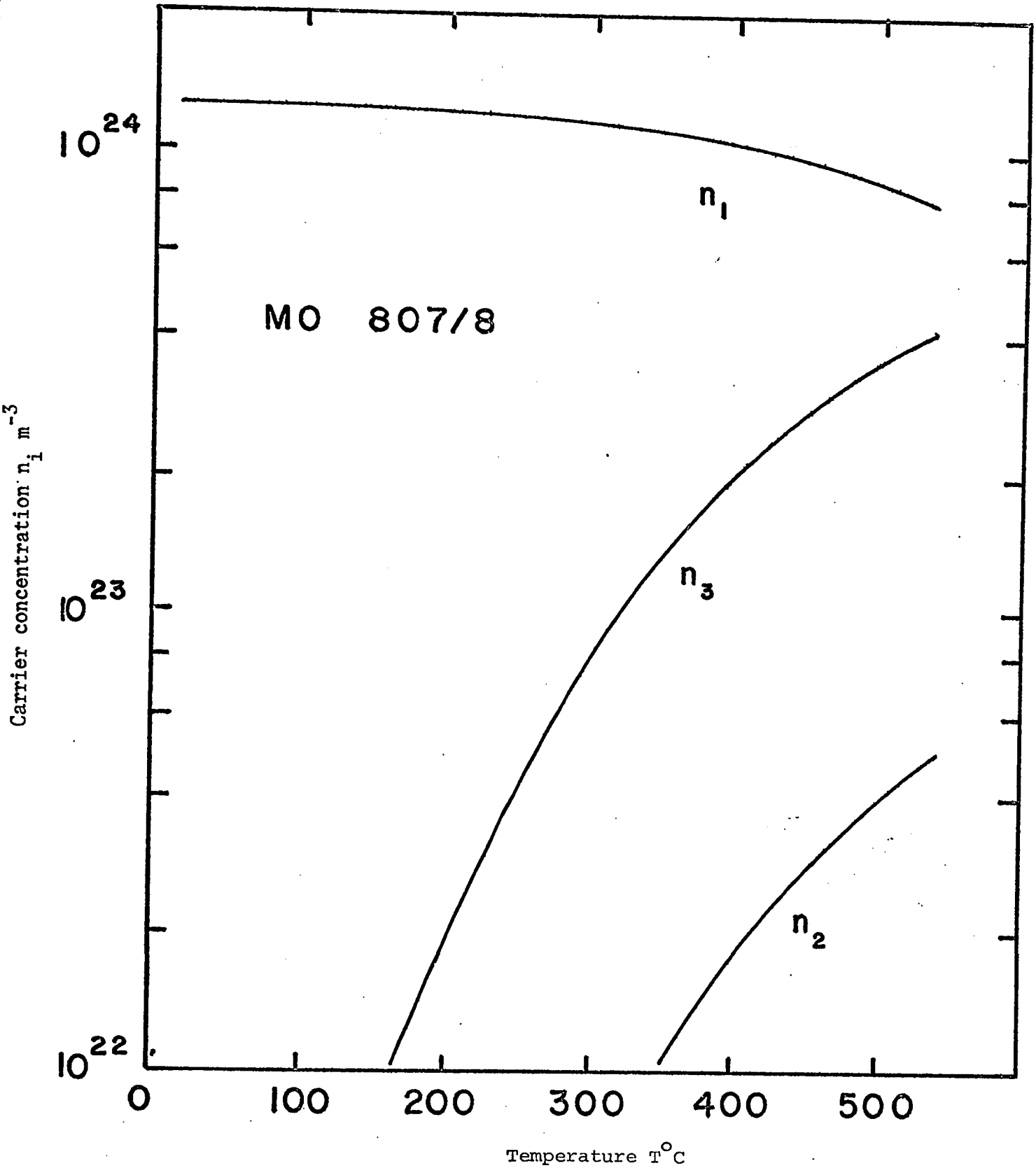

Fig. V-3 A semi-log plot of carrier concentration n_1, n_2 and n_3 in the three conduction minima Γ_1, L_1 and Δ_1, with $\mu_2(300) = 0.065$ m^2/V.sec and $E_{30} = 0.380$ eV.

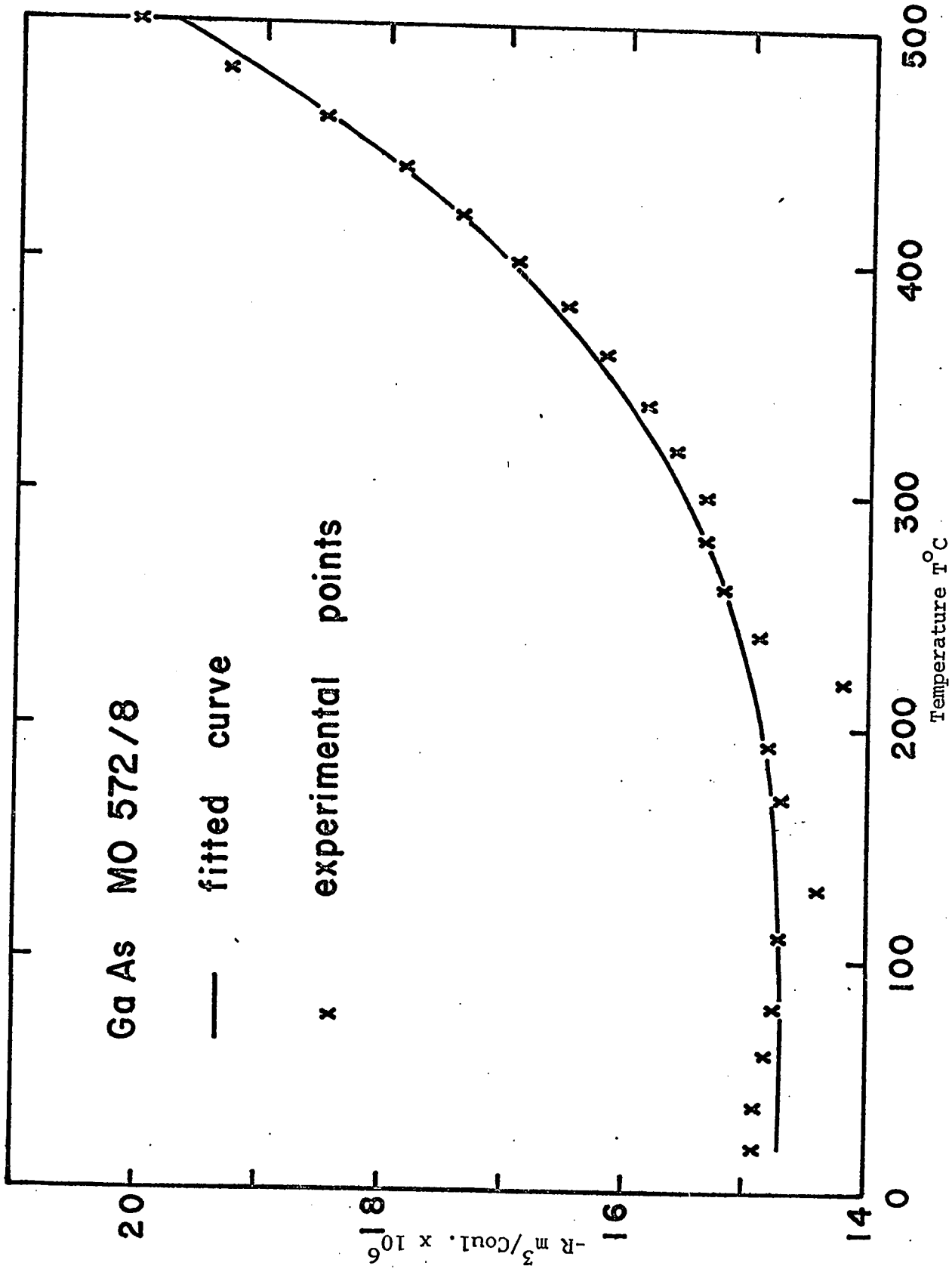

Fig. V-4 The Hall coefficient vs temperature for sample MO572/8 of n-GaAs. The solid line is the fitted curve for the three conduction band model Γ_1, L_1, Δ_1(or X_1). The crosses are experimental points.

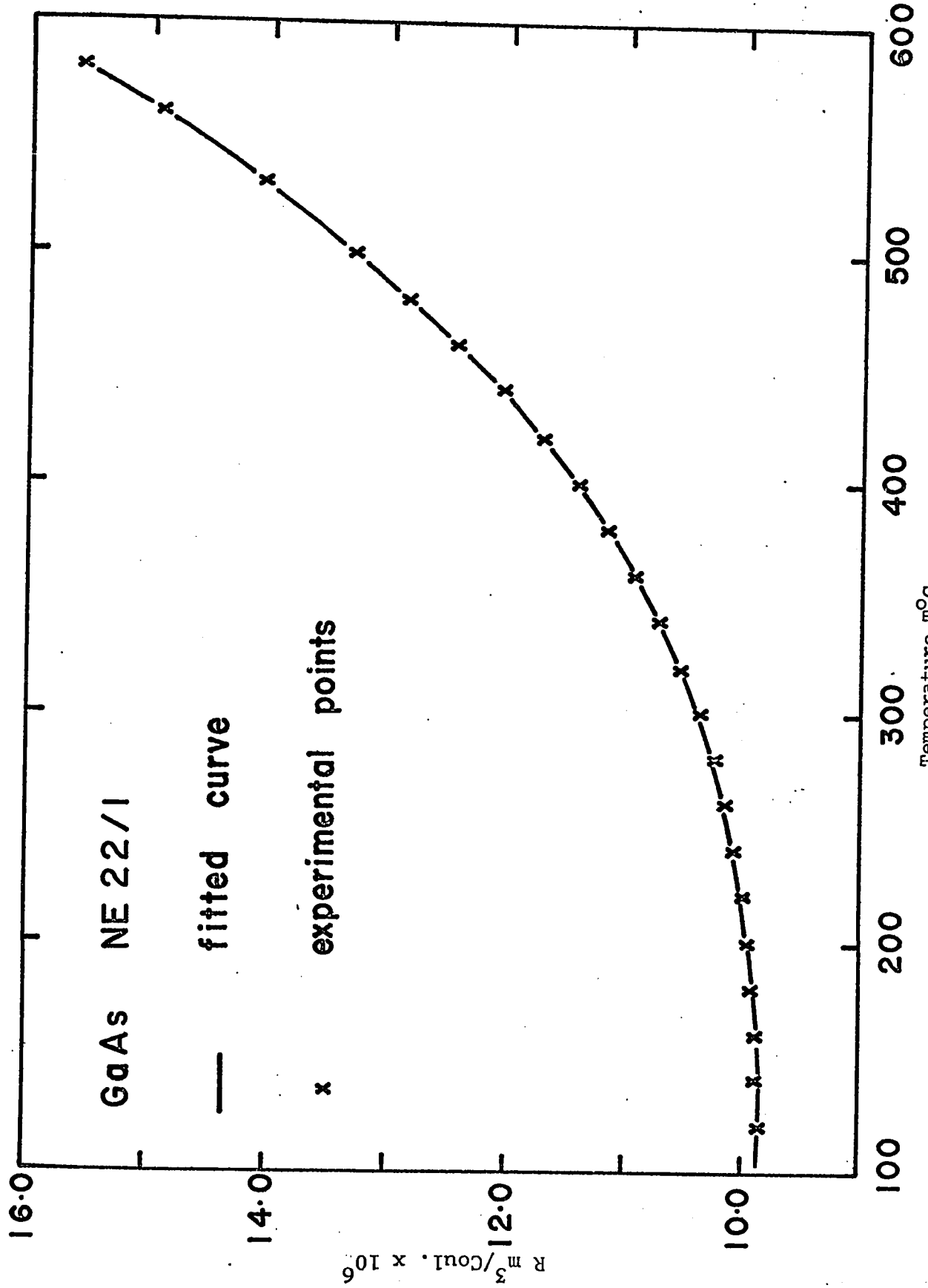

Fig. V-5 The Hall coefficient vs temperature for sample NE22/1 of n-GaAs. The solid line is the fitted curve for the three conduction band model Γ_1, L_1, Δ_1(or X_1). The crosses are experimental points.

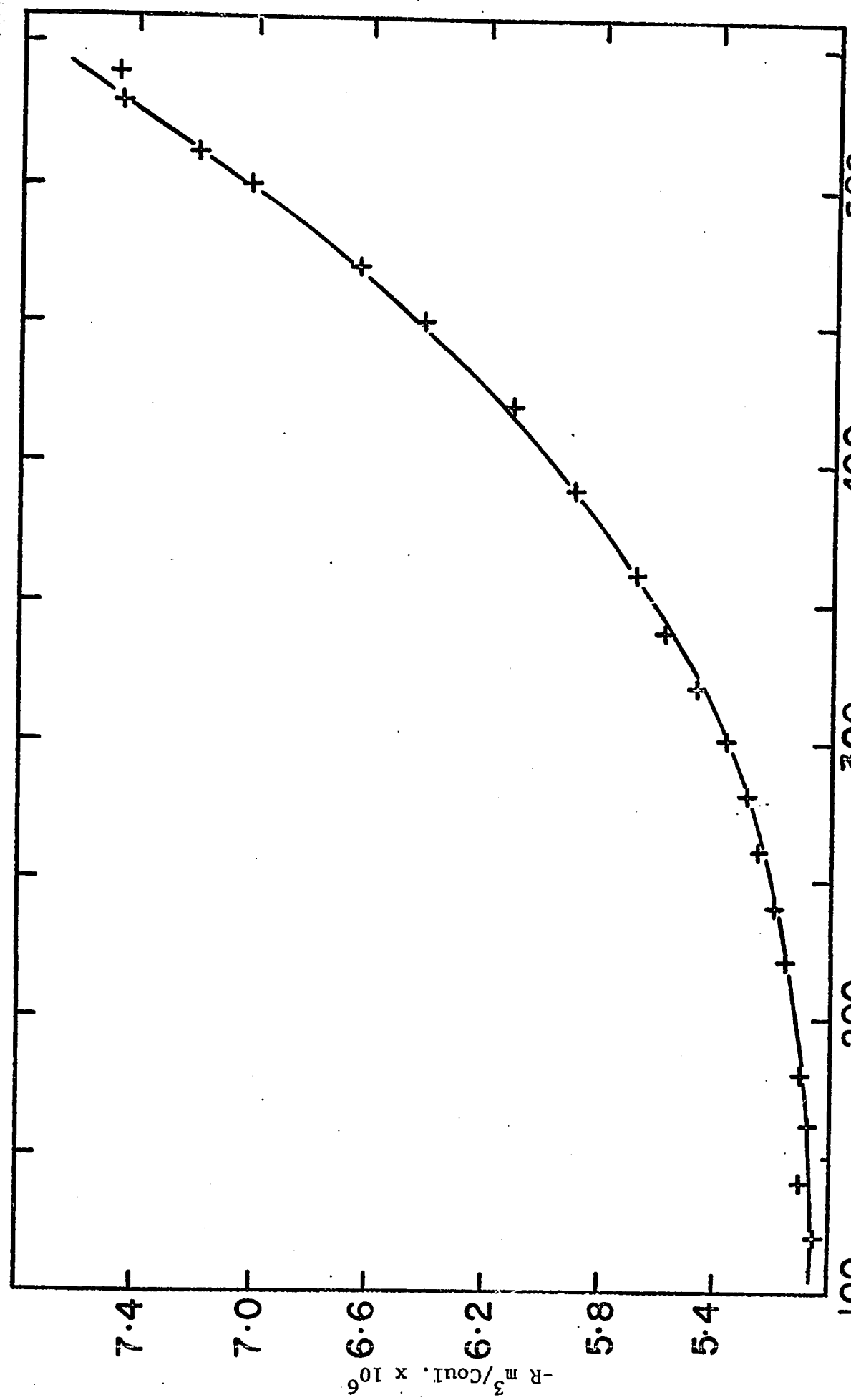

Fig. V-6 The Hall coefficient vs temperature for sample M0807/8 of n-GaAs. The solid line is the fitted curve for the three conduction band model Γ_1, L_1, Δ_1(or X_1). The crosses are experimental points.

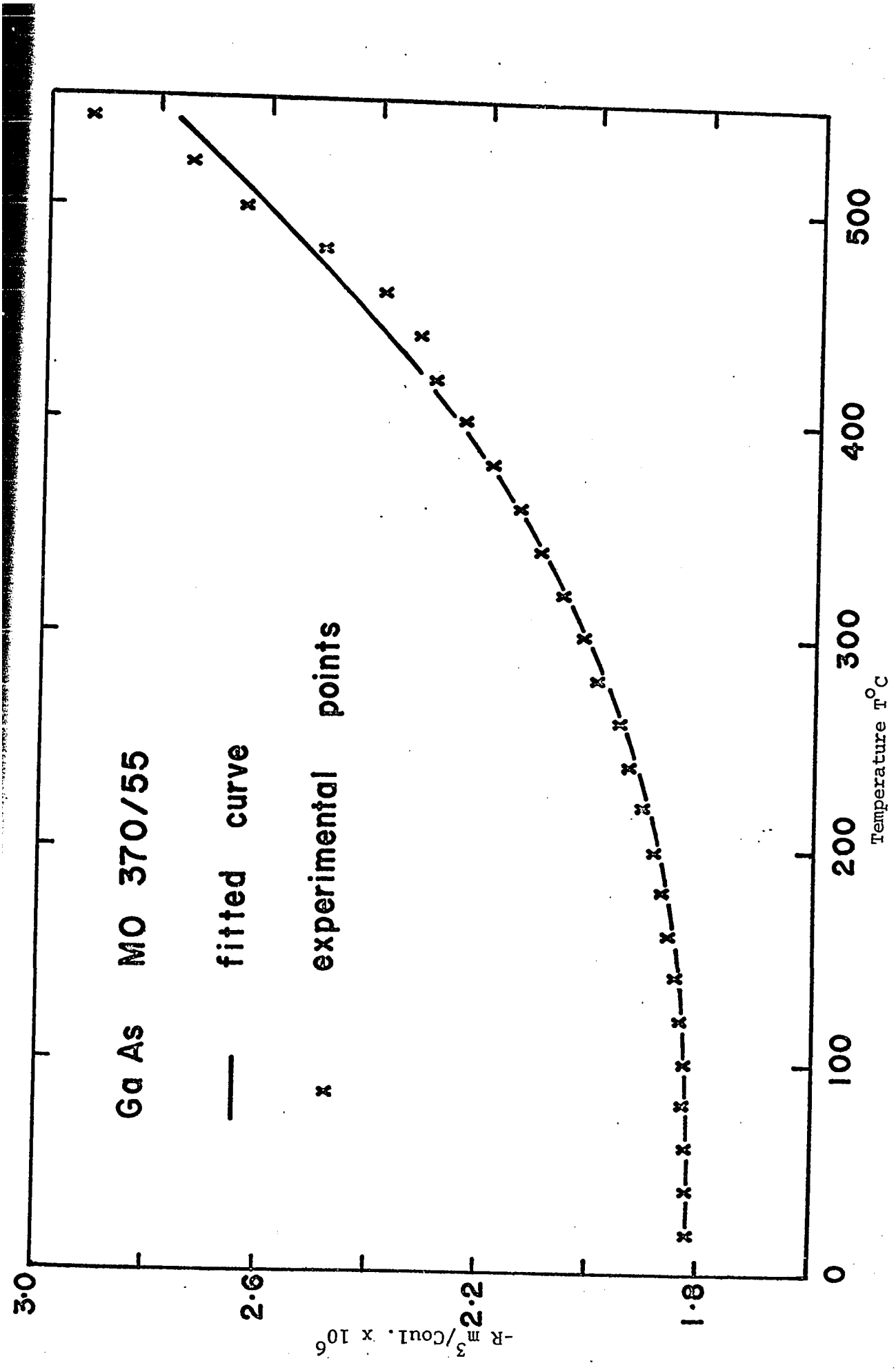

Fig. V-7 The Hall coefficient vs temperature for sample MO370/55 of n-GaAs. The solid line is the fitted curve for the three conduction band model Γ_1, L_1, Δ_1 (or X_1). The crosses are experimental points.

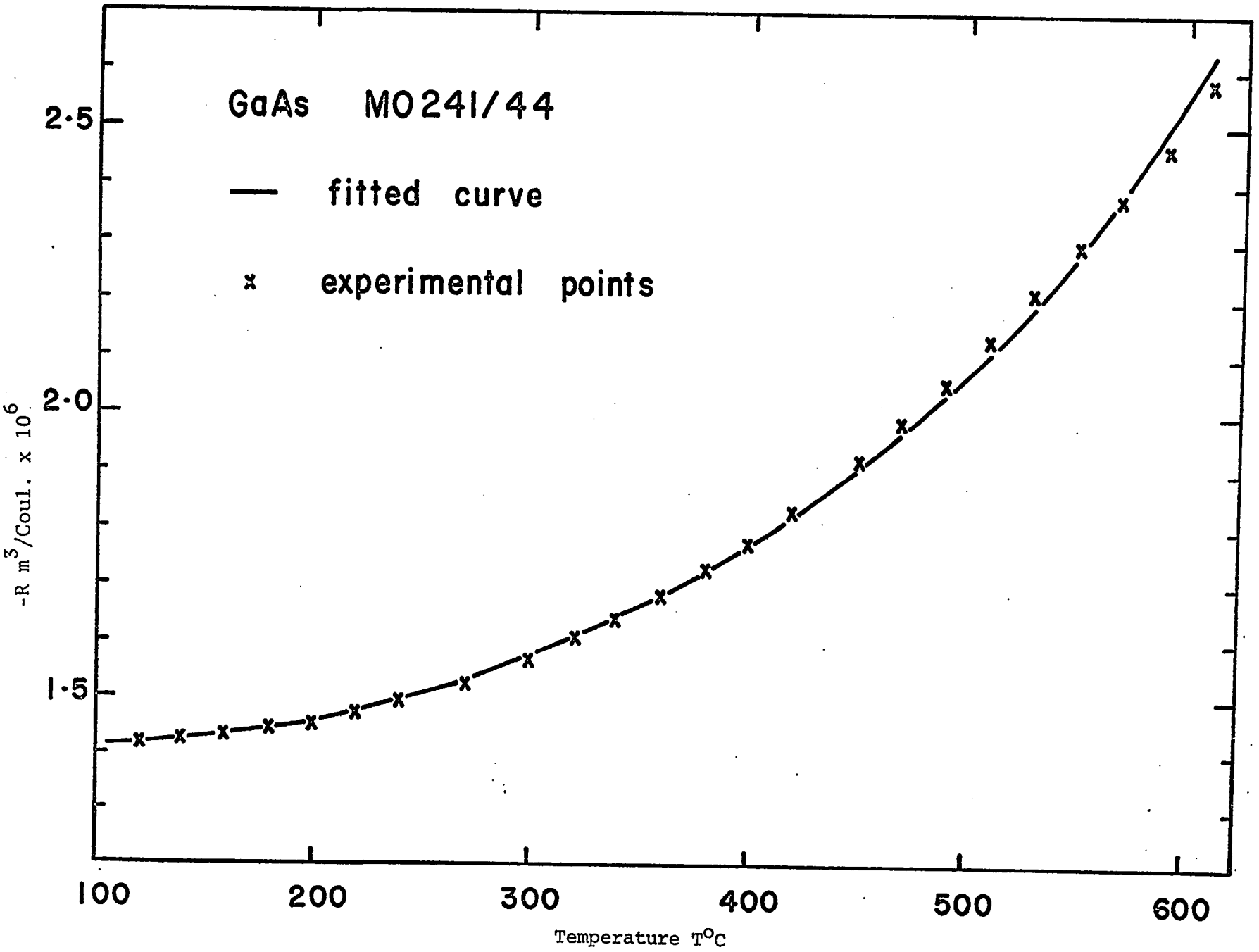

Fig. V-8 The Hall coefficient vs temperature for sample MO241/44 of n-GaAs. The solid line is the fitted curve for the three conduction band model Γ_1, L_1, Δ_1 (or X_1). The crosses are experimental points.

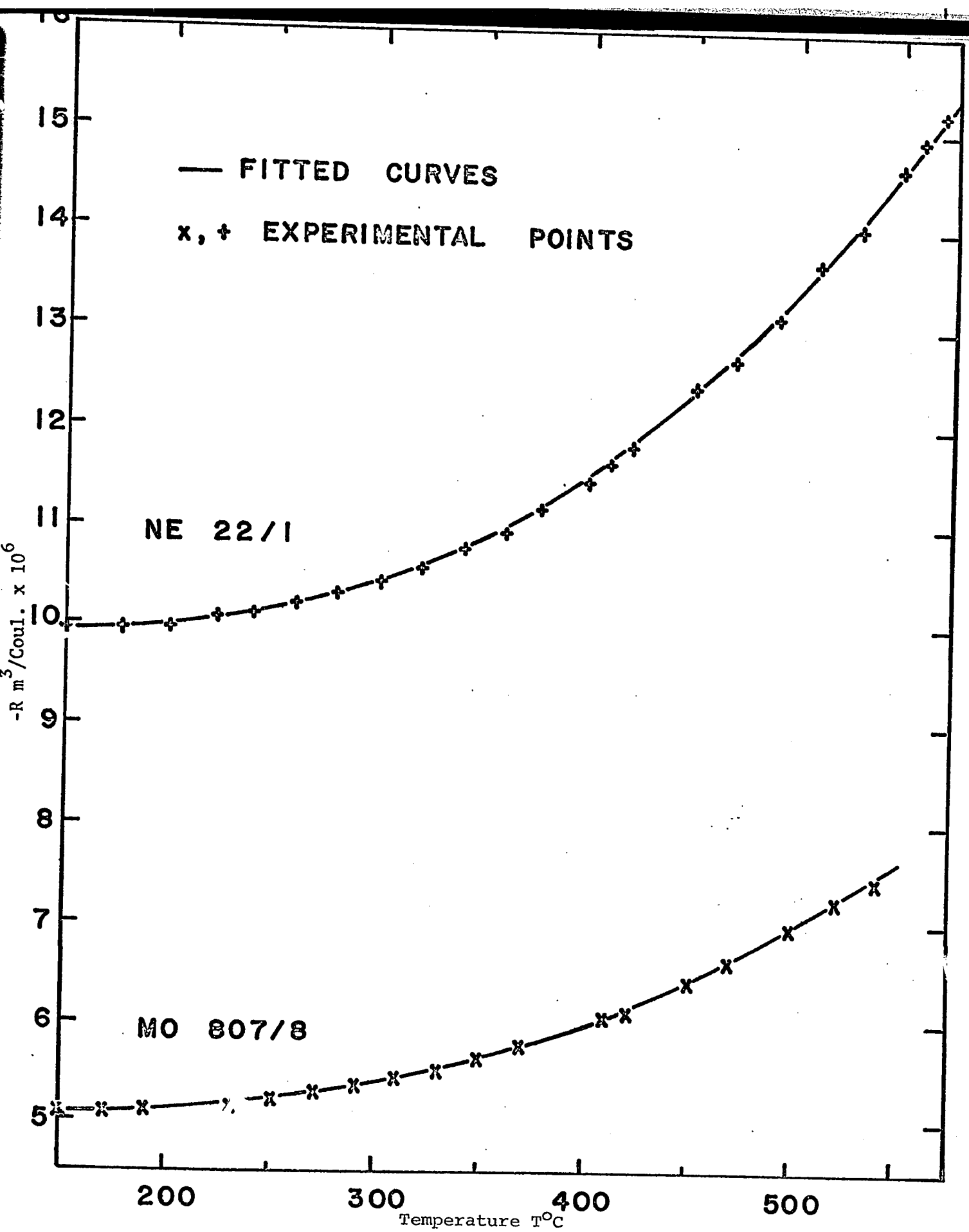

Fig. V-9 The Hall coefficient vs temperature for samples MO807/8 and NE22/1 of n-GaAs. The solid line is the fitted curve for the two conduction model Γ_1 and Δ_1.

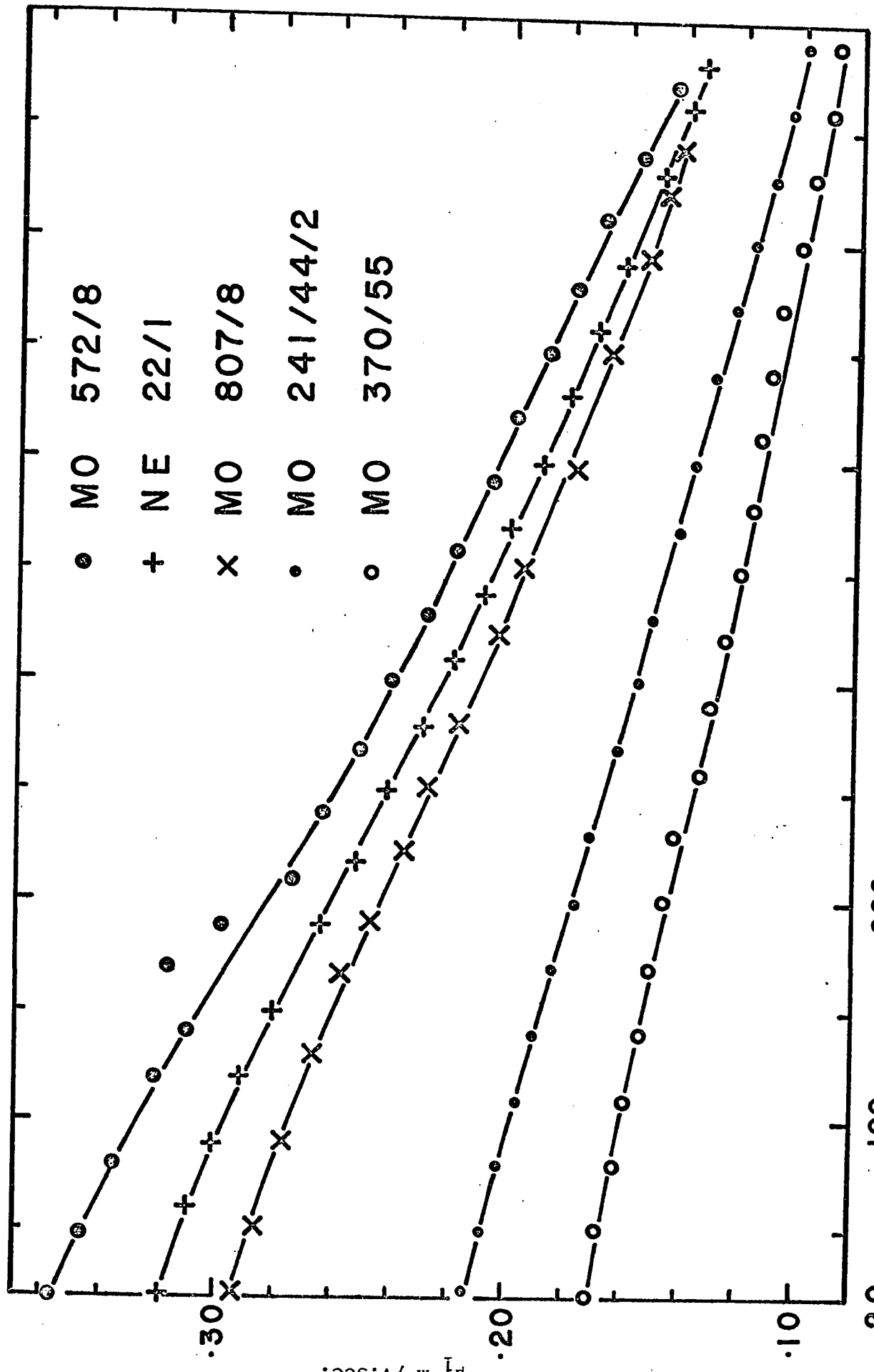

Fig. V-10 Electron mobility in the Γ_1 minimum vs temperature obtained by fitting R(T) with the three conduction band model Γ_1, L_1, Δ_1 (or X_1).

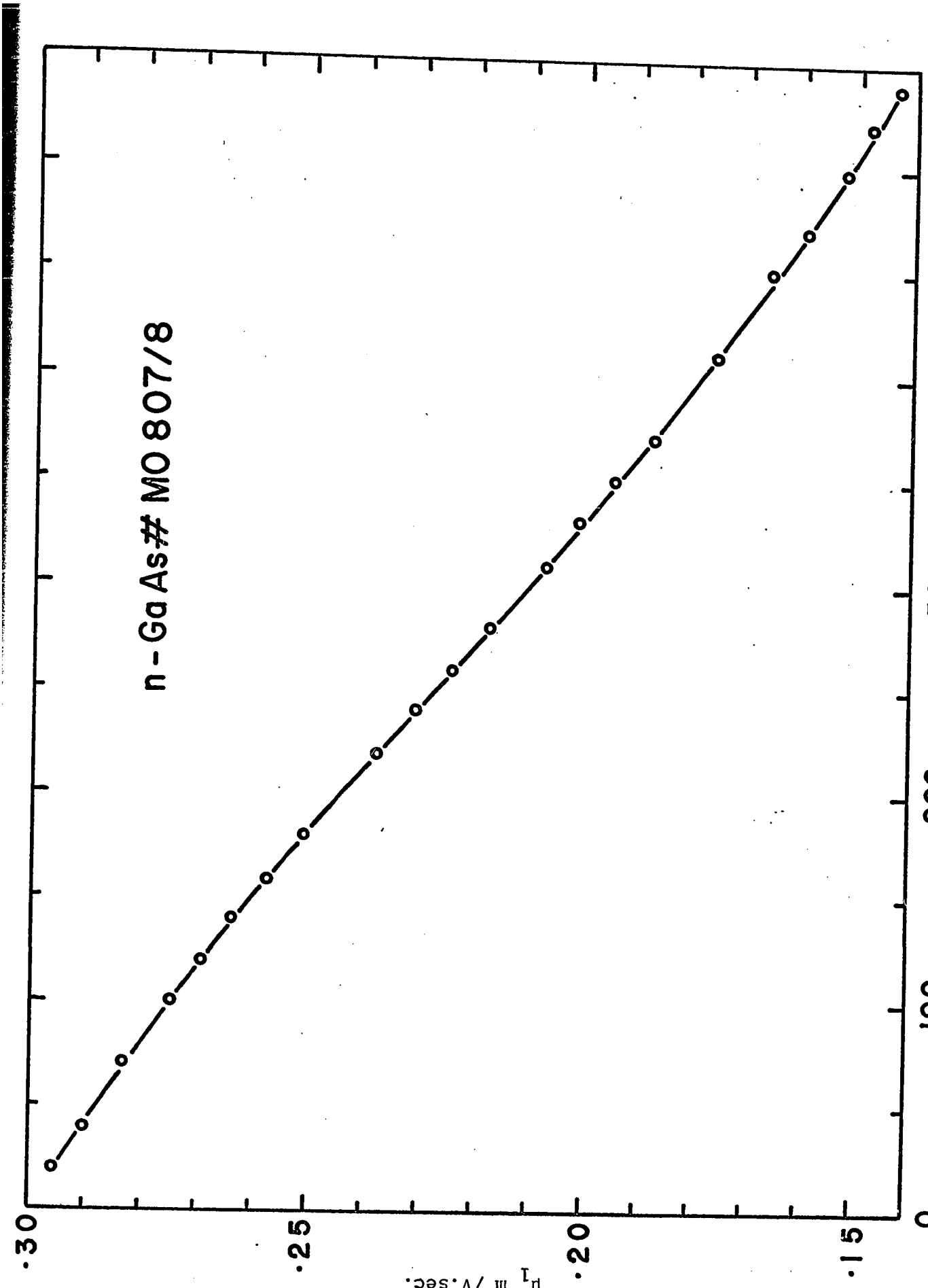

Fig. V-11 Electron mobility in the Γ_1 minimum vs temperature for sample MO807/8, obtained by fitting R(T) with the three conduction band model Γ_1, L_1, Δ_1 (or X_1).

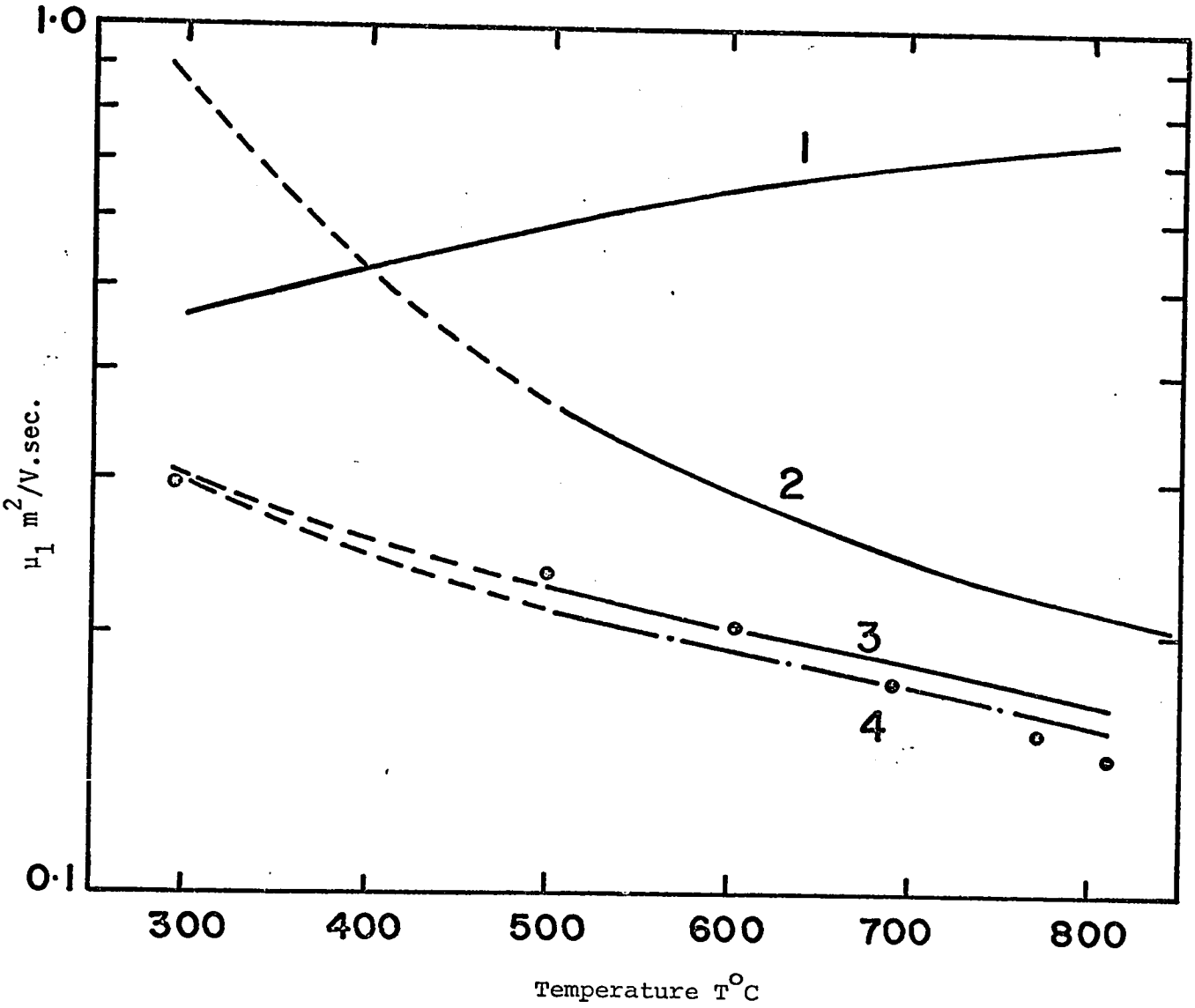

Fig. V-12 Electron mobility in the Γ_1 minimum vs temperature for sample MO807/8. (1) Ionized impurity mobility μ_I(B-H) N_I = 1.24 X10^{24}m^{-3}. (2) Lattice mobility μ_ℓ using Ikoma's results. (3) Combined μ_I and μ_ℓ mobilities. (4) Combined μ_I, μ_ℓ and μ_a.

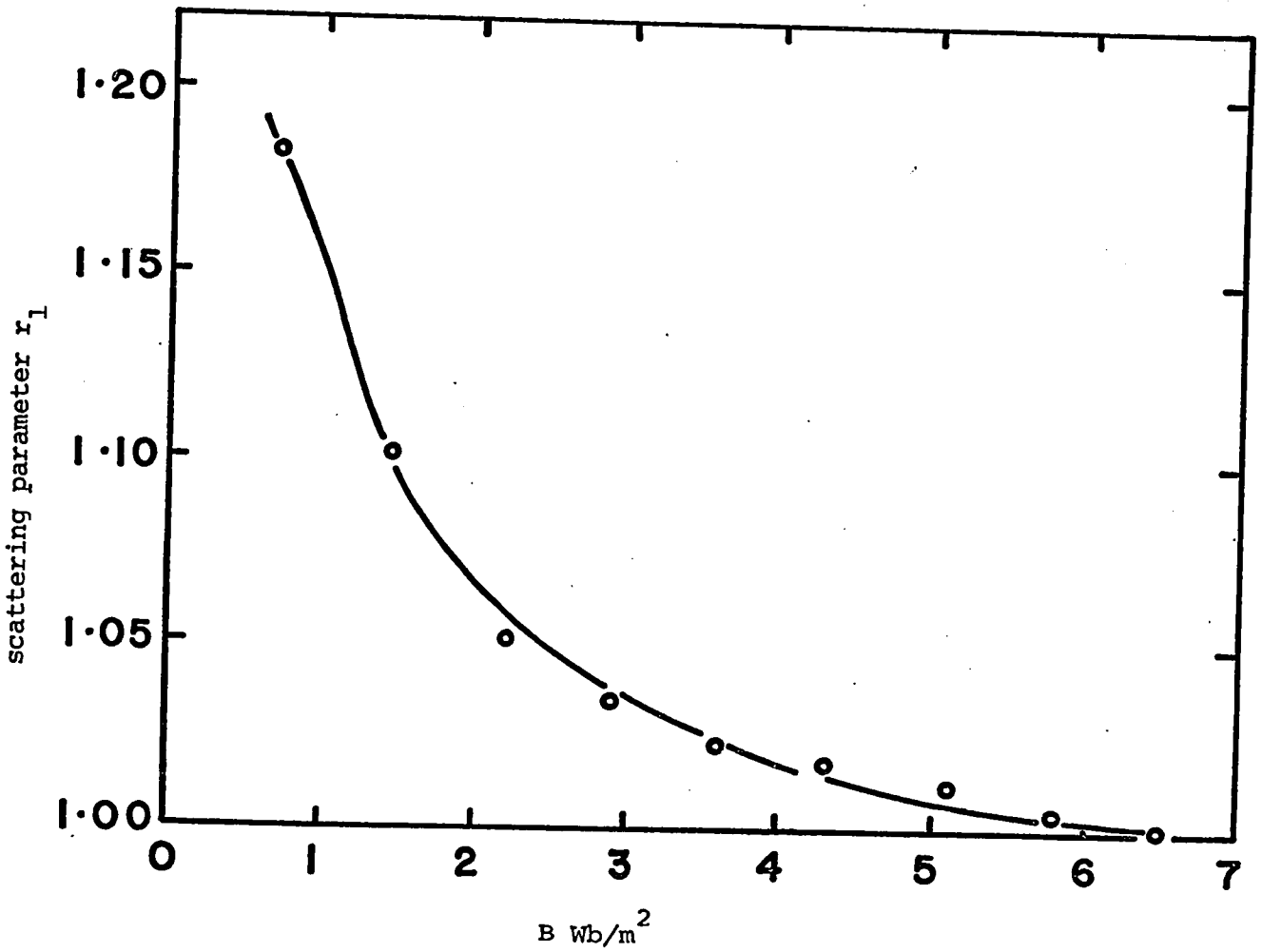

Fig. V-13: Variation of the Hall scattering parameter, r_1, with magnetic field, B, for sample NE22/1 at -50°C.

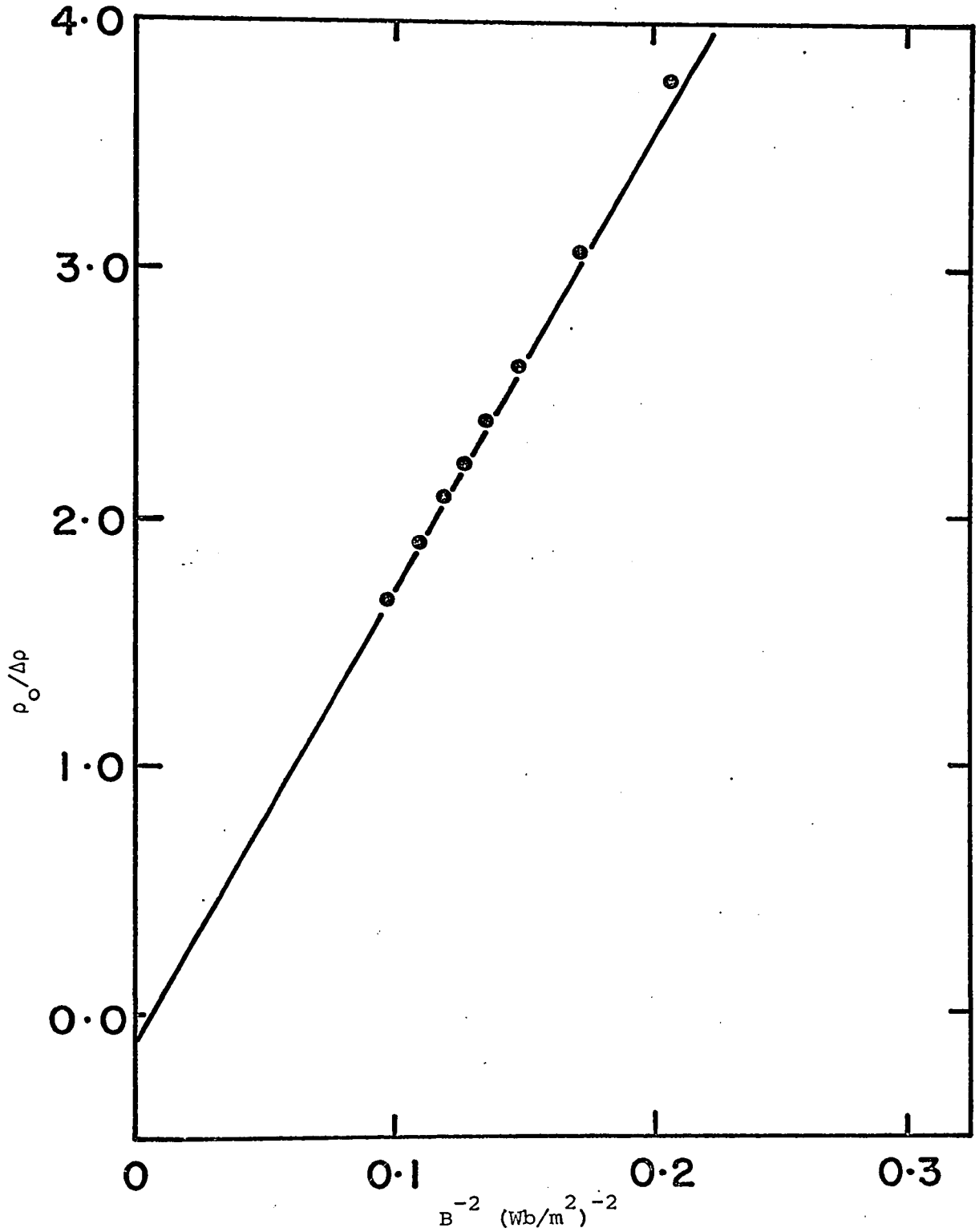

Fig. V-14: Variation of $\rho_o/\Delta\rho$ with B^{-2} for sample M018/60, at 400°C.

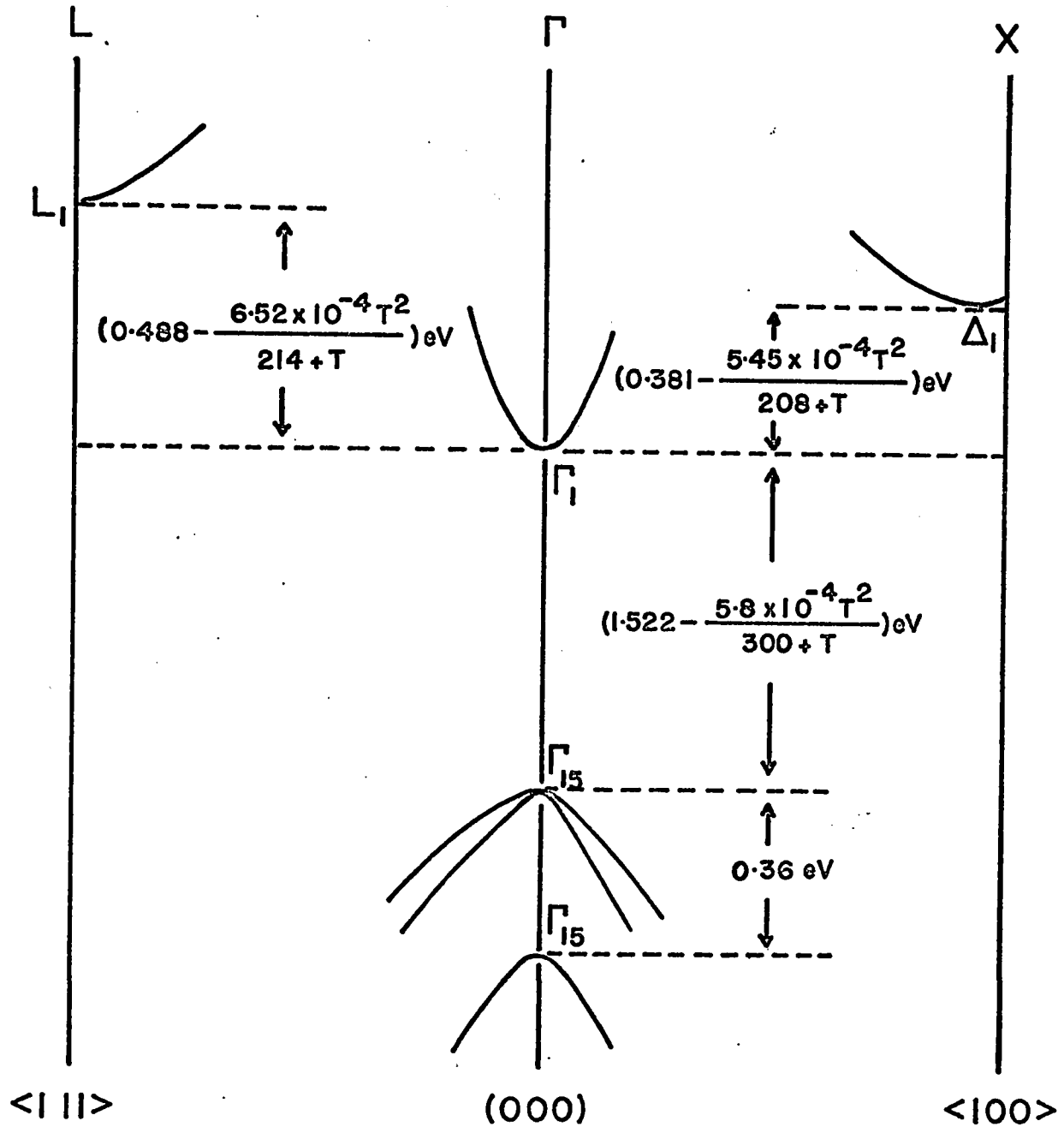

Fig. V-15 Schematic of the band structure of GaAs. Includes the previously established parameters as well as those estimated in this thesis.

APPENDIX A

Harland (65H1) made magnetoresistance and Hall coefficient measurements as a function of magnetic field on several n-type GaSb samples at 4.2°K. He analysed these to obtain R_1, R_2, σ_1 and σ_2, from which values he calculated n_1, n_2, μ_1 and μ_2. His analysis involved expanding the two band Hall coefficient and magnetoresistance in terms of ascending powers of B^2 and relating the coefficients to the band parameters R_1, R_2, σ_1 and σ_2. We have re-analysed his data using our method which does not involve the approximation made by expansion in terms of B^2, the results are shown in Table A-1, together with Harland's results. It can be seen that the two methods give very similar results for R_1, σ_1 and σ_2 but the value of R_2 obtained by Harland is smaller than that determined by the present method. This would tend to over-estimate the total carrier density. The results based on the present analysis were fitted to determine the value of E_2 at 4.2°K, a value of E_2 = 0.093 eV was obtained. This essentially is the value at absolute zero, i.e. E_{20}.

	HARLAND'S ANALYSIS				THIS WORK			
Sample	$-R_1$ m^3/Coul. x 10^6	$-R_2$ m^3/Coul. x 10^6	σ_1 $\Omega^{-1}m^{-1}$ x 10^{-5}	σ_2 $\Omega^{-1}m^{-1}$ x 10^{-4}	R_1 m^3/Coul. x 10^6	R_2 m^3/Coul. x 10^6	σ_1 $\Omega^{-1}m^{-1}$ x 10^{-5}	σ_2 $\Omega^{-1}m^{-1}$ x 10^{-4}
6	4.817	8.59	2.005	.944	4.814	8.95	2.007	.955
7	3.898	.541	2.101	4.917	3.954	.786	2.083	5.158

TABLE A-1

Table A-1: Comparison of analysis of Harland's (65H1) data of magnetoresistance as a function of magnetic field and Hall coefficient at 4.2^oK

REFERENCES

1917 (17C1) J. CZOCHRALSKI, Z. Physik. Chem. 92, 219.

1928 (28B1) F. BLOCH, Z. Physik. 52, 555.

1930 (30K1) R. de L. KRONIG and W. G. PENNEY, Proc. Roy. Soc. (London), A130, 499.

1950 (50B1) J. BARDEEN and W. SHOCKLEY, Phys. Rev. 80, 1, 72.

(50C1) E. M. CONWELL and V. F. WEISSKOPF, Phys. Rev., 77, 388.

1951 (51B1) H. BROOKS, (and HERRING), Phys. Rev., 83, 879.

1952 (52C1) R. G. CHAMBERS, Proc. Phys. Soc. A65, 903.

1953 (53B1) L. BRILLOUIN, "Wave Propagation in Periodic Structures", McGraw-Hill Book Co., Inc. (1946), Dover Publcations Inc.

(53K1) C. KITTEL, "Introduction to Solid State Physics", J. Wiley & Sons, Inc., 3rd Edition (1967).

1955 (55B1) H. BROOKS, in Advances in Electronics and Electron Physics (Academic Press, Inc., New York) Vol. 7.

(55D1) R. G. DINGLE, Phil. Mag., 46, 831.

(55D2) G. DRESSELHAUS, A. KIPP and C. KITTEL, Phys. Rev., 98, 368.

(55D2) G. DRESSELHAUS, Phys. Rev., 100, 580.

(55P1) R. H. PARMENTER, Phys. Rev., 100, 573.

1956 (56E1) H. EHRENREICH and A. OVERHAUSER, Phys. Rev., 104, 649.

(56H1) C. HERRING and E. VOGT, Phys. Rev., 101, 944.

(56K1) E. O. KANE, Phys. Chem. Sol., 1, 83.

1957 (57E1) H. EHRENREICH, Phys. Chem. Sol. 2, 131.

(57G1) LOUIS GOLD and LAURA M. ROTH, Phys. Rev., 107, 358.

(57K1) E. O. KANE, Phys. Chem. Sol., 1, 249.

1958 (58P1) J. C. PHILLIPS, Phys. Rev., 112, 685.

(58S1) R. J. SLADEK, Phys. Chem. Sol. 5, 155.

(58W1) J. C. WOOLLEY and B. A. SMITH, Proc. Phys. Soc., 72, 214.

1959 (59E1) H. EHRENREICH , Phys. Chem. Sol., 9, 129.

(59S1) R. A. SMITH, "Semiconductors", Cambridge University Press.

(59Z1) S. ZWERDLING, B. LAX, K. J. BUTTON and L. M. ROTH, Phys. Chem. Sol. 9, 320.

1960 (60E1) H. EHRENREICH, Phys. Rev., 120, 1951.

(60S1) A. SAGAR. Phys. Rev., 117, 93.

1961 (61B1) W. M. BECKER, A. K. RAMDAS and H. Y. FAN, J. Appl. Phys. Suppl. 32, 2094.

(61C1) M. CARDONA, Phys. Rev., 121, 752.

(61E1) H. EHRENREICH, J. Appl. Phys. Suppl. 32, 2155.

(61K1) J. KOLODZIEJCZAK, Acta. Phys. Pol., 20, 289.

(61S1) A. J. STRAUSS, Phys. Rev., 121, 1087.

(61W1) J. C. WOOLLEY and J. A. EVANS, Proc. Phys. Soc., 78, 354.

1962 (62B1) R. T. BATE, J. Appl. Phys., 33, 26.

(62C1) C. N. COCHRAN and L. M. FOSTER, J. Electrochem. Soc., 109, 149.

(62S1) M. D. STURGE, Phys. Rev., 127, 768.

(62T1) F. TRUMBORE, P. FREELAND and A. MILLS, J. Electrochem. Soc., 109, 645.

(62W1) L. R. WEISBERG, J. Appl. Phys., 33, 1817.

(62Z1) W. ZAWADZKI, Phys. Stat. Sol., 2, 285.

1963 (63B1) A. C. BEER, "Galvanomagnetic Effects in Semiconductors", Academic Press.

(63P1) H. PILLER, J. Phys. Chem. Sol., 24, 425.

(63S1) M. SHYAM, J. W. ALLEN and G. L. PEARSON, Trans. I.E.E.E., ED-13, 63

1964 (64B1) D. BRUST, Phys. Rev., 134A, 1337.

(64M1) D. MADELUNG, "Physics of II-V Compounds", John Wiley & Sons, Inc.

(64P1) H. PILLER, Proc. of 7th Intr. Conf. on Phys. of Semiconductors, Paris, 297.

(64S1) L. SOSNOWSKI, Proc. of 7th Intr. Conf. on Phys. of Semiconductors, Paris, 341.

1965 (65H1) H. B. HARLAND, Thesis, University of Ottawa.

(65M1) W. M. DE MEIS, Thesis, Harvard University Technical Report, No. HP-15.

(65R1) F. E. ROBERTS, Phys. Letters, 17, 21.

1966 (66B1) W. M. BECKER and T. O. YEP, J. Jap. Phys. Soc. 21, 366.

(66C1) M. L. COHEN and T. K. BERGSTRESSER, Phys. Rev., 141, 789.

(66M1) E. J. MOORE and H. EHRENREICH, Sol. Stat. Comm., 4, 407.

(66H1) H. B. HARLAND and J. C. WOOLLEY, Can. J. Phys., 44, 2715.

(66H2) C. HILSUM, Phys. Letters, 20, 136.

(66K1) E. O. KANE, Phys. Rev., 146, 558.

(66K2) J. KOLODZIEJCZAK, S. ZUKOTYNSKI and H. STRAMSKA, Phys. Stat. Sol., 14, 471.

(66P1) F. H. POLLAK, C. W. HIGGINBOTHAM and M. CARDONA, Proc. Intr. Conf. Phys. Semicond. Kyoto, J. Phys. Soc. Japan Suppl., 21, 20.

(66R1) Yu. I. RAVICH, Soviet Physics-Solid State, 7, 1466.

(66Y1) T. O. YEP and W. M. BECKER, Phys. Rev., 144, 741.

1967 (67B1) R. D. BAXTER, F. J. REID and A. C. BEER, Phys. Rev., 162, 718.

(67B2) J. BASINSKI and R. OLIVIER, Can. J. Phys., 45, 119.

(67H1) A. R. HUTSON, A. JAYARAMAN and A. S. CORIELL, Phys. Rev., 155, 786.

(67L1) J. LEES, M. P. WASSE and G. KING, Solid State Comm., 5, 521.

(67M1) W. J. MOORE, Phys. Rev., 160, 618.

(67P1) B. PISTULET, J. L. ROBERT and M. MARQUES, Phys. Stat. Sol., 24, 481.

(67S1) A. C. SMITH, J. F. JANAK and R. B. ADLER, "Electronic Conduction in Solids", McGraw-Hill Book Co.

(67V1) Y. P. VARSHNI, Physica, 34, 149.

(67Y1) T. O. YEP and W. M. BECKER, Phys. Rev., 156, 939.

1968 (68A1) M. AVEROUS, G. BOUGNOT and J. CALAS, Phys. Stat. Sol., 29, 807.

(68B1) I. BALSLEV, Phys. Rev., 173, 762.

(68B2) F. J. BLATT, "Physics of Electronic Conduction in Solids", McGraw-Hill Book Co.

(68C1) E. M. CONWELL and M. O. VASSELL, Phys. Rev., 166, 797.

(68H1) F. HERMAN, L. R. KORTUM, C. D. KUGLIN, J. P. VANDYKE and S. SKILLMAN, "Methods in Computational Physics" (edited by B. Adler, S. Fernbach and M. Rotenberg), Vol. 8, Academic Press, New York.

(68H2) C. W. HIGGINBOTHAM, F. H. POLLAK and M. CARDONA, Proc. Intr. Conf. on Phys. of Semiconductors, Moscow.

(68J1) L. W. JAMES, Ph.D. Thesis, Stanford University.

(68J2) L. W. JAMES, R. C. EDEN, J. L. MOLL and W. E. SPICER, Phys. Rev. 174, 909.

(68K1) B. B. KOSICKI, A. JAYARAMAN and W. PAUL, Phys. Rev., 172, 764.

(68K2) C. C. Y. KWAN and J. C. WOOLLEY, Can. J. Phys., 46, 1669.

(68L1) C. Y. LIANG, J. Appl. Phys., 39, 3866.

(68L2) J. LEES, Solid State Comm., 6, 11.

(68M1) H. C. MONTGOMERY, J. Appl. Phys., 39, 2002.

(68S1) W. E. SPICER and R. C. EDEN, Proc. Intr. Conf. on Phys. of Semiconductors, Moscow, 65.

(68S2) R. A. STRADLING and R. A. WOOD., J. Phys., C1, 1711.

(68T1) E. H. VAN TONGERLOO and J. C. WOOLLEY, Can. J. Phys., 46, 1199.

(68V1) Q. H. F. VREHEN, J. Phys. Chem. Solids, 29, 139.

(68W1) A. K. WALTON and U. K. MISHRA, J. Phys., C1, 533.

(68Z1) H. I. ZHANG and J. CALLAWAY, Solid State Comm., 6, 515.

1969 (69A1) M. AUBIN, Thesis, University of Ottawa.

(69A2) F. ADACHI, J. Phys. Chem. Sol., 30, 776.

(69A3) M. J. AUBIN, M. B. THOMAS, E. H. VAN TONGERLOO and J. C. WOOLLEY, Can. J. Phys., 47, 631.

(69B1) G. BORDURE, F. GUSTAVINS and C. LLINORES, Phys. Stat. Sol., 34, 759.

(69C1) T. M. CHAMBERLAIN and R. A. STRADLING, Solid State Comm., 7, 1275.

(69C2) W. M. CODERRE, Thesis, University of Ottawa.

(69C3) M. D'OLNE CAMPAS, L. GAUSKOV and A. NGUYEN VAN MAU, Phys. Stat. Sol., 35, 635.

(69J1) D. JONES and A. H. LETTINGTON, Solid State Comm., 7, 1319.

(69J2) L. W. JAMES and J. L. MOLL, Phys. Rev., 183, 740.

(69K1) H. KRESSEL and H. VON PHILIPSBORN, New York Meeting of the Electrochemical Soc., May 1969 (Abstract No. 61).

(69P1) M. B. PANISH and H. C. CASEY. Intr. J. Appl. Phys., 40, 163.

(69P2) G. D. PITT, High Temperature-High Pressure, 1, 111.

(69R1) JEAN LOUIS ROBERT, Thesis, University of Montpellier.

(69S1) D. G. SEILER and W. M. BECKER, Phys. Rev., 183, 784.

(69T1) E. H. VAN TONGERLOO and J. C. WOOLLEY, Can. J. Phys., 47, 241.

(69Z1) H. I. ZHANG and J. CALLAWAY, Phys. Rev., 181, 1163.

1970 (70A1) M. AVEROUS, G. BOUGNOT, J. CALAS and J. CHEVRIER, Phys. Stat. Sol., 37, 807.

(70B1) Z. BACHAN, E. KIERZEK-PECOLD and J. KOLODZIEJCZAK, Phys. Stat. Sol., 42, K101.

(70C1) T. C. COLLINS, D. J. STUKEL and R. N. EUWEMA, Phys. Rev. B, 1, 724.

(70F1) A. FORTINI, D. DIGNET and J. LUGAND, J. Appl. Phys., 41 3121.

(70G1) A. M. GRAY, Phys. Stat. Sol., 37, 11.

(70H1) J. S. HARRIS, J. L. MOLL and G. L. PEARSON, Phys. Rev. B, 1, 1660.

(70H2) H. G. B. HICKS and P. D. GREEN, Proc. of III Intr. Symposium and "Gallium Arsenide and related compounds" Aachen, Germany, October. (Published by the Institute of Physics, 1971).

(70I1) H. IKOMA, J. Phys. Soc., Japan, 28, 1474.

(70P1) G. D. PITT and J. LEES, Solid State Comm., 8, 491.

(70P2) G. D. PITT and J. LEES, Phys. Rev., B, 2, 4145.

(70R1) J. L. ROBERT and D. BARJON, Phys. Stat. Sol., (a), 3, 421.

(70S1) N. SAWAKI, A. YOSHIDA and T. ARIZUMI, J. Jap. Appl. Phys., 9, 922.

(70S2) NAN STELJAN, Rev. Romanian Physics, 15, 153.

(70S3) G. E. STILLMAN, C. M. WOLFE and J. O. DIMMOCK, J. Phys. Chem. Solids, 31, 1199.

(70S4) N. T. SHERWOOD, Ph.D. Thesis, Purdue University.

(70W1) J. P. WALTER, R. R. L. ZUCCA, M. L. COHEN and Y. R. SHEN, Phys. Rev. Letters, 24, 102.

1971 (71D1) G. DIONNE, Ph.D. Thesis, University of Ottawa.

(71K1) C.C.Y. KWAN, J. BASINSKI and J. C. WOOLLEY, Phys.Stat.Sol. (b), 48, 699.

(71S1) K. SZLANK and W. WALUKIEWICZ, Phys. Stat. Sol. (b) 48, K15.

(71Z1) W. ZAWADZKI and W. SZYMANSKA, J. Phys. Chem. Solids. 32, 1151.

1972 (72B1) D. BIMBERG and W. SCHAIRER, Phys. Rev. Letters, 28, 442.

(72D1) D. DEMARS, Ph.D. Thesis, University of Ottawa.

(72R1) S. ROSENBAUM, Ph.D. Thesis, University of Ottawa.

(72V1) Y. P. VARSHNI, Private communication.